

Air Force Institute of Technology

AFIT Scholar

Theses and Dissertations

Student Graduate Works

3-2006

Biological System Impedance Identification Using Stochastic Estimation and Control

Enrique Mendezaceves

Follow this and additional works at: <https://scholar.afit.edu/etd>



Part of the [Bioelectrical and Neuroengineering Commons](#)

Recommended Citation

Mendezaceves, Enrique, "Biological System Impedance Identification Using Stochastic Estimation and Control" (2006). *Theses and Dissertations*. 3497.

<https://scholar.afit.edu/etd/3497>

This Thesis is brought to you for free and open access by the Student Graduate Works at AFIT Scholar. It has been accepted for inclusion in Theses and Dissertations by an authorized administrator of AFIT Scholar. For more information, please contact AFIT.ENWL.Repository@us.af.mil.



BIOLOGICAL SYSTEM IMPEDANCE IDENTIFICATION USING
STOCHASTIC ESTIMATION AND CONTROL

THESIS

Enrique Mendezaceves, Second Lieutenant, USAF

AFIT/GE/ENG/06-41

DEPARTMENT OF THE AIR FORCE
AIR UNIVERSITY

AIR FORCE INSTITUTE OF TECHNOLOGY

Wright-Patterson Air Force Base, Ohio

APPROVED FOR PUBLIC RELEASE; DISTRIBUTION UNLIMITED.

The views expressed in this thesis are those of the author and do not reflect the official policy or position of the United States Air Force, Department of Defense, or the United States Government.

AFIT/GE/ENG/06-41

BIOLOGICAL SYSTEM IMPEDANCE IDENTIFICATION USING
STOCHASTIC ESTIMATION AND CONTROL

THESIS

Presented to the Faculty
Department of Electrical and Computer Engineering
Graduate School of Engineering and Management
Air Force Institute of Technology
Air University
Air Education and Training Command
In Partial Fulfillment of the Requirements for the
Degree of Master of Science in Electrical Engineering

Enrique Mendezaceves, B.S.E.E.
Second Lieutenant, USAF

March 2006

APPROVED FOR PUBLIC RELEASE; DISTRIBUTION UNLIMITED.

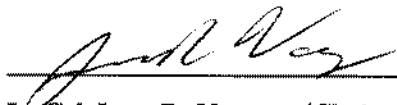
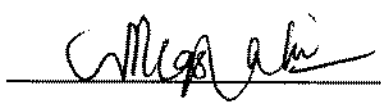
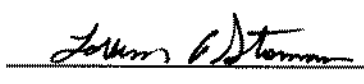
AFIT/GE/ENG/06-41

BIOLOGICAL SYSTEM IMPEDANCE IDENTIFICATION USING
STOCHASTIC ESTIMATION AND CONTROL

Enrique Mendezaceves, B.S.E.E.

Second Lieutenant, USAF

Approved:

 _____	<u>13 Mar 06</u>
Lt Col Juan R. Vasquez (Chairman)	Date
 _____	<u>10 MAR 06</u>
Dr. Saber Hussain (Member)	Date
 _____	<u>6 MAR 06</u>
Maj LaVern Starman (Member)	Date

Abstract

In an effort to find a less invasive way of testing for different cell abnormalities and finding more practical tests for different cellular mutations, this project makes use of a well known technique called cellular impedance spectroscopy coupled with stochastic estimation.

Impedance spectroscopy, the measurement of the complex resistance of a biological body, is not a new technology; it has been around for many years and has been used to make electrical representations of different biological systems. The problem with this procedure is that the models cannot be used for system identification. Stochastic estimation can complement a model produced by analysing the input/output characteristics of the cell to account for modeling inadequacies produced by linear modeling of electrical impedance spectroscopy alone.

In this thesis, biological cell samples were submitted to a sinusoidal voltage at a different range of frequencies. The cell samples created an output which was used to model the electrical behavior of the biological system. This electrical representation was used to build a fixed-interval stochastic smoother. The stochastic smoother was then used to estimate the output measurements of different cell samples and ultimately identify a cell type based on the evaluation of the residuals produced.

Results showed that, given residual values, one could apply a binary logic windowing technique that would show a difference in the cell samples tested thereby being able to identify the cell sample in question.

Table of Contents

	Page
Abstract	iii
List of Figures	vii
List of Tables	xiv
I. Introduction	1-1
1.1 Background	1-1
1.1.1 Impedance Spectroscopy.	1-1
1.1.2 System Measurements	1-2
1.2 Problem Statement	1-4
1.3 Research Focus	1-4
1.4 Methodology	1-5
1.5 Assumptions/Limitations	1-6
1.6 Thesis Overview	1-8
II. Literature Review	2-1
2.1 Overview of Electrical Impedance Spectroscopy	2-1
2.1.1 EIS Measurements	2-2
2.1.2 Other Electrical Impedance Spectroscopy Avenues	2-12
2.1.3 Cell Samples Being Tested	2-17
2.2 Overview of Control Systems	2-19
2.2.1 Transfer Functions	2-19
2.2.2 Bode Plots	2-20
2.2.3 System Identification	2-21
2.3 Overview of Stochastic Estimation and Control	2-23
2.3.1 The Kalman Filter	2-23

	Page	
2.3.2	The Stochastic Smoother	2-23
2.3.3	Residual Monitoring	2-26
2.4	Synthesis	2-26
III.	Theory	3-1
3.1	Collection of Sampled Data	3-3
3.2	System Identification (SID)	3-4
3.2.1	The Linear, Ready-made Model (LRM)	3-4
3.2.2	Parameter Prediction	3-6
3.3	Stochastic Estimation and Control (SEC)	3-8
3.3.1	The Kalman Filter (KF)	3-9
3.3.2	Residual Monitoring	3-14
3.4	Summary	3-15
IV.	Results	4-1
4.1	Measurement Equipment	4-1
4.1.1	Oscilloscope	4-1
4.1.2	Function Generator	4-2
4.1.3	Probes	4-2
4.1.4	Computer Interface	4-3
4.2	Cell-type Samples	4-7
4.2.1	Cell Test Samples	4-10
4.3	System Modeling	4-20
4.4	Modeling of Stochastic Smoother	4-26
4.5	Residual Analysis	4-33
4.5.1	Residual Results	4-33
4.5.2	Results from Windowing	4-37

	Page
V. Conclusions and Recommendations	5-1
5.1 Restatement of Research Goals	5-1
5.2 Summary of Results	5-1
5.3 Significant Contributions of Research	5-3
5.3.1 The Military Sector	5-3
5.3.2 The Civilian Sector	5-3
5.4 Recommendation for Future Research	5-4
5.4.1 More Accurate Experimentation	5-4
5.4.2 MEMS	5-5
5.4.3 Noninvasive Designs	5-7
5.5 Conclusion	5-7
Bibliography	BIB-1

List of Figures

Figure		Page
1.1.	Very basic mathematical system model. The input (u) goes into an unknown system to produce the output (y). The perturbation (e), is described as noise entering the system. The perturbation is usually modeled statistically (i.e., as random white noise).	1-3
1.2.	Comparison of two cellular representative circuits that have the same output. Both Circuit A and Cirtuit B will perform the same function, but the dyelectric properties are distributed differently. Note that circuit B components are written in terms of Circuit A component values.	1-7
2.1.	Plot of resistance and reactance; the real and imaginary part of impedance in rectangular coordinates. Impedance is also plotted in polar coordinates through its magnitude and phase.	2-2
2.2.	Basic theory behind EIS measurements. An input is placed into the biological sample and the output signal is recorded. Based on these two measurements, an impedance measurement is produced.	2-3
2.3.	Basic mammal cell cross section (above picture) (14). Below is a circuit representation of such cell. Extra cellular material is considered resistive. The membrane of the cell has capacitive and resistive components. The intra cellular material is resistive except for different specifice components (like the nucleus) (2).	2-4
2.4.	Diagram of high frequency and low frequency signals passing through a cell sample (27).	2-5
2.5.	Diagram of dispersion denoting three different regions. These regions affect measurements of different parts of the cell (2).	2-6

Figure		Page
2.6.	Typical probing method of the EndOhm-12. The sample well consists of a cylinder with a 12 mm diameter. This device makes use of the 4-point probe method. Current goes through the outside electrodes (which encircle the point electrodes in the middle), while voltage differential is measured via the point electrodes. This technique has the potential of reducing errors produced by other media inside the sample well in the EIS machine (4).	2-8
2.7.	Typical oscilloscope readings. Blue denotes sinusoidal input. Red denotes sinusoidal output.	2-10
2.8.	Basic diagram delineating a EIS measurement via a non-invasive technique. The a current is passed through a coils which in turn produces an electromagnetic field. The eddy current of the epidermal layer (the skin), cancels some of this field, thereby reducing the current in the system, the reduced current is measured and analyzed (32).	2-13
2.9.	Fabrication of impedance probes through alternative polyimide substance (38).	2-15
2.10.	This diagram shows different manipulation techniques that need to be used for different sized cells in different environments (40).	2-17
2.11.	The Bode plot of the transfer function depicted in Equation 2.14. It consists of two graphs. The frequency is plotted logarithmically. The magnitude (top plot), is plotted in dB. The bottom plot is in degrees (y scale).	2-21
2.12.	This is the typical application of a Kalman filter. It takes all measurements into account, including erros, to come up with the best estimate of the system state. This estimate is then updated by actual system measurements to get a better overall ouput (22).	2-24
2.13.	Typical smoother representation in conjunction with Kalman filter representation. $P(t_i^+)$ is the covariance of the forward Kalman filter. $P_b(t_i^+)$ is the backward propagation of the same filter. When optimaly combined into a smoother, the covariance $P(t_i/t_f)$ is significantly reduced, providing more confidence in the estimate (22). . .	2-25

Figure	Page	
3.1.	Diagram denoting the theoretical experimental process used in this thesis. The red section denotes the acquisition of measurements of live cell samples via EIS. The green section denotes the System Identification (SID) process to produce a model. The yellow section shows the creation of the stochastic smoother based on the identified system characteristics and the subsequent use of the filter with an unrelated cell sample. The yellow section also points to the residual monitoring of the stochastic smoother. Finally, the blue section shows a decision being made based on the aforementioned process.	3-2
3.2.	Block diagram representing the ARX model. A represents the Auto Regression portion of the model, B denotes an extra input, and e denotes noise entering the system.	3-6
4.1.	Agilent 54641D oscilloscope used in the measurement of the input and output signals of the test samples.	4-2
4.2.	Agilent 33250A function generator used in this experiment. The function generator was used to input a sine wave at different frequencies into the cell sample.	4-3
4.3.	Fabrication schematic of probe interface. The probe interphase was specifically designed to fit into a well containing a biological cell sample.	4-4
4.4.	Picture of fabricated probe interface. This specific probe interface fits into a 24 sample well (see figure 4.10). Two probe interface types were considered: two leads and four leads. The four lead probe was not used because subsequent experiments found that the two inner probes did not take cell sample measurements but only measured extra-cellular material. This resulted from cells sticking to the bottom of the sample wells, where the middle leads could not properly test.	4-4
4.5.	Figure of measurement and experimental equipment used to send an input and record an output of the cell sample. The function generator (bottom left) sends a sinusoidal input into the cell sample. The oscilloscope (top left) measures the input and registers the output of the cell sample. The laptop (on the right) directs the input and output, and records the measurements at every sample time.	4-5

Figure	Page	
4.6.	The flowchart depicts the process of taking different cellular measurements automatically. The computer specifies the input of the function generator. The output is read by the oscilloscope and recorded into a computer file at each frequency. The automated process then moves on to the next frequency increment to take a measurement until measurements from the entire frequency range are taken.	4-6
4.7.	Control HEL-30 sample at 10x magnification.	4-7
4.8.	Control PC-12 cell sample at 60x magnification.	4-8
4.9.	Figure displaying results of MTT tests. This is a comparison between the normalized data of the 308 samples tested with an input signal and the control test samples, which were not excited by an electrical input.	4-8
4.10.	Depiction of 24 well cell sample plate. Each well contains either a sample of HEL-30 cells or PC-12 cells. Probes are connected to test the electrical characteristics of an individual cell sample within the plate.	4-9
4.11.	HEL-30 control cell without MTT marker. Photographs used to compare the structure of the cell of anomilies.	4-10
4.12.	HEL-30 cell control samples with MTT marker.	4-11
4.13.	Typical frequency response over a 200KHz-1MHz range with a 2Vpp amplitude. There is no significant response change between the input and the output. It was for this reason that a range of 1MHz to 80 MHz in the β dispersion frequency range was chosen. X label denotes sample points (100 per frequency measurement). Frequencies labeled in their specific partitions.	4-14
4.14.	Input/output relationships of representative HEL-30 cell samples used in the system modeling. Top scale and dividers denote frequencies and boundaries respectively. Bottom scale denotes number of sample points. Y scale denotes units in volts (V). This figure denotes a frequency range of 1MHz-40MHz at 1MHz steps.	4-16

Figure	Page
4.15. Input/output relationships of representative HEL-30 cell samples used in the system modeling. Top scale and dividers denote frequency changes. Bottom scale denotes number of sample points. Y scale denotes units in volts (V). This figure denotes a frequency range of 41MHz-75MHz at 1MHz steps.	4-17
4.16. Input/output relationships representative of PC-12 cell samples. Top scale and dividers denote frequency. Bottom scale denotes number of sample points. Y scale denotes units in volts (V). This is from a frequency range 1MHz-40MHz at 1MHz steps and an amplitude of 250 mVpp.	4-18
4.17. Input/output relationships of representative PC-12 cell samples. Top scale and dividers denote frequency. Bottom scale denotes number of sample points. Y scale denotes units in volts (V). This is from a frequency range 41MHz-75MHz at 1MHz steps and an amplitude of 250 mVpp.	4-19
4.18. Comparison of PC-12 sample and HEL-30 sample outputs (Blue denotes HEL-30 samples while Red denotes PC-12 samples). Upper scale denotes frequency changes. Lower scale denotes sample steps. Y scale denotes amplitude in volts (V). These plots show response over a frequency range of 1MHz-40MHz.	4-21
4.19. Comparison of PC-12 sample and HEL-30 sample outputs (Blue denotes HEL-30 samples while Red denotes PC-12 samples). Upper scale denotes frequency changes. Lower scale denotes sample steps. Y scale denotes amplitude in volts (V). These plots show response over a frequency range of 41MHz-75MHz.	4-22
4.20. Figure of Ident, a GUI used within MATLAB [®] to build system models based on ARX models. This tool is used to estimate transfer functions based on input and output measurements.	4-23
4.21. The figure depicts 13 different models that very closely resemble the output characteristics of the samples at different frequencies. These models were produced by different iterations of the ARX algorithm. From these models, one was chosen as best depiction. The line in black is the system measured response, the smooth multi-colored lines depict the different models.	4-24

Figure		Page
4.22.	Figure depicts the model that was to be used in the development of the stochastic smoother.	4-25
4.23.	This figure shows the difference between the smoothed output estimated and the measured output of a representative HEL-30 cell sample. Red shows the cell sample output. Blue shows the estimate output. Upper scale denotes frequencies. Lower scale shows sample intervals. Y scale shows magnitude in volts (V).	4-29
4.24.	This figure shows the difference between the smoothed output estimated and the measured output of a representative HEL-30 cell sample. Red shows the cell sample output. Blue shows the estimate output. Upper scale denotes frequencies. Lower scale shows sample intervals. Y scale shows magnitude in volts (V).	4-30
4.25.	The figure shows the difference between the smoothed output estimate and the measured output of a representative PC-12 cell sample. Red shows the cell sample output. Blue shows the estimated output. Upper scale denotes frequencies. Lower scale shows sample intervals. Y scale shows magnitude in volts (V).	4-31
4.26.	The figure shows the difference between the smoothed output estimate and the measured output of a representative PC-12 cell sample. Red shows the cell sample output. Blue shows the estimated output. Upper scale denotes frequencies. Lower scale shows sample intervals. Y scale shows magnitude in volts (V).	4-32
4.27.	Typical comparison between residuals from HEL-30 cell sample and PC-12 cell sample. Black line delineates allowable threshold error in the estimate.	4-34
4.28.	Plot of comparison between residual values of HEL-30 cell sample (Red), and PC-12 sample (Blue). Upper scale measured the frequency. Lower scale shows sample point. Y scale is amplitude in volts (V).	4-35
4.29.	Plot of comparison between residual values of HEL-30 cell sample (Red), and PC-12 sample (Blue). Upper scale measured the frequency. Lower scale shows sample point. Y scale is amplitude in volts (V).	4-36

Figure		Page
4.30.	Flow diagram describing the process of windowing. Windowing is a method to determine if residuals are consistently above a certain threshold.	4-38
4.31.	Window plot representing flags from windowing the data in residual plots from Plate 14 and Plate 11.	4-39
4.32.	Window plot representing extreme amount of flags from windowing the data in residual plots from Plate 14 (top) and Plate 11 (bottom).	4-41
4.33.	Comparison between residuals from HEL-30 cell sample and PC-12 cell sample. Black line delineates allowable threshold error in the estimate.	4-42
4.34.	Window plot representing minute amount of flags from windowing the data in residual plots from Plate 14 (Top) and Plate 11 (bottom).	4-43
4.35.	Comparison between residuals from HEL-30 cell sample and PC-12 cell sample. Black line delineates allowable threshold error in the estimate.	4-44
5.1.	MEMS probe designed during this research but never implemented. Probe is $100\mu\text{m}$ long and $10\mu\text{m}$ wide and is made of polysilicon overlaid with gold. Probe thickness is $6\mu\text{m}$. Gold wire (Blue) connects probe to wire bonded gold pad.	5-5
5.2.	Probe array designed for cell testing. Given that different cells vary in size, this probe is designed to be fit around a cell and then probe from different angles for best measurement accuracy. Each of these probes are the same as in Figure 5.1.	5-6

List of Tables

Table		Page
4.1.	This table denotes the results of Cell Sample Plate 1. HEL-30 cell samples were tested. There were no control samples in this plate because boundaries needed to be tested.	4-12
4.2.	This table denotes the results of HEL-30 Cell Sample Plate 2. This plate was mainly tested to find input boundaries that could be used for experimentation.	4-13
4.3.	This table denotes the input that each HEL-30 cell sample plate was subjected to. The cell samples that have already been displayed are referenced from other tables. There were only 22 test samples in each plate because 2 test samples were always used for control	4-15
4.4.	This table denotes inputs that PC-12 sample plates were subjected to. MTT test column delineates survival of all test samples. There were only 22 test samples in each plate because 2 test samples were always used for control	4-20
4.5.	The table shows how many flags each of the samples in Plate 11 (made up of 21 HEL-30 samples), and Plate 14 (made up of PC-12 samples) raised as a result of their residuals not being below acceptable thresholds. Based on this data, it can be safe to assume that system identification is possible based on the number of times the residuals of the data exceed a specific limit	4-40

BIOLOGICAL SYSTEM IMPEDANCE IDENTIFICATION USING STOCHASTIC ESTIMATION AND CONTROL

I. Introduction

Electrical Impedance Spectroscopy (EIS), a method of finding the electrical properties of materials, has been catalytic in some of the technologies used today. Many of the technologies that required batteries in WWII were developed with EIS. The combination of this measuring technique with an estimating algorithm (like Stochastic Estimation and Control (SEC)), could become the next evolution in EIS. By applying an optimal estimation algorithm and being able to account for the unknown processes in a material (like a biological cell), identification through electrical means could be a possibility. The positive consequences of being able to identify a cell in-vivo could be limitless. Soldiers could test for internal bleeding with a device that does not break the skin. Tumors could be classified as cancerous or benign by applying a Micro Electro Mechanical Systems (MEMS) probe into a live individual, completely bypassing the need for a myoscopy. The problem addressed in this research is: How could one interface these two powerful fields of research?

1.1 Background

A brief background on EIS and SEC is reported in the following paragraphs. The culmination of the chapter will entail the synthesis of these subjects to come up with a method for the identification of specific cell types using smoothing algorithms and residual monitoring.

1.1.1 Impedance Spectroscopy. Electrical impedance is the complex resistance created by trying to pass current through a material. Just about every material on earth will have some sort of interaction when a current is passed through it. This interaction, in the vast majority of cases, will resist the flow of electrons. This resistance (or impedance, if the resistance is complex or frequency dependent), limits the flow rate of electrically charged particles when such particles are present in the system. Given the many different

fundamental microscopic processes that take place in a cell, this impedance behavior is often unique to one type of system depending on the size, shape, interface with the probing material and composition of the material being tested. Scientists have been able to exploit this knowledge to electrically characterize different compounds, both biological and electrochemical. Since the shape and structure of many compounds are unique, it stands to reason that the impedance (capacitive or inductive), of such materials would also be unique and could possibly help in characterizing such a compound. This is the main reason EIS was developed (2, 11).

EIS is a method for characterizing the electrical properties of a sample (3, 11, 23) . The theory for such a measurement has been around for more than a century, but the actual practice of using EIS measurements is relatively new. Computer and digital technologies have made it easier to implement measurements over a vast frequency spectrum with relatively good accuracy. One of the best qualities of an EIS measurement is its dynamic range of implementation. Almost all chemical processes change the electrical conductivity of the particle in question, which leaves a lot of leeway for test and measurement investigation. It is the experience of many researchers that EIS provides a means for investigating almost anything seen hystorologically in a microscope (2). EIS measurements can identify tissue structures (such as size, shape, cell orientation, amount of liquid inside and outside of the cell, and cell membrane structure), and uniquely characterize them between samples that are of the same cell type, and also within samples that are of different cell type. This allows different characterization of a regular cell and a modified cell of the same sort (i.e., between a cancerous and a healthy cell) (1, 7, 41).

The characterization of a cellular system via electrical methods allows for the modeling of such a system in terms of control theory. This is based on the fact that the measurements taken by EIS are dependent on an input and an output signal. Assuming that the system is linear, a control system model for the cell can be approximated via electrical components such as resistors, capacitors and inductors (2, 11).

1.1.2 System Measurements. The creation of a cellular model based on electrical components is based on the premise of model behavior. Given a specific input, a specific

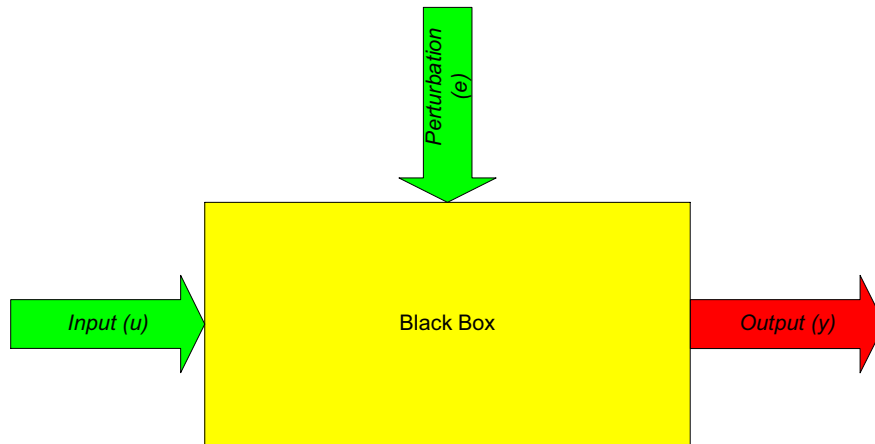


Figure 1.1 Very basic mathematical system model. The input (u) goes into an unknown system to produce the output (y). The perturbation (e), is described as noise entering the system. The perturbation is usually modeled statistically (i.e., as random white noise).

output is created that can be characterized by some combination of circuit components. There are many techniques for modeling the behavior of a system which will be discussed in Chapter 2. Most of these techniques involve differential equations to represent the complexity of the system.

The end result is that, based on a representative model (if not a perfect model, at least one that reasonably depicts the behavior of relevant system modes), one can write a mathematical equation for such a system. The mathematical model is very important, it has to accurately represent relevant information for a biological system's behavior over certain boundaries (i.e., frequency boundaries). A basic "black box" depiction of a system is represented in Figure 1.1 (21).

There are many ways to assess the network inside the black box. In some cases, it may be accurate enough to manually determine the system model from input/output data such as frequency domain magnitude and phase (Bode plot). In the vast majority of cases though, one has to use different techniques, such as curve-fitting the frequency data to minimize some error criterion. Depending on the system being studied and the algorithm used, one can get a reasonably reliable assessment of the correct representative model (20).

1.2 Problem Statement

Overall, EIS measurements have proven very useful to scientists and researchers. Because of the fact that many different structures (chemical and biological) are based on many different material and mechanical parameters (even the temperature of an object can increase or decrease its conductivity and therefore its impedance), it is very easy to individually identify a very specific specimen if care is taken to measure within specific parameters. EIS is constantly being used in experimentations with cancer cells and based on EIS measurements, many generalizations can be made.. For example, researchers now know that a cancerous cell will increase in impedance. Researchers also know that an irritated cell will allow more electricity through (or have less impedance) (1, 2, 6, 11).

The problem with EIS measurements is that they account for too many parameters of the cell. An example of this is that cells at different stages of growth (duplication, maturity, confluence, or death), will exhibit different impedances. While this may be the desired result in some experiments, it does not allow the tool to be used for cell identification. The reason is that cells may be going through different natural processes that may fundamentally alter their basic composition, thereby exhibiting different impedances. This would make it difficult to identify a cell via EIS based on a model built from a completely different cell that was of the same cell-type, but in a different growth stage. As a result, scientists and researchers are restricted to making generalized statements about impedance spectroscopy (i.e., smaller sized cells generally have a lower impedance than bigger sized cells) (2, 41).

1.3 Research Focus

There are two primary goals of this study. The first is whether or not EIS measurements at higher frequencies can produce a good and unique model for the characterization of cells. Secondly, whether or not SEC could be exploited in the study of biological systems if it is interfaced with EIS.

Given prior research efforts, and the study of industry standards, it is an accepted practice to test biological systems (and some electrochemical ones as well), at low frequen-

cies (most commercial tools test cells in the 1mHz to 1MHz range) (6, 10, 11). Preliminary results of this research indicate that more distinct magnitude and phase changes occurred in the high frequency range. Based on this, it was decided that the biologically representative circuit models would be based on the responses of the higher frequency spectrums.

Once these frequency models are determined, the next part of this thesis involves applying SEC to correctly estimate and identify a biological system. As mentioned before, statistical modeling and electrical component modeling has been used to build models in the biological community for some time (11). SEC is an extension of this statistical modeling, revolving around the Kalman filter (an optimal estimation filter). The hypothesis of this thesis is that SEC can be used to identify the cell-type from sampled data.

This research is mainly conducted to answer the question: "Can a biological system be identified via SEC?" This is important, because if different biological systems can be identified, then markers could be found for different processes within the system. Given the flexibility of EIS, the next step after identifying different types of systems would be to identify a specific process within the same system, such as the production of a specific protein, or the early mutation of a cell. The possibility of future studies using this technology could be limitless and beneficial both for the military and the civilian sectors.

1.4 Methodology

Initially EIS measurements will be taken with a signal generator and an oscilloscope. The results of these measurements will be used to build a model based on a sample of cells. The mathematical model created will be used to build a stochastic smoother (an evolution of the Kalman filter). Statistical properties of the smoother, such as a noise term, will be modified for more accurate estimation. Finally, the results of other samples (from the same cell-types and different cell-types) will be run through the smoother. The smoother will estimate the model behavior, known as the internal states of the model. Given a proper combination of these states, we can form an estimate of the actual measurements. The residuals (the difference between the estimated measurements and the actual measurements) will be monitored. Based on the divergence between the actual measurements and the filter estimate, the sample will be either identified as the same cell-type or a dif-

ferent one. Specifically, if the residual is small this implies the model matches the newly measured sample. A large residual indicates the model and the new sample are different. The accuracy with which the filter correctly identifies a system of the same type will be recorded and discussed.

1.5 Assumptions/Limitations

Assumption 1: One of the main limitations in this research is the assumed linearity of the biological system over the observed frequency range (26). This assumption permits the use of well understood system identification tools for linear systems. The process of curve-fitting the frequency data will allow a minimization of a least squares error and thus strive to estimate the nonlinear component of the system. Lastly, the stochastic theory is significantly simplified if a nonlinear system is assumed to be linear. Nonlinear estimation techniques exist, but are beyond the scope of this research (22).

Assumption 2: The model of the system is unique over the frequency range used in the experiments. As mentioned before, the typical frequency range for testing is between 1mHz and 1MHz (11). The experimentation of this thesis revealed that more meaningful measurements existed over a frequency range between 1MHz and 100MHz. While this study accepts that meaningful EIS measurements are more commonly taken over a lower frequency range, the range used for this experiment was chosen based on experimental data. Limitations in existing equipment precluded data collections of frequencies above 100MHz.

Assumption 3: Lumped system properties are assumed adequate in modeling the system. A lumped system implies that internal subsystems are adequately represented by evenly distributed parameter values (11). The problem with this is that the vast majority of biological systems' electrical properties are not lumped, but distributed unevenly. This leaves questions on whether or not the represented system is truly representative of the system. An example of this is portrayed in Figure 1.2, where two separate circuits would have the same response, but are internally different. It is the contention of this study that the most relevant goal is to model the output as effectively as possible. Therefore, the focus will be on input/output relationships of lumped linear systems.

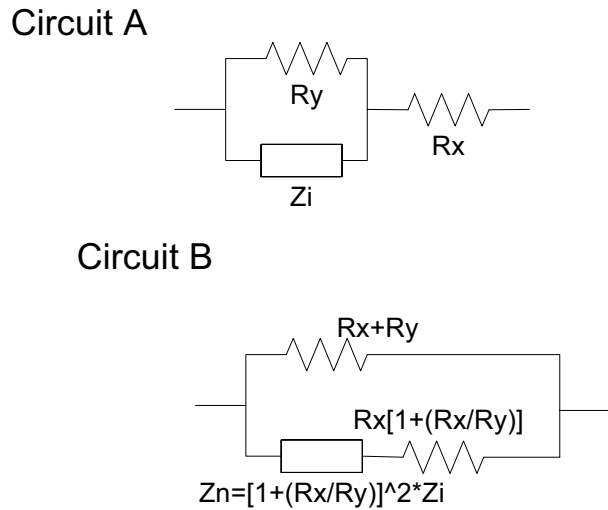


Figure 1.2 Comparison of two cellular representative circuits that have the same output. Both Circuit A and Circuit B will perform the same function, but the dielectric properties are distributed differently. Note that circuit B components are written in terms of Circuit A component values.

Assumption 4: The cellular system being tested is assumed to be time-invariant and has a steady state response. This is a significant assumption given the unknown effects an electrical stimulus has on the cell at high frequencies. It is known that cell samples can stand high electrical magnitudes as some studies show that cells can survive with electrical stimuli up to 46 volts (28). If the cells die during the test, then their response would change in the middle of the experiment. This has serious implications as it suggests that our method could not be used with live subjects. Secondly, it implies that the dead cells would obviously have different electrical properties than live cells. In assuming time-invariance, we essentially declare that the system response is independent of when the stimulus is applied and thus the model characteristics are constant. A steady-state response implies that the cells do not die or radically change their behavior when excited by the stimulus. In order to validate this assumption, a series of 3-(4, 5-dimethylthiazol-2-yl)-2, 5-diphenyltetrazolium bromide tests to mitochondrial reactions (or MTT tests for short), were conducted to determine if the cells remained alive after prolonged stimulation. A more thorough discussion of MTT tests is given in Section 2.1.1.6.

1.6 Thesis Overview

Chapter 2 goes through a basic history and evolution of the theories presented in this thesis. Basic concepts are discussed along with aspects of other research with EIS. This chapter will also present the process of EIS measurements. Also, System Identification (SID) will be introduced in the most basic manner. Finally, the basic ideas of SEC and the smoothing algorithm will be presented.

Chapter 3 will delve in the theory and mathematical analysis used in this thesis. Its main purpose is to present all the theories and postulations made. Some of the hardware issues will also be discussed, given their pertinence to this thesis.

Chapter 4 will present the details of the experimentations that constitute the actualization of the theories in Chapter 3. This chapter will discuss data collection methods and solutions to different experimental difficulties that were encountered. This chapter will be very specific in nature regarding the complete experimentation procedure and the results. It will discuss methods of data acquisition of EIS measurement, methods used for SID, implementation of the smoother for SEC and finally the results of the residual monitoring.

Finally, Chapter 5 will summarize all the results acquired in Chapter 4. The chapter will conclude with different recommendations for the improvement of the research. This chapter will summarize the possible future avenues for research in this field.

II. Literature Review

The main purpose of this chapter is to give some background information on the diverse subjects this thesis covers. Publications concerning different measurement methods, inputs, and mathematical analyses will be discussed. The Electrical Impedance Spectroscopy (EIS) section will conclude with a discussion on how this technology evolved.

A section of control system theory will be provided in order to describe how EIS can be interfaced with Stochastic Estimation and Control (SEC). Next, there will be a section discussing some of the theories behind SEC. Finally, there will be a brief discussion on the stochastic smoother and residual monitoring.

2.1 Overview of Electrical Impedance Spectroscopy

The concept of impedance was first introduced in the 1880's by Oliver Heavyside. Shortly thereafter, A. E. Kennelly, and C. P. Steinmetz developed the vector diagrams and complex representation of electrical impedance that are currently in use (11). Impedance has become a very fundamental concept in electrical engineering. EIS is an electrical measurement constituting resistance, capacitance and inductance. So, it is recognized that EIS is just another type of electrical measurement. Impedance, $Z = R + jX$, where R is the resistance or the real part of impedance, and X is the reactance or the complex part of impedance is represented in Figure 2.1. Note that $j = \sqrt{-1}$. In polar coordinates, one can represent impedance as $Z = |Z| e^{j\theta}$. The magnitude is given by $|Z| = \sqrt{R^2 + X^2}$, and θ is the change in phase, or the phase angle; $\theta = \arctan(\frac{X}{R})$.

The development of electricity as a medical means began in the 20th century, when two doctors, Cerletti and Bini invented the Electroconvulsive Therapy machine (ECT). The ECT is a machine that delivers about 100 volts of shock to schizophrenic patients (31). Needless to say, this was more torture than treatment, but the focus here is the development of a machine that took full-body impedance into account.

EIS on cellular samples began in earnest in 1925. EIS however, was not developed specifically for biology. There is an enormous amount of documentation concerning non-catalytic energy conversion based on the electrochemical processes measured by EIS.

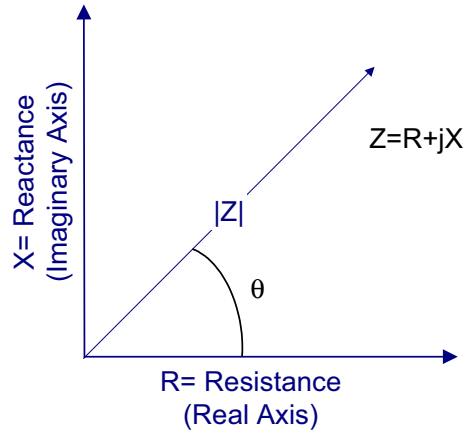


Figure 2.1 Plot of resistance and reactance; the real and imaginary part of impedance in rectangular coordinates. Impedance is also plotted in polar coordinates through its magnitude and phase.

This was done to create more efficient batteries during WWII. It was not until the late 1970's that the technology was implemented to the extent it is now applied. The reason for this new found implementation was due to improvements in automation technology. The practice of taking thousands of measurements (in some cases), over a high range of frequencies suddenly became more commonplace. Once the process was established, people in the medical community were able to apply this technology to biological research. An important study happened in 1979, when D. C. Salter, from the Slade Hospital in Oxford England qualified electricity as a method of influencing cell activities and taking measurements (35). D. C. Salter studied some of the electrical properties of the skin by applying electricity through a probe system. He measured the impedance of the skin over a frequency range.

2.1.1 EIS Measurements. The most general approach to taking EIS measurements is to apply an electrical stimulus (either voltage or current) to a system, then observe the response of the system (Figure 2.2). Time-invariance is initially assumed, but then either confirmed or disproved based on the results. Also, a perfectly smooth interphase between the probe material and the material being tested is assumed. Needless to say, there are many point defects, chemical impurities, structure abnormalities and chemical processes that influence the actual measurements taken. Assuming these outside per-

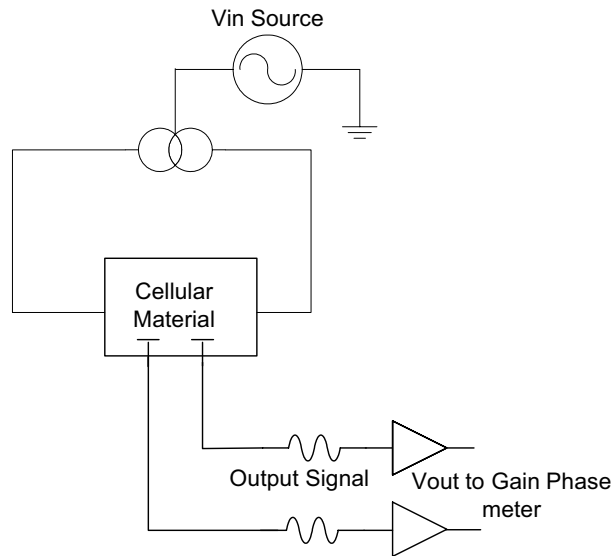


Figure 2.2 Basic theory behind EIS measurements. An input is placed into the biological sample and the output signal is recorded. Based on these two measurements, an impedance measurement is produced.

turbations are negligible, the result of EIS measurements allows for the development of a cellular model based on its electrical characteristics.

2.1.1.1 Advantages and Disadvantages of EIS Measurements. Results from EIS measurements can be readily correlated to many physical and chemical properties of materials such as form-mass transport, material conductivity mapping, chemical reaction rates, and material density. EIS can also predict the performance of chemical sensors and is used in many studies involving cell membranes (2, 11). The fact that EIS can be interpreted and modeled as bulk electrical components also allows for added flexibility in terms of system analysis.

The main disadvantage of EIS revolves around the ambiguities of the representative electrical system. Unfortunately, the dielectric properties of some materials are not lumped in an area, but distributed throughout the system (unlike the lumped system properties of electrical components). It has been found that a finite amount of summed constant elements could not fully predict a cellular system, but approximations become more accurate once distributed impedance elements are used within a frequency range (11). This raises

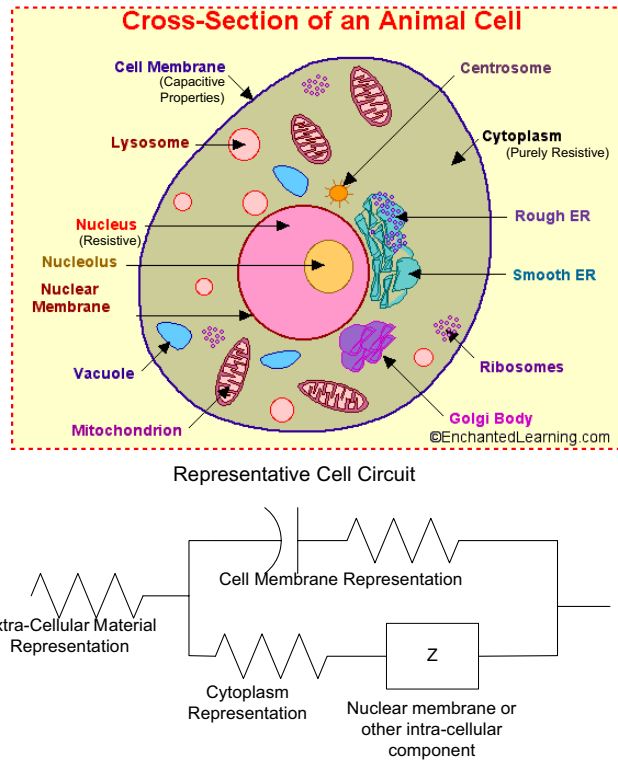


Figure 2.3 Basic mammal cell cross section (above picture) (14). Below is a circuit representation of such cell. Extra cellular material is considered resistive. The membrane of the cell has capacitive and resistive components. The intra cellular material is resistive except for different specific components (like the nucleus) (2).

the question of how many components would be needed to properly represent the cellular models' properties.

2.1.1.2 Biological Measurements of Electrical Impedance Spectroscopy. The properties of the cell manifest themselves as different electrical phenomena. The cellular membrane's semipermeable properties allow for some, but not all, ions to pass through the membrane. This property creates the capacitance and some of the resistance seen in an EIS measurement. In addition, both the inside and outside of the cell (the nutrient environment and the cytoplasm within), represent, purely resistive properties (see Figure 2.3). EIS is useful in measuring the resistive properties and thus identifying properties of biological systems.

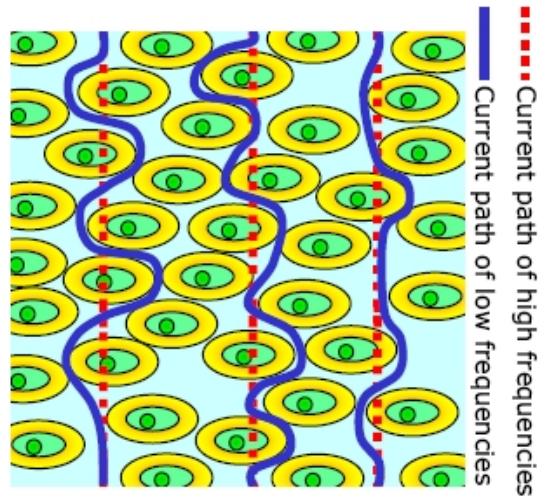


Figure 2.4 Diagram of high frequency and low frequency signals passing through a cell sample (27).

The impedance of such a cellular structure is also dependent on high frequencies. Normally, low frequencies affect the extra-cellular environment (outside the cell), while higher frequencies affect the intra cellular environment (inside the cell). Cell membranes have a high capacitance, acting as high pass filters. This limits the propagation of lower frequency currents to the outside of the membranes, or the extra-cellular medium. Higher frequencies pass through the cell. These attributes explain the high variations of impedance over the frequency spectrum (please refer to Figure 2.4).

Another phenomenon that allows for a unique impedance spectrum is the process of dispersion. While the theory of dispersion entails the molecular movement of cells given a physical phenomena (i.e., electricity) it is beyond the scope of this paper. Dispersion is seen where impedance is decreased at a given frequency (2). Figure 2.5 shows some dispersive characteristics of a biological material. Shwan was the first to notice these dispersive characteristics in cells (2, 3). He identified three frequency regions where dispersion occurred. According to Shwan, the dispersion in the medically relevant information about the cell usually occurs in the β region, constituting measurement of structural changes and polarization of cell membranes and edema. The α region represents polarizations of ionic clouds around the cell. The γ dispersion reflects relaxation of water molecules.

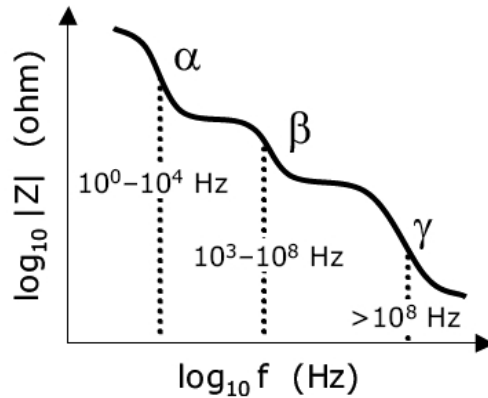


Figure 2.5 Diagram of dispersion denoting three different regions. These regions affect measurements of different parts of the cell (2).

2.1.1.3 *EIS Measurement Methods.* EIS uses a very basic premise: Ohm's Law. In the simplest case; $V = RI$, or voltage, V , is directly proportional to the current, I , by a factor of R , the resistance of the medium by which such current is transferred. In the complex domain, the DC voltage $v(t)$ becomes a time-dependent sinusoidal waveform as in Equation (2.1):

$$v(t) = V_0 \sin(\omega t) \tag{2.1}$$

Where V_0 is the peak-to-peak voltage, ω is the frequency in rads/s, and t delineates time. Likewise, $i(t)$ becomes time-dependent:

$$i(t) = I_0 \sin(\omega t + \theta) \tag{2.2}$$

Where I_0 is the peak-to-peak current running through the circuit, and θ is the phase shift. If a system has a purely resistive behavior, $\theta = 0$.

In the time domain, the voltage and current are related to the capacitive and inductive elements via differential equations. For capacitive elements, current is defined as the change in voltage over time taking into account the constant capacitance of the element:

$$i(t) = [dv(t)/dt]C \tag{2.3}$$

where C is capacitance in Farads. Likewise, for inductive elements, voltage is the change in current over time taking into account the constant inductive element:

$$v(t) = [di(t)/dt]L \quad (2.4)$$

where L is inductance in Henrys. For the most simple systems, solving for these differential equations might not be a problem. The Fourier transform provides a means to transform a mathematical system from the time domain to the frequency domain. The resulting frequency domain relations are:

$$I(jw) = CjwV(jw) \quad (2.5)$$

and

$$I(jw) = \frac{V(jw)}{Ljw} \quad (2.6)$$

Finally, using Equations (2.3)-(2.6), One can derive Equations (2.7) and (2.8) from Equations (2.1) and (2.2)

$$V(jw) = V_o\pi \quad (2.7)$$

$$I(jw) = I_o\pi \exp(\theta j) \quad (2.8)$$

Once transformed into the frequency domain, impedance can be solved for in a manner resembling Ohm's law for resistances:

$$I(jw) = \frac{V(jw)}{Z(jw)} \quad (2.9)$$

where $Z(jw)$ is defined as the impedance function. For capacitive and inductive responses $Z(jw)$ is $\frac{1}{C(jw)}$ and $L(jw)$, respectively. When using the Fourier transform, linearity, causality and stationarity of the system have to be assumed. This directly implies that EIS measurements are assumed to be continuous over time and that the outputs are a direct result of the inputs.

At present, there are machines that can automatically make EIS measurements. A typical machine of this sort measures impedance somewhere in the range of 1mHz to

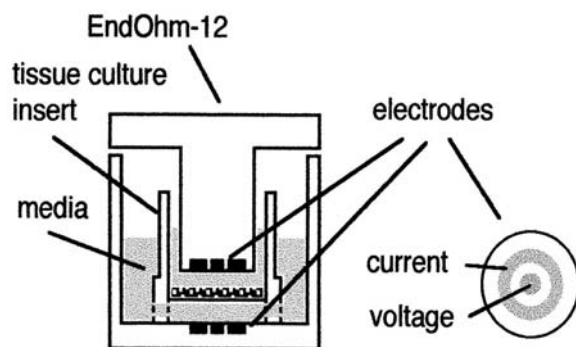


Figure 2.6 Typical probing method of the EndOhm-12. The sample well consists of a cylinder with a 12 mm diameter. This device makes use of the 4-point probe method. Current goes through the outside electrodes (which encircle the point electrodes in the middle), while voltage differential is measured via the point electrodes. This technique has the potential of reducing errors produced by other media inside the sample well in the EIS machine (4).

1MHz, depending on the machine and the material being tested (11). The End-Ohm 12 by World Precision Instruments, is a popular impedance spectroscopy machines (see Figure 2.6) (4, 19). In practice, the most common EIS measurements of biological material are taken in the range of 1kHz to 1MHz (4, 10). Typical input magnitudes vary from equipment to equipment and sometimes are produced with a signal generator. There have been studies which used an amplitude of up to 46 volts without cell damage (28). There is however a convention of

$$V_T = \frac{RT}{F} = \frac{kT}{e}$$

or 25mV at 25°C (R is the gas constant, T is absolute temperature, F are units of electric charge in Faraday, k is the Boltzman constant, and e is the proton charge of the particle being tested). It is theorized that at this voltage, the signal would become linear in nature (11).

EIS can be measured in the time domain or the frequency domain. Time domain measurements are not as common, and will not be covered because they are not used for this research. For the frequency domain, the application of a sine wave as an input is often the best way to produce a transfer function of the system. This practice was first developed to determine the transfer function of a battery cell, and thus the reaction of the

mechanistic and kinetic parameters of the cell. J. R. Macdonald and J. A. Garber (17), were among the first to use the transfer function of EIS for these purposes.

EIS Measurement by Audio Frequency Bridges. Before the invention of digital computers, most EIS measurements were taken from analog signal inputs in either the time or frequency domain. In the past, a reactively substituted Wheatstone bridge was the best way to accomplish such measurements. This method of testing proved to be very useful in the audio range (20-20000Hz) (29). Armstrong et al., wrote some of the theory behind this technique which is well derived and documented, but no longer used mainly due to their frequency limitations. The limitation of this EIS measurement is that it is only valid in the audio frequencies. Nonlinearities cannot be calculated past the 100 kHz frequency. At low frequencies, there is too much noise and the signal to noise ratio is not big enough to provide useful measurements (29).

Many other variations of a bridge were implemented to achieve a higher range of frequencies. These methods included Transformer Ratio Arm Bridges, Berberian-Cole Bridges, the Wien Bridge and the autobalance bridge. The premise behind all these bridges is to match the unknown impedance of the sample through bridge adjustment. Once the impedances are matched, the measurement is derived from the electrical component settings.

The Oscilloscope as an EIS Measuring Technique. EIS oscilloscope measurements work on a simple premise. The magnitude of the impedance can be calculated by Equation (2.10):

$$|Z| = \frac{R |V_{Out}(jw)|}{|V_{in}(jw)|} \quad (2.10)$$

The real and imaginary part of the impedance can be calculated as

$$R = |Z| \cos(\theta)$$

and

$$X = |Z| \sin(\theta)$$

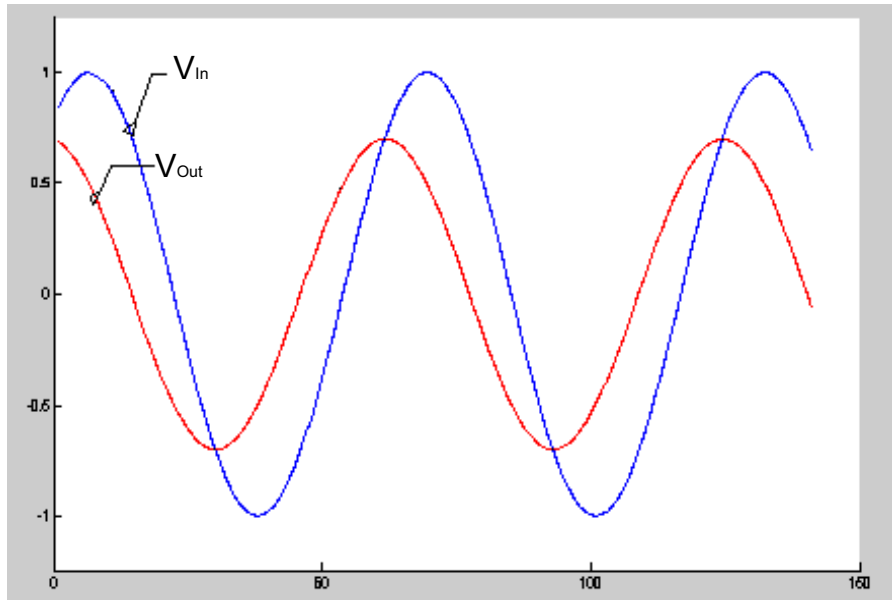


Figure 2.7 Typical oscilloscope readings. Blue denotes sinusoidal input. Red denotes sinusoidal output.

respectively. Figure 2.7, denotes the different input and output waveforms.

2.1.1.4 EIS Input Variations. While there have been many methods of measuring EIS, the inputs to these methods have become standard over the years. There are three main types of inputs. They are described in order of the least used to most used.

Step Voltage. Step Function Transient Measurements (SFTM) is an established EIS measurement method, although seldom used. This measurement takes advantage of a regular step function.

$$\left\{ \begin{array}{l} v(t) = V_o \text{ for } t \geq 0 \\ \text{and} \\ v(t) = 0 \text{ for } t < 0 \end{array} \right\} \quad (2.11)$$

This type of measurement focuses on the initial transient response. The transient response is referred to as the indicial impedance. Disadvantages to this type of measurement are that they need to be Fourier transformed and signal-to-noise ratio varies with different

frequencies. The advantages to this measurement technique are that the method is fairly easy to implement, and the transients vary depending on the magnitude of the input (11).

White Noise. Another type of measurement is the use of a random signal with a voltage offset. This random signal acts as white noise over all frequencies. The automation and digitization of testing is a requirement for this testing method. The output is typically measured as Fourier-transformed current. Advantages to this type of EIS measurement is that it allows for fast data collection. Also, given that white noise is being used, it gives out a better signal-to-noise ratio than the SFTM method. The main disadvantage is that there is no such thing as true random white noise (11).

Sinusoid. This type of EIS measurement is the most common measuring method. Impedance is measured by the input and output quotient, and the phase shift. The input is characterized as a sinusoid voltage signal. This technique for EIS is the one most frequently used. The instrumentation for this type of measurement is readily available. Very good signal-to-noise ratio can be achieved with this type of measurement, and the signals can be manipulated mathematically in both the time domain and the frequency domain (11).

2.1.1.5 The Cole-Cole Model. A major milestone that allowed electrical impedance to be developed in the cellular scenario was the Cole-Cole model (2, 11). This model identified, via electrical components, distributed dielectric properties in biological systems. EIS was implemented in medical and biological studies once the Cole-Cole model was used to estimate biological samples.

Bioimpedance within a frequency range is usually curve-fit to a Cole-Cole model. The advantage of this model is that the model can be fitted to cellular-pertinent values, such as the conductivity of the membrane, and the intra/extra-cellular resistivity. In the Cole equation, the impedance Z is a frequency dependent function:

$$Z(f) = R_{\infty} + \frac{R_o - R_{\infty}}{1 + (i \frac{f}{f_c})^{1-\alpha}} \quad (2.12)$$

Here, f_c is the center frequency (or characteristic frequency) of dispersion, R_o is the low frequency resistance, while R_∞ is the high frequency resistance, α represents the heterogeneity of the system ($0.0 \leq \alpha \leq .5$), 0.0 represents a very homogenous tissue. This model is valid for only one dispersion (see Figure 2.5). There are some Cole-Cole models that take all three dispersions into account, but these models are much harder to estimate given the extent of the extra variables that need to be curve-fit (2).

2.1.2 Other Electrical Impedance Spectroscopy Avenues. While this study is mainly concerned with basic EIS measurements, the actual technology has advanced past basic measurements. While measurements all hold the same basic premise, the evolution has mainly focused on the application of such devices. The application has mainly changed in the size of the interface, or the type of interface used.

2.1.2.1 Phase Mapping. Phase Mapping makes use of EIS to produce an image of the cell being studied. The image is produced by making simultaneous EIS measurements at different parts of the cell. Given that each probe measurement will produce slightly different measurements, an image will be made which is dependent on the lump impedance found at each probe (1, 4, 37). In 2002, Todd E. Kerner et al. used this technique to study the human breast in an effort to produce an alternative to the mammogram (37).

2.1.2.2 Noninvasive Technique. While many members of the scientific community have used probes that interphase with materials being tested, other people have tried different noninvasive ways. The basic premise behind these types of systems is that by introducing a current through a wire, there would be a natural electric field created. If this wire were placed close to someone's skin, then the eddy current from the skin would cancel out some of the electrical field created in this wire, thereby canceling out some of the current going through the wire. This change in current would then be measured to identify changes in the skin layer. In 1998 Richard Petty et al., used this method for a tissue schema (schema is a type of skin irritation) measurement (refer to Figure 2.8). Their tests were conclusive but not completely accurate. In 2001, C. H. Riedel et al., tried to

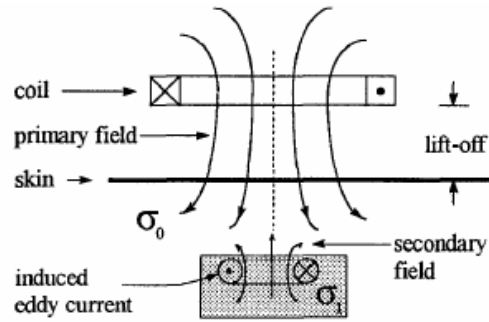


Figure 2.8 Basic diagram delineating a EIS measurement via a non-invasive technique. The a current is passed through a coils which in turn produces an electro-magnetic field. The eddy current of the epidermal layer (the skin), cancels some of this field, thereby reducing the current in the system, the reduced current is measured and analyzed (32).

validate this method to test impedance of the skin and produced more favorable results (16, 32).

In 1988, Ionescu-Tirgoviste et al., studied the responses that the nervous system had by indirectly and noninvasively measuring different electrical responses created by the body to different stimuli (16). The electro dermal response to different stimuli was the focus of the study. In 1995 Mark R. Prausnitz decided to test the impact of different pulsed voltages through a cell. In his study, he found that the skin went through structural changes due to high voltage pulsing (28). He characterized the changes that he saw as dramatic increases in transdermal flux, and the effect enhanced the transport of macro molecules, enlarged transport pathways, and increased skin permeability.

2.1.2.3 Micro Electro Mechanical Systems (MEMS). MEMS started as a natural evolution to Very Large Scale Integration (VLSI). Transistor structures were bulk fabricated by metal deposition and etching. Once it was found that other structures could be "machined" into micro mechanical devices, the world of MEMS evolved (5).

MEMS applications in the biomedical realm are becoming more and more diverse. Some advantages to this technology include its small size, the strength of the material, its electrical characteristics, and the fact that silicon, and other MEMS materials are benign to some cells (18, 38).

Bio MEMS. MEMS fabricated Poly-silicon have many advantages when dealing with cellular objects as stated earlier. However, several disadvantages exist to include:

- Poly-silicon is expensive to use in microfabrication, considering that sometimes hundreds of cell samples have to be processed.
- Poly-silicon MEMS have to be grown and released in a clean room.
- The conductivity of silicon is not ideal for fabricating MEMS probes (38), and
- Traditional MEMS for biological purposes are not always bio compatible.

A bio compatible material is designed to exist and perform specific functions within living organisms. While poly-silicon is benign to most organic systems, some living systems reject invading materials by synthesizing protein to build a permeable membrane which prohibits nutrient intake. Two consequences of synthesizing protein; 1) The living organism may wall itself off from oxygen and nutrients, thereby starving and asphyxiating itself, and 2) may create inaccurate measurements due to protein synthesis around the measurement instrument.

Currently, polymeric materials are being investigated since they are less expensive and have shorter cycle times. In addition, these materials can be fabricated for specific hardness, hydrophobicity, and surface bulk chemistries that can be adjusted for different applications (38). In a study done by the University of Tokyo, PDMS (polydimethylsiloxane) was used to build a template on a glass substrate to grow PDMS micro-structures. As stated in (38), glass substrate is coated with fluorocarbon and covered with a thin sacrificial layer, PDMS and CYTOP are spin coated on the substrate. A layer of photoresist is spun and patterned by exposing to UV-light through a mask. Gold is then deposited and patterned using a lift-off technique. After removal of the CYTOP by oxide ashing, a thin layer of PDMS is deposited on top of the electrode by spin coating. Figure 2.9 illustrates the fabrication process.

Probe Fabrications. In 2000, R. Ivanic et al., introduced a paper about the system characterization of MEMS electrodes (30). The modeling of these electrodes

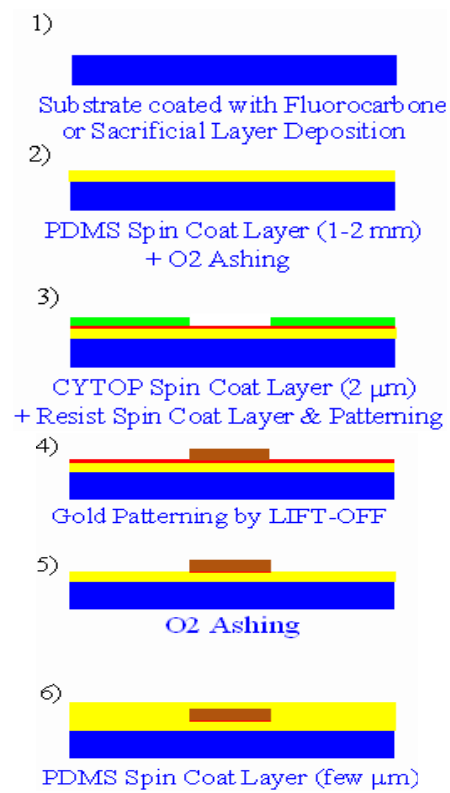


Figure 2.9 Fabrication of impedance probes through alternative polyimide substance (38).

encompassed the relative electromagnetic effect within the cell area. Ivanic made a direct relation between the thickness of skin and the vector electromagnetic field created. These measurements and formulas were simulated using circuit-dependent calculating software and it was determined that, when dealing with MEMS probes, modeling of these structures correctly is critical. This is due to the scale of the probes were approximately the size of the actual cell. Probing of this cell in the micro-scale would have adverse effects on the measurements because the probe may have certain reactances that hide the true response of the cell.

A major drawback of using planar stimulating electrodes is the large current densities produced near the edge of the electrode. Through experimentation, it is been shown that a small recess at the tip of the electrode can minimize the large current densities. Iridium coated electrodes are ideal for impedance measurements in cell research, but these electrodes are subject to current irregularities which could damage the probes and the cells being studied. A method for making sure this does not happen is to remove the excess iridium coating with oxygen plasma (39).

Building a channel is another method for measuring cell impedance. This method takes advantage of the ability to build air tight chambers with MEMS technologies. Some of these systems make use of only two electrodes. This method only works for certain cell sizes, since the chamber cannot be bigger than $10\mu\text{m}$ wide and $4\mu\text{m}$ high. This size is ideal for smaller types of cells, like red blood cells. This idea is primitive as the separating of a cell and putting it into the chamber is difficult (13).

Atomic Force Mover (ATM). Using EIS at a microscopic scale is very hard to accomplish. At the micro-scale one needs to isolate an individual sample for testing. Even if one manages to isolate a cellular sample within the three dimensions (a microscope can only allow for imaging in two dimensions), the correct force needs to be applied to the cell so that the cell can be moved. This is difficult enough to accomplish, yet researchers also have to keep in mind that too much force could kill the cell and that cells come in different sizes (Please refer to Figure 2.10) (40). Examining the figure below, the type of manipulation to use (contact, or non contact), as well as the environment of

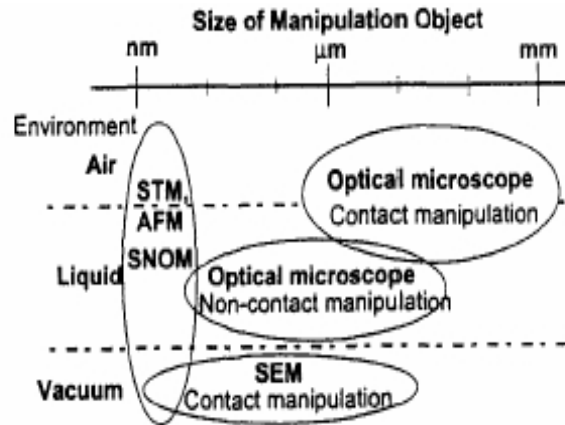


Figure 2.10 This diagram shows different manipulation techniques that need to be used for different sized cells in different environments (40).

separation, depends on the size of the manipulating cell. Most animal cells are the around 20-150 μm (40). This means that the most efficient method of manipulation would take place with contact manipulation using a light microscope while the biological organism is in liquid. Regardless of the above fact, manipulation is still very difficult to accomplish accurately. This is partly due to the fact that the tri-axial manipulators have to have a movement of nanometers while the user interface has to work in the order of centimeters (40). Still, other sources of errors are also due to alignment error, elastic and thermal deformation, slide, and pressure sensor vibration.

The cutting edge technology in the manipulation of living cells is the Tele-Micro robot (12). The two main parts are the cell interface that manipulate the particles and the human interface that is used to operate the system. The cell interface has clamps and three-dimensional movement on two arms. The human counterpart is a scaled replica of the micro-counterpart. The operator can move the macro replica, which will identically move the micro replica. It scales all movements down to a $1\mu\text{m}$ resolution, and scales all forces by the same resolution. This allows for the operator to “feel” the cell and any interactions that happen at a microscopic level, allowing for nanometer accuracy (12). This device is also equipped with a laser spectrometer. This allows for the accurate measurement of cells.

2.1.3 Cell Samples Being Tested. While this section does not directly correlate to EIS, completeness of this research would require a background on the cellular samples

being used. E. B. Wilson, a renowned classic biologist said in 1925: “The key to every biological problem must finally be sought in the cell.” (14) This was a significant insight back in 1925, when the now antiquated light microscope was cutting edge technology. Its technical limitations were not made apparent until the 1940’s, before then the cell was merely viewed as a bag of enzymes, the protoplasm.

2.1.3.1 The HEL-30 Cell. This type of cell is a keratinocyte cell line of a rodent. They are mainly selected because they are epidermal cells, effectively simulating a working model of skin cells. It was specifically chosen for its resistance to different stimuli, such as resistance to temperature fluctuation as well as ultraviolet rays to some extent. These cells have been immortalized. In nature, the vast majority of cells can be cultured and grown, but then they die. With the right nutrients, they can be made to reproduce, but only for a set number of generations. Immortalized cells can reproduce for an unlimited number of generations. HEL-30 cell samples are grown in Ham’s Nutrient Mixture F-12, pH 7.25 with 5% FBS, and 1% antibiotic mixture of penicillin and streptomycin. In order to grow, these cells need to be kept at a constant 37°C. An incubator with an atmosphere consisting of 5% CO₂ is used for this purpose. The cells are used when they are 90-95% confluent, where 100% confluence is defined as a cell growth that covers the entire growth surface (8, 34).

2.1.3.2 The PC-12 Cell. The PC-12 cell is a neuroendocrine cell. These cells resemble nerve cells. This cell line has the capacity to produce dopamine and contain functional dopamine metabolism pathways. The PC-12 cell line is derived from *rattus norvegicus* pheochromocytoma (stock number CRL-1721 from the American Type Tissue Culture (ATTC) organization). These cells are grown in RPMI-1640 media supplemented with 5% fetal bovine serum and 10% horse serum (both heat inactivated), and 1% penicillin–streptomycin in a humidified atmosphere with 5% CO₂ at 37°C cells. The cells are cultured on rat-tail collagen coated flasks, plates, and slides. This cell line is used for testing dopamine depletion. These cells are normally grown to 80% sample confluence before being used (33).

2.1.3.3 The MTT Test. Sometimes, one can look through a microscope and immediately determine whether a cell is alive or dead. Sometimes, this cannot be determined by visual analysis. In such cases, many researchers rely on a test which determines whether or not mitochondria within the cell is functioning to the correct levels. This determination is made by the MTT assay for mitochondrial function (Carmichael, et al. 1987). Mitochondrial function, via the MTT assay is evaluated spectrophotometrically by measuring the degree of mitochondrial reduction of the tetrazolium salt, 3-(4, 5-dimethylthiazol-2-yl)-2, 5-dyphenyltetrazolium bromide to formazan by succinic dehydrogenase (Carmichael et al., 1987). This salt is placed into a cell sample so that it reacts as a catalyst with the mitochondria of the cells. After an incubation (typically 30 minutes), the sample is exposed to a light spectrum, and is evaluated based on the resulting light spectrum. If the cellular sample has any mitochondrial activity, the resulting light spectrum will be reddish in color. If there is no mitochondrial activity, then the cells are dead and will give off a green spectrum (8, 33, 34).

2.2 Overview of Control Systems

James Watt was the first person to make a significant contribution in the field of Control System in the 1800's. His contribution to the field was a centrifugal central governor for the speed control of a steam engine. Nyquist also made a significant contribution by making a simple mapping of closed-loop systems that used a steady state sinusoidal input in 1932. Bode made a similar contribution in the 1940's. He was able to build a plotting technique of a system in the frequency domain. In the 1950's, the root locus method was developed by Evans. All these contribution lead to the study of stable control systems that satisfied a set of performance requirements. In the two decades that followed (1960's to 1980's), optimal control by deterministic and stochastic methods were fully studied, which brings us to modern control theory (24).

2.2.1 Transfer Functions. Mathematical models of dynamic systems are defined as a set of equations that identify system behavior as accurately as possible. Most systems can be portrayed as input/output characteristic relationships of components. These sys-

tems are assumed as linear and time-invariant. They are mostly represented in differential equation form. The driving function, or input, and the response function, or output, are defined by the following variables:

$$a_0y^{(n)} + a_1y^{(n-1)} + \dots + a_{n-1}\dot{y} + a_ny = b_0x^{(m)} + b_1x^{(m-1)} + \dots + b_{m-1}\dot{x} + b_mx, (n \geq m)$$

Where y is the input, and x is the output (a and b are constants). Ogata (24) defines transfer functions as the ratio of the Laplace transformed output to the Laplace transformed input of a linear, time-invariant differential equation. The assumption is that all initial conditions are zero. The transfer function can be defined mathematically as:

$$\begin{aligned} \text{Transfer Function} = G(s) &= \frac{\mathcal{L}[\text{output}]}{\mathcal{L}[\text{input}]} = \frac{Y(s)}{X(s)} \\ &= \frac{b_0x^{(m)} + b_1x^{(m-1)} + \dots + b_{m-1}\dot{x} + b_mx}{a_0y^{(n)} + a_1y^{(n-1)} + \dots + a_{n-1}\dot{y} + a_ny} \end{aligned} \quad (2.13)$$

The transfer function is extensively used in the analysis of many different control systems. It is independent of the input. This allows it to be used to study system response by providing different inputs. If the transfer function of a system is unknown, it can be found by providing an input to the system and studying the output. A transfer function can fully describe the dynamic characteristics of a system. The transfer function is also independent of the physical system description, which means that electrical, mechanical, physical or biological (as in our case) systems can be described by the same transfer function.

2.2.2 Bode Plots. Bode Plots map the response of a transfer function over a range of frequencies. The Bode plot consists of two graphs. The first graph is the plot of the magnitude of the transfer function over a range of frequencies. The second part of a Bode plot consists of a graph of the phase shift between the input signal and the output signal versus frequency. Normally, the frequencies are plotted on a logarithmic scale. It is also common practice to scale the magnitude in decibels (dB), while phase is plotted in

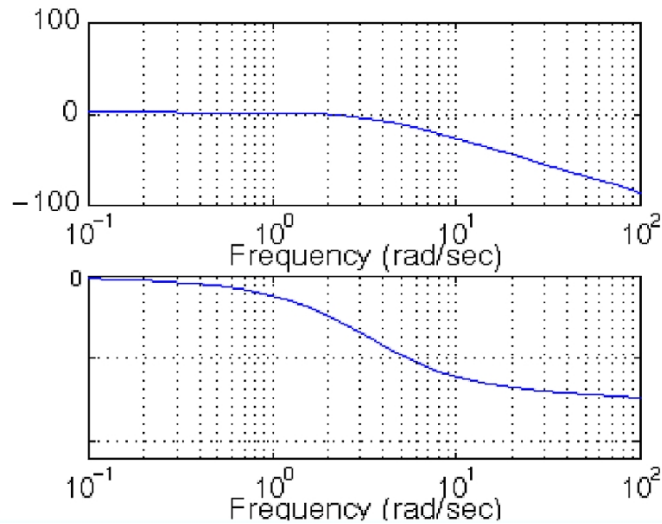


Figure 2.11 The Bode plot of the transfer function depicted in Equation 2.14. It consists of two graphs. The frequency is plotted logarithmically. The magnitude (top plot), is plotted in dB. The bottom plot is in degrees (y scale).

degrees. Please refer the Figure 2.11 for a visualization of a Bode Plot (26).

$$\frac{.5}{s^9 + 9s^2 + 30s + 40} \quad (2.14)$$

A Bode plot provides an easy way of evaluating simple transfer functions, like the one shown in Figure 2.11. When the Bode plots get too complicated for visual estimation, one must find different methods of determining the transfer function from the input and the output. The algorithms used to evaluate a system's transfer function are called System Identification (SID).

2.2.3 System Identification. Finding the transfer function of a system could be a very complex task. One has to decide which variables and quantities are significant and how they interrelate. Simple tests are sometimes made on the system to evaluate the response. The two most common tests used in industry to identify a system are the step response and the impulse response. The practice of describing a system by one of these method is called transient analysis (24).

To find a system with the step response (or transient response), a step function is applied to the system, and the output is observed. For the impulse response, a pulse of short duration is applied to the system. These two techniques are mainly used because, if somewhat limited, they allow for quick insights of the input/output relationships, time delays, and static gains of the system. One limitation is the inability to account for equipment noise. The system may also be intolerant to a wide range of inputs (24).

There are many techniques presently used for the modeling of an unknown system. Frequency analysis is a way to directly estimate the frequency response of a system. Within frequency analysis, one could use a sinusoidal input and record the output. Once the output is recorded, changes in magnitude and phase shift are recorded and used to estimate the transfer function of the system. Frequency analysis is very easy to use, especially with current technology that can generate thousands of measurements in seconds. The requirements needed for frequency analysis is that the system has to be linear and possess a steady-state response. This type of estimation is useful because it can help build a transfer function pertaining to specific frequency ranges (24).

Disadvantages to the frequency analysis method of estimating are that the estimates first come out as a magnitude and phase. While this gives a good Bode plot estimation of the system, it does not directly provide the transfer function. A range of frequencies must be used to get an accurate depiction of the output of the system. This may be sufficient for some applications, but it is detrimental when the change of the input is detrimental to the physical parameters of a real-world system. Also, the relevant frequencies may not be attainable with present interfacing technology (for example, one needs to excite a mechanical system for a response in the gigahertz range).

EIS measurements require an input and an output at different frequencies. Frequency analysis may be used to build a transfer function that models the response of the cellular samples. If a sinusoidal input is used (which is the most common input used), the output could be recorded and used to build the magnitude and phase characteristics of the system, and the subsequent transfer function.

2.3 Overview of Stochastic Estimation and Control

Because no one can predict the total behavior of a cell, it would be advantageous for the estimation of a cellular system to have an added statistical perturbation that would model some of the unknown processes not depicted in the system identified transfer function. Using stochastic modeling of these unknown processes provided a theoretical basis for handling these uncertainties. A common method applicable to linear systems (such as those assumed in this thesis) is the use of a linear Kalman filter.

2.3.1 The Kalman Filter. A Kalman filter is an optimal recursive data processing algorithm. The Kalman filter is optimal in the sense that it uses all available measurements available to improve accuracy. A Kalman filter takes into account, the input, the output, the system error sources, and measurement errors. In short, it makes use of all available data to compute the optimal estimate of the system as shown in Figure 2.12 (22). The algorithm of the Kalman filter is described in Chapter 3.

2.3.2 The Stochastic Smoother. The stochastic smoother is an evolution of the Kalman filter. While it has been shown that the Kalman filter is the optimal estimation tool in real time, there are other evolutions of the filter that could give better estimates once all the measurements have been taken. These algorithms are not practical for most applications of the Kalman filter. The Kalman filter is for the most part implemented to estimate real time measurements for flight control and navigation. The smoother algorithms are therefore better suited for a post processing (22).

The basic premise behind a smoothing filter is to run two Kalman filters in conjunction with each other. The first filter runs forward from time t_0 to t_{final} . The second filter is set to run backwards from t_{final} to t_0 . Finally, once all values have been estimated by both filters, the estimates are combined in the most optimal manner. This achieves a higher measurement accuracy than each Kalman filter by itself. The drawback to this filter is that it is difficult to use in a real time implementation. A typical smoother implementation is portrayed in Figure 2.13 (22).

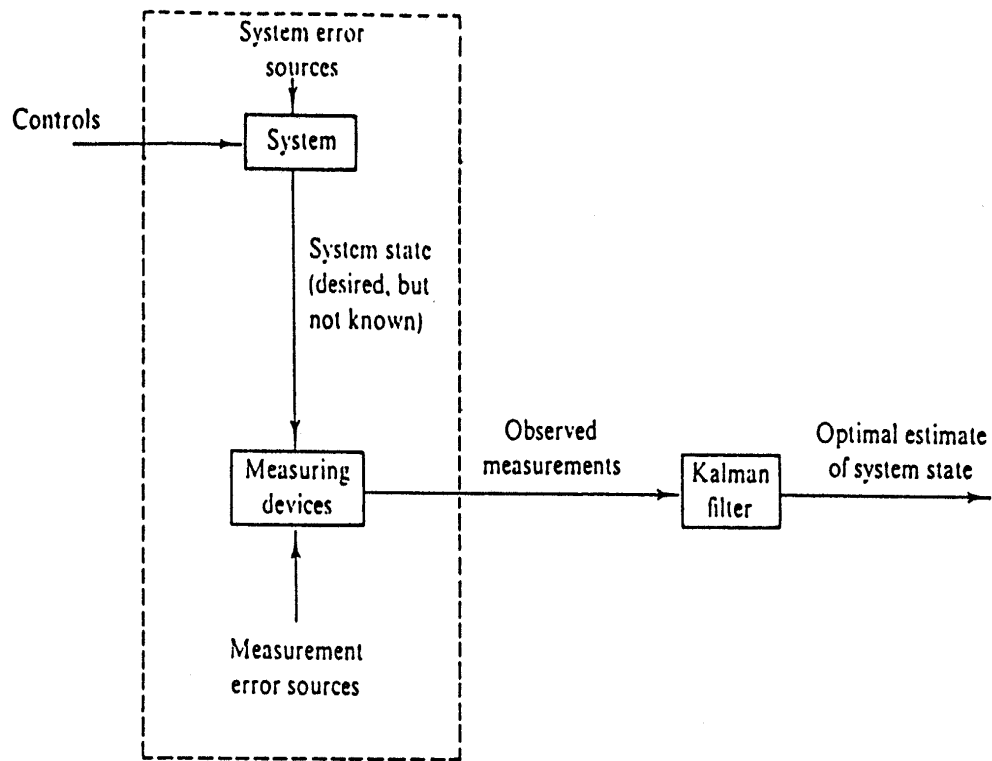


Figure 2.12 This is the typical application of a Kalman filter. It takes all measurements into account, including errors, to come up with the best estimate of the system state. This estimate is then updated by actual system measurements to get a better overall output (22).

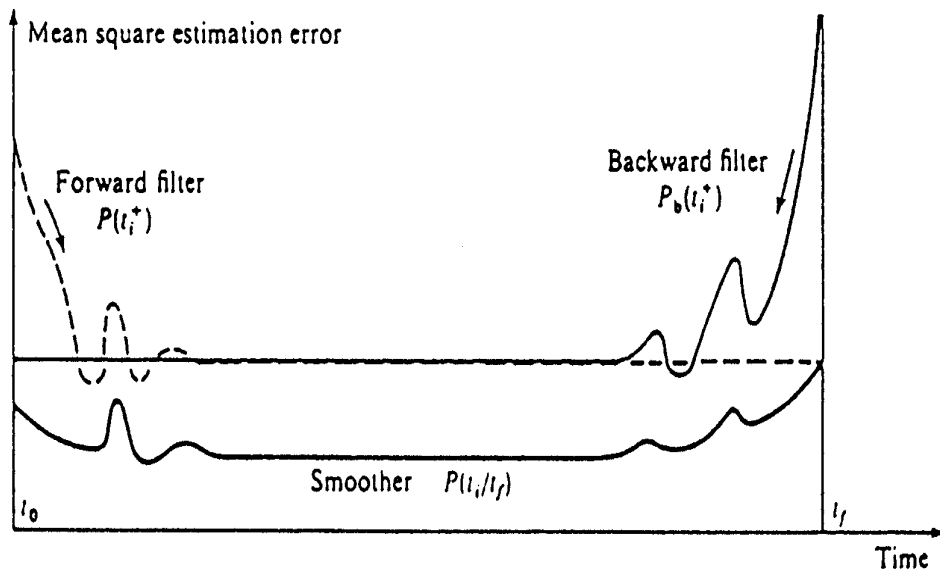


Figure 2.13 Typical smoother representation in conjunction with Kalman filter representation. $P(t_i^+)$ is the covariance of the forward Kalman filter. $P_b(t_i^+)$ is the backward propagation of the same filter. When optimally combined into a smoother, the covariance $P(t_i/t_f)$ is significantly reduced, providing more confidence in the estimate (22).

2.3.3 Residual Monitoring. Residuals are defined by Dr. Peter S. Maybeck as: "The difference between the current measurement value z_i , and the best prediction of its value before the measurement is actually taken" (22). In other words, it is a measure of the accuracy of the estimate the filter produced as compared to the measurement itself. Residual monitoring is a way to validate the adequacy of a system. If the residual measurements of a system in question are constantly low, then there is a good confidence that the filter being used adequately estimates the correct response of the system. Equations and theory on residual monitoring will be presented in the next chapter following a mathematical discussion of the Kalman filter and the stochastic smoother.

2.4 Synthesis

The theories above will all be combined into a method of cell identification. Initially EIS measurements will be taken of HEL 30 cell samples. A sinusoidal input will be applied and the output will be recorded. The assumption will be made that the system is linear, time-invariant and adequately represents the steady-state response. A mathematical model based on the input/output magnitude and phase shift will be produced via frequency analysis. This mathematical model will be used to build a smoother. The smoother will estimate measurements based on other cell samples. Based on residual monitoring, the process may or may not adequately identify a specific cell type from the samples taken of both cells. If the process is successful, future experiments will test the adequacy of the research

III. Theory

Since Electrical Impedance Spectroscopy (EIS) and Stochastic Estimation and Control (SEC) have never been integrated before, a brief introduction of the experimental procedure will be presented regarding the synthesis of the two subjects.

This experiment begins by acquiring cell sample data (refer to the red section in Figure 3.1) via EIS. Cell samples from two different cell-types will be obtained for the following purposes:

- To develop an input that provides the most readable, definable outputs of the cell samples.
- To develop a model that accurately estimates the electrical behavior of a cell-type over a frequency range.
- As independent data to be used in the validation of the cell behavior model.

The model that estimates the electrical response of a cell-type will be built via System Identification (SID) theory (refer to the yellow section in Figure 3.1). The model will be built on the input-output relationship of the samples. The model will be built in the form of a transfer function. This transfer function will then be changed into a state-space model representation with the same behavioral characteristics.

The stochastic smoother will be created from the characteristic matrices of the state-space model (refer to the yellow section of Figure 3.1). The remainder of the cell sample data will then be sent through the smoother to generate estimates of the system states. The data from two different cell-types will be sent through the smoother. The first cell sample data tested will be from the same cell-type used to design the smoother. The second cell sample data tested will be from a different cell-type. The results of this process will be analyzed through residual monitoring (the process of analyzing the difference between the smoother estimated output and the measured data output of the samples).

It is the postulation of this research that the residuals associated with the same cell-type data will be distinguishable from the residuals for the different cell-type data.

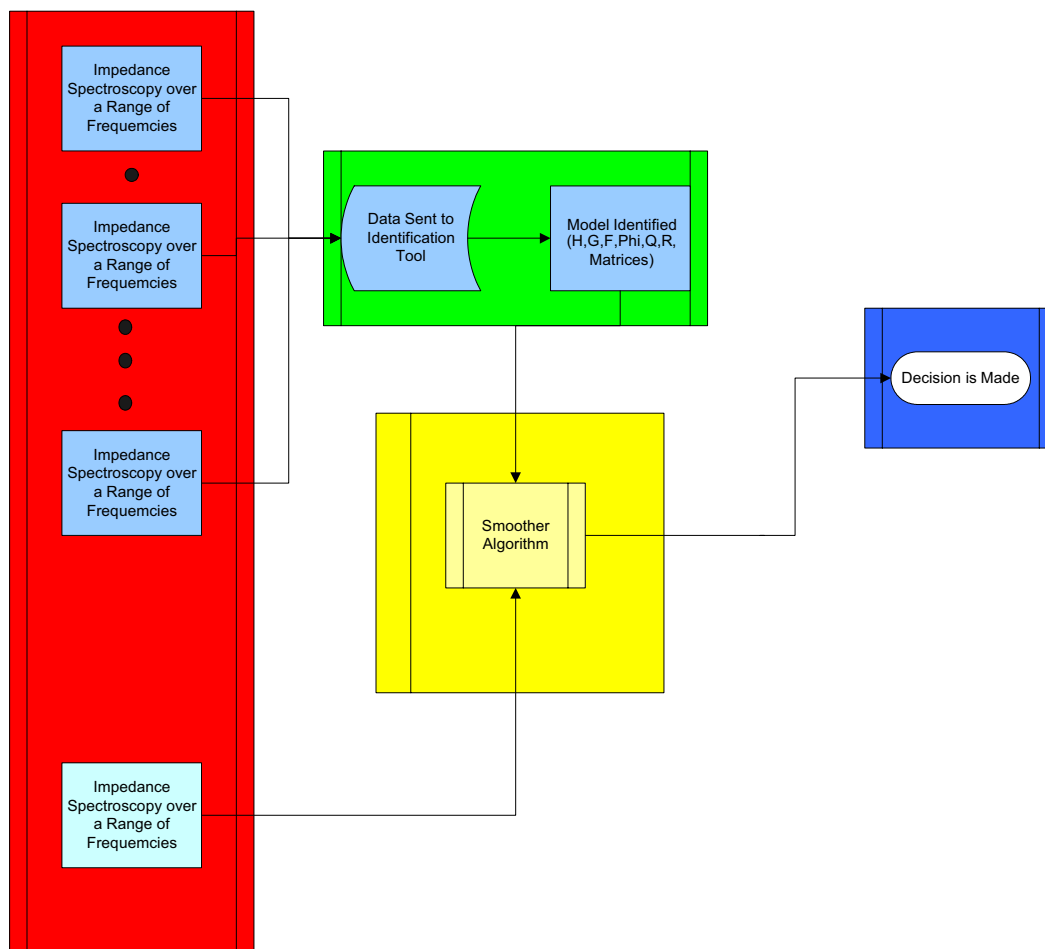


Figure 3.1 Diagram denoting the theoretical experimental process used in this thesis. The red section denotes the acquisition of measurements of live cell samples via EIS. The green section denotes the System Identification (SID) process to produce a model. The yellow section shows the creation of the stochastic smoother based on the identified system characteristics and the subsequent use of the filter with an unrelated cell sample. The yellow section also points to the residual monitoring of the stochastic smoother. Finally, the blue section shows a decision being made based on the aforementioned process.

If so, decision logic will be employed to identify each cell sample through its electrical characteristics (refer to the blue section of Figure 3.1).

3.1 Collection of Sampled Data

The main focus of this part of the experimental process is to obtain values that will be used in the estimation of a transfer function from the input and output data. As explained in Chapter 2.1.1.3, electrical impedance spectroscopy gives the basic theory that accounts for the change in magnitude and phase of the input and the output in a cell sample. The process of dispersion also accounts for different input/output relationships at different frequencies (11).

Based on the input and output data and assuming the system is linear and time-invariant, a transfer function can be created. By using Fourier transformations (as it was shown in Chapter 2.2.1), one can write the transfer function relationship of Equation (3.1), (20).

$$Y(s) = G(s)U(s) \quad (3.1)$$

Where $Y(s)$ is the Fourier transformed input function, $U(s)$ is the Fourier transformed output function and $G(s)$ is the transfer function that describes the linear system. In the frequency domain, complex functions can be analyzed with simple algebra, so Equation (3.1) becomes (11):

$$G(s) = \frac{Y(s)}{U(s)}$$

which describes the transfer function $G(s)$ based on an input and output relationship. Using this relationship is simple if the input and output functions are known. Most of the time, however, only sampled values are obtained from the data. If the only available data is composed of sampled values, the following approximation can be used (20):

$$Y(s) = t \sum_{k=1}^N y(kt) e^{-jwkt} \quad (3.2)$$

and

$$U(s) = t \sum_{k=1}^N u(kt) e^{-jwkt} \quad (3.3)$$

Where $y(kt)$ and $u(kt)$ are sampled values, $k = 1, 2, \dots, N$, and t is the sampling interval (20). Although this method will approximate a transfer function, it has many inherent disadvantages. This form of analysis gives arbitrary accuracy only if pure sinusoids are used as the input of the system. If the input is not a pure sinusoid (as inputs rarely are) then the estimate has an error equal to the noise to signal ratio $\frac{V(s)}{U(s)}$, where $V(s)$ is the Fourier transform of the disturbance over the interval of the samples (20, 21). $V(s)$ is more fully derived in Section 3.2.2 Equations (3.18) and (3.20).

3.2 System Identification (SID)

Based on the discussion in the previous section, a better model identification algorithm needs to be used in order to properly build a model of the cell sample that will accurately estimate the cell sample's electrical properties. Based on the fact that there is very little known about the cell system, there is no a priori knowledge of the system behavior. In cases such as these, a Linear, Ready-made Model (LRM) may be used to characterize the system (20).

3.2.1 The Linear, Ready-made Model (LRM). LRM's, or black-box models are models that have been found to work with multiple applications. These models are only used as vehicles to describe the input and output relationships since they have no direct physical relation to interpret the actual system being modeled (21).

LRM's are used when there is no physical insight into the actual system being modeled. The lack of insight into the properties of a system could be due to reactions of the system that are too complex, or the construction of the system is unknown. In such cases, models that have a wide range of applications are used. Most of these models are linear in nature (20, 21).

In LRMs, the general form is a discrete-time model as in Equation (3.4) (20):

$$y(t) = \eta(t) + w(t) \quad (3.4)$$

where $y(t)$ is a sampled measurement, $w(t)$ is defined as the noise in the system, and $\eta(t)$ is the noise-free measurement. This equation is used as most unknown systems are modeled based on their input and output, which are for the most part sampled. We can represent $\eta(t)$ as:

$$\eta(t) = G(s, \theta)u(t) \quad (3.5)$$

where $G(s, \theta)$ is a Fourier transformed rational function in terms of s , which denotes the frequency domain and θ represents the unknown parameters of the system. Likewise, $w(t)$ can be written as:

$$w(t) = H(s, \theta)e(t) \quad (3.6)$$

where $e(t)$ is white noise, and $H(s, \theta)$ is a Fourier transformed rational function in terms of s and θ .

Now, $G(s, \theta)$ and $H(s, \theta)$ can be defined as:

$$G(s, \theta) = \frac{B(s)}{A(s)} = \frac{b_1s^{-nk} + b_2s^{-nk-1} + \dots + b_{nb}s^{-nk-nb+1}}{1 + a_1s^{-1} + \dots + a_{na}s^{-na}} \quad (3.7)$$

$$H(s, \theta) = \frac{C(s)}{A(s)} = \frac{1}{1 + a_1s^{-1} + \dots + a_{na}s^{-na}} \quad (3.8)$$

and the sampled measurement output $y(t)$ can now be summarized as:

$$y(t) = G(s, \theta)u(t) + H(s, \theta)e(t) \quad (3.9)$$

Thus $y(t)$ can now be described by a set of two transfer functions with structural parameters na , nb , and nk denoting the orders of the various polynomials which make up these transfer functions. These parameters denote the number of poles and the zeros of the transfer functions. When the number of poles and zeros have been chosen, the equations can be curve-fitted to the θ vector coefficient parameters a_i and b_i .

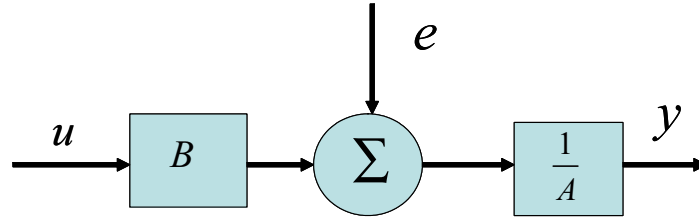


Figure 3.2 Block diagram representing the ARX model. A represents the Auto Regression portion of the model, B denotes an extra input, and e denotes noise entering the system.

Finally, using Equation (3.9) and multiplying the function $y(t)$ by $A(s)$ gives Equation (3.10):

$$A(s)y(t) = B(s)u(t) + e(t) \quad (3.10)$$

This ready-made model is called the Auto Regression eXtra input (ARX) model. The $A(s)y(t)$ denotes the auto-regression of the system model. The $B(s)u(t)$ denotes the extra input. A block diagram of the ARX model is pictured in Figure 3.2 (20).

3.2.2 Parameter Prediction. It is possible to predict the output $y(t)$ based on measurements of $u(T)$ and $y(T)$, where $T \leq t - 1$ (20). The prediction for the ARX case uses old values of the output (details to follow), and the prediction can be calculated by dividing the model in Equation (3.9) with the transfer function $H(s, \theta)$:

$$H^{-1}(s, \theta)y(t) = H^{-1}(s, \theta)G(s, \theta)u(t) + H^{-1}(s, \theta)e(t) \quad (3.11)$$

or

$$y(t) = [1 - H^{-1}(s, \theta)]y(t) + H^{-1}(s, \theta)G(s, \theta)u(t) + H^{-1}(s, \theta)e(t) \quad (3.12)$$

Further mathematical analysis of $[1 - H^{-1}(s, \theta)]$ results in the following:

$$[1 - H^{-1}(s, \theta)] = 1 - \frac{A(s)}{C(s)} = \frac{C(s) - A(s)}{C(s)} = \frac{1 - A(s)}{1} \quad (3.13)$$

$$= -a_1s^{-1} - \dots - a_nas^{-na} \quad (3.14)$$

Combining Equations (3.13) and (3.14) reveals that $[1 - H^{-1}(s, \theta)]y(t)$ is made up entirely of previous values of $y(t)$. The entire right side of Equation (3.12) is known except for component $e(t)$, which has already been established as unpredictable (20). So the prediction of values for the ARX model can be obtained from Equation (3.11) by deleting $e(t)$:

$$\hat{y}(t | \theta) = [1 - H^{-1}(s, \theta)]y(t) + H^{-1}(s, \theta)G(s, \theta)u(t) \quad (3.15)$$

Where $\hat{y}(t | \theta)$ denotes the predicted value of $y(t)$ at $T = t-1$. Furthermore, $H^{-1}(s, \theta)G(s, \theta)$ reduces to:

$$H^{-1}(s, \theta)G(s, \theta) = b_1s^{-nk} + b_2s^{-nk-1} + \dots + b_nbs^{-nk-nb+1} \quad (3.16)$$

Expansion of Equation (3.15) using (3.16) gives the following prediction equation:

$$\begin{aligned} \hat{y}(t | \theta) = & -a_1y(t-1) - \dots - a_nay(t-na) \\ & + b_1u(t-nk) + \dots + b_nbu(t-nk-nb+1) \end{aligned} \quad (3.17)$$

Using the following expression for the prediction error (20):

$$\varepsilon(t, \theta) = y(t) - \hat{y}(t | \theta) \quad (3.18)$$

one can determine the parameter vector θ such that this error is minimized. One method is to minimize the variance of the prediction error using:

$$\hat{\theta}_N = \arg \min_{\theta} V_N(\theta) \quad (3.19)$$

where

$$V_N(\theta) = \frac{1}{N} \sum_{t=1}^N \varepsilon^2(t, \theta) \quad (3.20)$$

A transfer function of a proper form is obtained from the estimated parameter θ resulting in:

$$G(s) = \frac{b_0 s^m + b_1 s^{m-1} + \dots + b_{m-1} s + b_m}{a_0 s^n + a_1 s^{n-1} + \dots + a_{n-1} s + a_n}$$

Once a transfer function is obtained, it is important to change it to a state-space model so it can be implemented in a stochastic smoother.

The transfer function $G(s)$ can now be represented via linear system theory as (25):

$$\dot{\mathbf{x}}(t) = \mathbf{F}(t)\mathbf{x}(t) + \mathbf{B}(t)\mathbf{u}(t) \quad (3.21)$$

$$y = \mathbf{H}(t_i)\mathbf{x}(t_i) \quad (3.22)$$

While Equation (3.21) is the depiction of the perfect model, practicality denotes the fact that neither the measurements or the model will be perfect. This may be due to inaccuracy of sensors, noise within the signals, or the simplicity of the model (11, 20). Within the model itself are often characterized as stochastic noise, $\Gamma(t)\mathbf{w}(t)$ to get:

$$\dot{\mathbf{x}}(t) = \mathbf{F}(t)\mathbf{x}(t) + \mathbf{B}(t)\mathbf{u}(t) + \Gamma(t)\mathbf{w}(t) \quad (3.23)$$

Expanding on this concept, the measurement will also have added noise $\mathbf{v}(t)$ to get:

$$\mathbf{z}(t_i) = \mathbf{H}(t_i)\mathbf{x}(t_i) + \mathbf{v}(t_i) \quad (3.24)$$

where t_i denotes discrete time measurements ($i = 1, 2, \dots, n$)

3.3 Stochastic Estimation and Control (SEC)

The theory behind Stochastic Estimation and Control revolves around optimal estimation of a system modeled with stochastic processes. The stochastic filter uses the tools of probability to more accurately predict the incoming measurement. While many stochastic filters have been developed, this research is only concerned with two: the Kalman filter (KF) and the Fixed Interval Smoother (FIS).

3.3.1 *The Kalman Filter (KF).* The linear Kalman filter is an optimal recursive data processing algorithm (22). This tool is used when deterministic analysis is not sufficient to estimate the state variables. It assumes a linear dynamics model driven by white Gaussian noise of known statistics (22). The KF uses a Bayesian approach to incorporate noise corrupted measurements. It makes use of all available measurements, regardless of their accuracy, to come up with the best estimate of the system state. The KF makes use of a time propagation cycle and a measurement cycle when discrete-time measurements are available. A complete derivation of the Kalman filter is given in (22).

3.3.1.1 *State and Measurement Model Equations.* The system dynamics of a KF assume linearity. The model is depicted in state-space form as (22):

$$\dot{\mathbf{x}}(t) = \mathbf{F}(t)\mathbf{x}(t) + \mathbf{B}(t)\mathbf{u}(t) + \mathbf{\Gamma}(t)\mathbf{w}(t) \quad (3.25)$$

where:

$\mathbf{x}(t)$ = the system state vector

$\mathbf{F}(t)$ = the state dynamics matrix

$\mathbf{B}(t)$ = the control input matrix

$\mathbf{u}(t)$ = the control input

$\mathbf{\Gamma}(t)$ = the noise input matrix

$\mathbf{w}(t)$ = the dynamics driving noise vector

For the purposes of this research there are no control inputs, so the \mathbf{B} and \mathbf{u} terms will be dropped from any subsequent equations. The discrete-time representation of the Equation (3.25) is given by:

$$\mathbf{x}(t_{i+1}) = \mathbf{\Phi}(t_{i+1}; t_i)\mathbf{x}(t_i) + \left[\int_{t_i}^{t_{i+1}} \mathbf{\Phi}(t_{i+1}; \tau)\mathbf{\Gamma}(\tau)d\beta(\tau) \right] \quad (3.26)$$

Where β is a vector valued Brownian motion process of diffusion $\mathbf{Q}(t)$ and $\mathbf{\Phi}(t_{i+1}; t_i)$ is the state transition matrix from t_i to t_{i+1} and, assuming a time invariant \mathbf{F} matrix, is given by:

$$\Phi(t_{i+1}; t_i) = \Phi(\Delta t) = e^{F\Delta t} \text{ where } \Delta t \equiv t_{i+1} - t_i \quad (3.27)$$

Equivalently, the discrete time model can be described as

$$\mathbf{x}(t_{i+1}) = \Phi(t_{i+1}; t_i)\mathbf{x}(t_i) + \mathbf{B}(t_i)\mathbf{u}(t_i) + \Gamma_d(t_i)\mathbf{w}_d(t_i) \quad (3.28)$$

where

$$\mathbf{w}_d(t_i) = \int_{t_i}^{t_{i+1}} \Phi(t_{i+1}; \tau)\Gamma(\tau)\beta(\tau) \quad (3.29)$$

This is defined as the discrete-time white Gaussian dynamics driving noise, with statistics (22):

$$E \{ \mathbf{w}_d(t_i) \} = 0 \quad (3.30)$$

$$E \{ \mathbf{w}_d(t_i)\mathbf{w}_d^T(t_i) \} = \mathbf{Q}_d(t_i) \quad (3.31)$$

$$= \int_{t_i}^{t_{i+1}} \Phi(t_{i+1}; \tau)\Gamma(\tau)\mathbf{Q}(\tau)\Gamma^T(\tau)\Phi^T(t_{i+1}; \tau)d\tau \quad (3.32)$$

$$E \{ \mathbf{w}_d(t_i)\mathbf{w}_d^T(t_j) \} = 0, t_i \neq t_j \quad (3.33)$$

The measurement output depicted as:

$$\mathbf{z}(t_i) = \mathbf{H}(t_i)\mathbf{x}(t_i) + \mathbf{v}(t_i) \quad (3.34)$$

Where $\mathbf{z}(t_i)$ is defined as the measurement taken. $\mathbf{H}(t_i)\mathbf{x}(t_i)$ is defined as the true noise-free measurement and $\mathbf{v}(t_i)$ is the noise added given imperfect measurements. The statistics of the measurement corruption noise are described by (22):

$$E \{ \mathbf{v}(t_i) \} = 0 \quad (3.35)$$

$$E \{ \mathbf{v}(t_i)\mathbf{v}^T(t_j) \} = \left\{ \begin{array}{l} \mathbf{R}(t_i) \text{ for } t_i = t_j \\ 0 \text{ for } t_i \neq t_j \end{array} \right\}, \quad (3.36)$$

Also,

$$E \{ \mathbf{w}_d(t_i)\mathbf{v}^T(t_j) \} = 0 \text{ for all } t_i \text{ and } t_j \quad (3.37)$$

which means that the driving noise $\mathbf{w}_d(t_i)$ and the measurement corruption noise $\mathbf{v}(t_j)$ are assumed independent of each other.

3.3.1.2 Kalman Filter Equations. Kalman filters are typically propagated forward in time from t_{i-1}^- to t_i^- where the superscript "-" indicates state values prior to measurement incorporation. Whereas t_i^+ denotes the time after a measurement update as indicated by the "+" superscript. Initial conditions used in the first propagation are described by $\hat{\mathbf{x}}(t_0)$ and $\mathbf{P}(t_0)$, where $\mathbf{P}(t_0)$ is the initial covariance and $\hat{\mathbf{x}}(t_0)$ is the initial state estimate. Also, the " $\hat{}$ " notation on the state vector represents an estimate of $\mathbf{x}(t)$ (22). The propagation cycle is described by the following equations:

$$\hat{\mathbf{x}}(t_i^-) = \Phi(t_i, t_{i-1})\hat{\mathbf{x}}(t_{i-1}^+) \quad (3.38)$$

$$\mathbf{P}(t_i^-) = \Phi(t_i, t_{i-1})\mathbf{P}(t_{i-1}^+)\Phi^T(t_i, t_{i-1}) + \Gamma_d(t_{i-1})\mathbf{Q}_d(t_{i-1})\Gamma_d^T(t_{i-1}) \quad (3.39)$$

Once the filter has been propagated, measurements updates are calculated by:

$$\mathbf{A}(t_i) = \mathbf{H}(t_i)\mathbf{P}(t_i^-)\mathbf{H}^T(t_i) + \mathbf{R}(t_i) \quad (3.40)$$

$$\mathbf{K}(t_i) = \mathbf{P}(t_i^-)\mathbf{H}^T(t_i)\mathbf{A}(t_i)^{-1} \quad (3.41)$$

$$\mathbf{r}(t_i) = \mathbf{z}_i - \mathbf{H}(t_i)\hat{\mathbf{x}}(t_i^-) \quad (3.42)$$

$$\hat{\mathbf{x}}(t_i^+) = \hat{\mathbf{x}}(t_i^-) + \mathbf{K}(t_i)\mathbf{r}(t_i) \quad (3.43)$$

$$\mathbf{P}(t_i^+) = \mathbf{P}(t_i^-) - \mathbf{K}(t_i)\mathbf{H}(t_i)\mathbf{P}(t_i^-) \quad (3.44)$$

Note that $\mathbf{z}_i = \mathbf{z}(t_i)$ for convenience.

Ideally, if the filter is properly designed (the noise statistics and the model are commensurate to the real world), it would have a zero-mean residual vector, $\mathbf{r}(t_i)$, with an associated filter-computed covariance $\mathbf{A}(t_i)$. Once the filter has been propagated and updated, the new values for $\hat{\mathbf{x}}(t_i^+)$ and $\mathbf{P}(t_i^+)$ are used for the next propagation cycle.

3.3.1.3 Optimal Smoother. The traditional Kalman filter is optimal when working in real time. Propagations and updates only go forward in time, but take into account all previous measurements. Optimal stochastic smoothers are an evolution to the

KF. These stochastic smoothers make use of future data to improve the state and covariance estimate. While there are three classes of smoothers (the Fixed-interval Smoother (FIS), Fixed-point Smoothers (FPS), and Fixed-lag Smoothers (FLS)), this research will use the fixed-interval smoother because it has been shown to give the best estimates provided that all the data has been acquired prior to the estimation (22).

Conceptually, a fixed-interval smoother can be defined as a combination of two stochastic filters. A traditional forward-running Kalman filter, and a backward-running Kalman filter that is typically implemented using an inverse covariance formulation (22). Estimates are calculated by optimally combining the forward and backward portions of the filter estimates and covariance matrices. The forward filter approximates state estimate $\hat{\mathbf{x}}(t_k^-)$ and error covariance $\mathbf{P}(t_k^-)$ before \mathbf{z}_k (the new measurement where $k = 1, 2, \dots, i$) is taken. When \mathbf{z}_k is incorporated, the forward smoother estimates $\hat{\mathbf{x}}(t_k^+)$ and $\mathbf{P}(t_k^+)$. In the case of the backward filter $\hat{\mathbf{x}}_b(t_k^-)$ and $\mathbf{P}_b(t_k^-)$ denotes the state and covariance before the measurement \mathbf{z}_k is incorporated, and $\hat{\mathbf{x}}_b(t_k^+)$ and $\mathbf{P}_b(t_k^+)$ after the measurement \mathbf{z}_k has been incorporated.

The Forward Filter. The forward filter of a stochastic smoother is basically a KF given the following initial conditions:

$$\hat{\mathbf{x}}(t_0) = \hat{\mathbf{x}}_0 \quad (3.45)$$

$$\mathbf{P}(t_0) = \mathbf{P}_0 \quad (3.46)$$

The system is propagated using:

$$\hat{\mathbf{x}}(t_{k+1}^-) = \Phi(t_{k+1}, t_k) \hat{\mathbf{x}}(t_k^+) \quad (3.47)$$

$$\mathbf{P}(t_{k+1}^-) = \Phi(t_{k+1}, t_k) \mathbf{P}(t_k^+) \Phi^T(t_{k+1}, t_k) + \mathbf{\Gamma}_d(t_k) \mathbf{Q}_d(t_k) \mathbf{\Gamma}_d^T(t_k) \quad (3.48)$$

Once the system has been propagated, it is updated by the following equations:

$$\mathbf{K}(t_k) = \mathbf{P}(t_k^-) \mathbf{H}^T(t_k) [\mathbf{H}(t_k) \mathbf{P}(t_k^-) \mathbf{H}^T(t_k) + \mathbf{R}(t_k)]^{-1} \quad (3.49)$$

$$\hat{\mathbf{x}}(t_k^+) = \hat{\mathbf{x}}(t_k^-) + \mathbf{K}(t_k) [\mathbf{z}_k - \mathbf{H}(t_k) \hat{\mathbf{x}}(t_k^-)] \quad (3.50)$$

$$\mathbf{P}(t_k^+) = \mathbf{P}(t_k^-) - \mathbf{K}(t_k)\mathbf{H}(t_{ki})\mathbf{P}(t_k^-) \quad (3.51)$$

The update and propagation equations are used iteratively for $k = 1, 2, \dots, i$. This produces a set of estimated state variables $\hat{\mathbf{x}}(t_i^+)$ at every sample period.

The Backward Filter. The backward filter is initialized in much the same way as the forward filter, but with one slight exception:

$$\hat{\mathbf{y}}_b(t_f^-) = \mathbf{0} \quad (3.52)$$

$$\mathbf{P}_b^{-1}(t_f^-) = \mathbf{0} \quad (3.53)$$

Where $\hat{\mathbf{y}}_b(t_f^-)$ is the final measurement estimate before the incorporation of \mathbf{z}_f and $\mathbf{P}_b^{-1}(t_f^-)$ is the final covariance. Measurement updates are instanced by:

$$\hat{\mathbf{y}}_b(t_k^+) = \hat{\mathbf{y}}_b(t_k^-) + \mathbf{H}^T(t_k)\mathbf{R}^{-1}(t_k)\mathbf{z}_k \quad (3.54)$$

$$\mathbf{P}_b^{-1}(t_k^+) = \mathbf{P}_b^{-1}(t_k^-) + \mathbf{H}^T(t_k)\mathbf{R}^{-1}(t_k)\mathbf{H}(t_k) \quad (3.55)$$

and the backward propagations are estimated by:

$$\mathbf{J}(t_k) = \mathbf{P}_b^{-1}(t_k^+)\mathbf{\Gamma}_d(t_{k-1}) [\mathbf{\Gamma}_d^T(t_{k-1})\mathbf{P}_b^{-1}(t_k^+)\mathbf{\Gamma}_d(t_{k-1}) + \mathbf{Q}_d^{-1}(t_{k-1})]^{-1} \quad (3.56)$$

$$\mathbf{L}(t_k) = \mathbf{I} - \mathbf{J}(t_k)\mathbf{\Gamma}_d^T(t_{k-1}) \quad (3.57)$$

$$\hat{\mathbf{y}}_b(t_{k-1}^-) = \mathbf{\Phi}^T(t_k, t_{k-1})\mathbf{L}(t_k) [\hat{\mathbf{y}}_b(t_k^+)] \quad (3.58)$$

$$\mathbf{P}_b^{-1}(t_{k-1}^-) = \mathbf{\Phi}^T(t_k, t_{k-1}) * \quad (3.59)$$

$$\{\mathbf{L}(t_k)\mathbf{P}_b^{-1}(t_k^+)\mathbf{L}^T(t_k) + \mathbf{J}(t_k)\mathbf{Q}_d^{-1}(t_{k-1})\mathbf{J}^T(t_k)\} \mathbf{\Phi}(t_k, t_{k-1})$$

A brief inspection of the indices in this equation does indeed show a backward propagation from $k = f, (f - 1), \dots, (i + 1)$ to finally generate $\hat{\mathbf{y}}_b(t_i^-)$.

The Smoothed Estimate. Once the forward filter has propagated and estimated $\hat{\mathbf{x}}(t_i^+)$ and $\mathbf{P}(t_i^+)$ and the backward filter has estimated $\hat{\mathbf{y}}_b(t_i^-)$ and $\mathbf{P}_b^{-1}(t_i^-)$, the

smoothed estimate is calculated by:

$$\mathbf{X}(t_i) = [\mathbf{I} + \mathbf{P}(t_i^+) \mathbf{P}_b^{-1}(t_i^-)]^{-1} \quad (3.60)$$

$$\mathbf{W}(t_i) = \mathbf{P}(t_i^+) \mathbf{X}^T(t_i) \quad (3.61)$$

$$\mathbf{Y}(t_i) = \mathbf{I} - \mathbf{W}(t_i) \mathbf{P}_b^{-1}(t_i^-) \quad (3.62)$$

$$\mathbf{P}(t_i/t_f) = \mathbf{Y}(t_i) \mathbf{P}(t_i^+) \mathbf{Y}^T(t_i) + \mathbf{W}(t_i) \mathbf{P}_b^{-1}(t_i^-) \mathbf{W}^T(t_i) \quad (3.63)$$

$$\hat{\mathbf{x}}(t_i/t_f) = \mathbf{X}(t_i) \hat{\mathbf{x}}(t_i^+) + \mathbf{P}(t_i/t_f) \hat{\mathbf{y}}_b(t_i^-) \quad (3.64)$$

where the notation (t_i/t_f) indicates values generated over the fixed interval of t_i to t_f . While there are methods of optimizing this code into algorithms that would require less computational cost, these are seldom used in a smoother. A fixed interval smoother is mostly used for post processing applications, so processing time and memory optimization is not required in most cases.

3.3.2 Residual Monitoring. A residual is defined as the difference between the measurement value estimated by a filter and the actual measurement provided to the filter. The residual value, $\mathbf{r}(t_i)$, is calculated from the measurements and the estimates of these measurements before they are incorporated into the state estimates:

$$\mathbf{r}(t_i) = \mathbf{z}(t_i) - \mathbf{H}(t_i) \hat{\mathbf{x}}(t_i^-) \quad (3.65)$$

The residual shows the error in the estimate based on the measurements. Because of this, residuals are useful tools in checking the reasonableness of the system. Large residuals mean that there is a big difference between the estimate and the measurement it is compared to. Small residuals mean that there is little or no difference between the estimates and measurements. Naturally, large residuals also mean that there is a model mismatch, since the model cannot produce good estimates. Small residuals mean that the model is adequate for the estimation of measurements.

3.4 Summary

The entire purpose of this research is to conceptualize a new experimental method useful in identification of cell samples. Measurement of a sinusoidal output, given a sinusoidal input, are taken and recorded. The measurements are used to build a state space model that accurately depicts the cell's electrical characteristics. The state space matrices are used to develop a stochastic smoother. The smoother is used to estimate the electrical behavior of different cells samples. Residual monitoring will be used to assess modeling errors. Based on residual values this research is hoping to distinguish between different cell-types.

IV. Results

This chapter presents the results acquired through the development of the theory in Chapter 3. The first couple of sections describe the practicalities of cell sample testing and the measurement process. The subsequent section deals with the analysis used in developing the state-space model that describes the electrical characteristics of a cell sample. The next section discusses the development of the stochastic smoother. Finally, a section describing residual analysis and windowing results will be presented

4.1 Measurement Equipment

One of the most important parts of this experiment is to record the electrical characteristics of the cell samples as accurately as possible. This research effort was somewhat constrained by financial factors; so the testing was done with the most accurate equipment on hand.

4.1.1 Oscilloscope. The oscilloscope used is an Agilent 54641D. Analog channels Ch1 and Ch2 have simultaneous acquisition. The range limits of the sample frequencies are from AC coupled 3.5 Hz to 350 MHz. The calculated rise time is $0.35/\text{bandwidth}$ or $\sim 1.0\text{ns}$. The Single Shot Bandwidth is 350 MHz maximum. The vertical amplitude scale ranges from 2 mV per division to 5 V per division, while the maximum input is 300 Vrms or 400 Vpk. The input resistance is 1 meg Ohm $\pm 1\%$ or 50-Ohm selectable. Input capacitance was ~ 13 pF. Figure 4.1 depicts the oscilloscope used for cell sample data collecting.

The oscilloscope provided measurements by re-scaling its resolution before each frequency measurement was taken. This guaranteed the most accurate measurement regardless of frequency. The amplitude of each frequency reading was recorded with a resolution of 100 points per sample at each frequency measurement. Scales varied from 10ns/sample to $2\mu\text{s}/\text{sample}$. Both channels recorded the input and output data simultaneously. Also, frequency and phase measurements were recorded at every frequency reading.

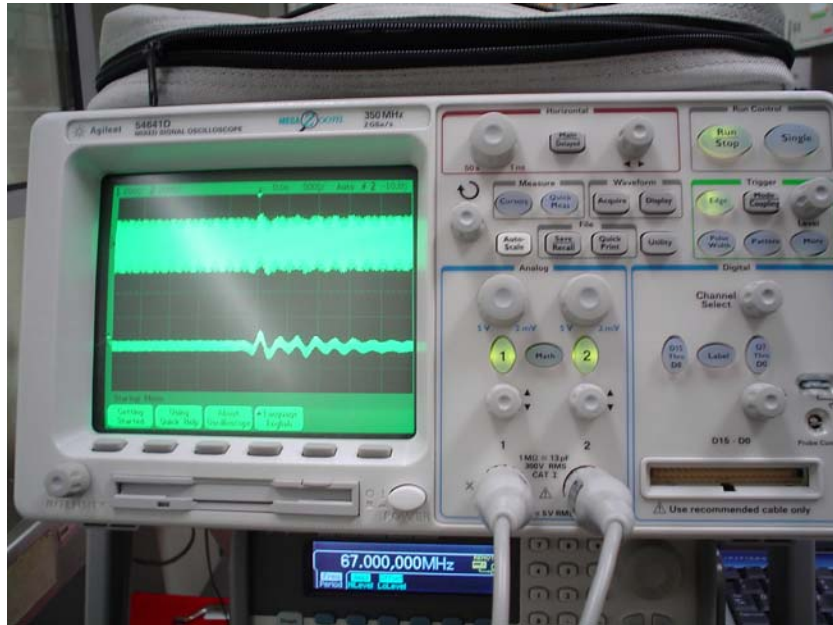


Figure 4.1 Agilent 54641D oscilloscope used in the measurement of the input and output signals of the test samples.

4.1.2 Function Generator. The function generator used was an Agilent 33250A. It is an arbitrary waveform generator with a sine function output frequency range of $1\mu\text{Hz}$ to 80MHz . The harmonic distortion is -30 dBc . The amplitude into 50 Ohms of resistance is 10mVpp to $10\text{Vpp} \pm 0.1\text{mVpp}$. Figure 4.2 depicts the function generator used during the experiment.

The function generator was used to provide a sine input at a set amplitude with varying frequencies. The oscilloscope subsequently recorded the input from the function generator and the output from a cell sample.

4.1.3 Probes. The actual oscilloscope-to-cell sample interface consisted of two components; the oscilloscope probes that came from the manufacturer and a second component used to acquire measurements from the cell sample. These Agilent probes were used for the purpose of isolating electromagnetic waves and losses in the transmission wires. They were also used because they worked with negligible reactance to the signal over the frequency range of experimentation.



Figure 4.2 Agilent 33250A function generator used in this experiment. The function generator was used to input a sine wave at different frequencies into the cell sample.

The second probing component consisted of an interface that was able to properly measure the response of a cell sample. Each cell sample was placed in a fabricated well and the probe device was customized to fit into standard biological cell sample wells. Figure 4.3 depicts the design schematics of these well-probe component, while Figure 4.4 shows the fabricated probe components. These probe components were used to connect the industry fabricated probes to the cell samples. These probe components were tested at the limits of the input and output devices for signal distortion. No significant changes in the input or output measurements were viewed or recorded.

4.1.4 Computer Interface. A Dell laptop was used to record all measurements and direct all instrument processes. A General Purpose Interface Buss (GPIB) card interfaced the oscilloscope and function generator to the laptop (15). Agilent Visual Engineering Environment (VEE) program was used to program the equipment to take measurements. Figure 4.5 displays the entire cell measurement setup.

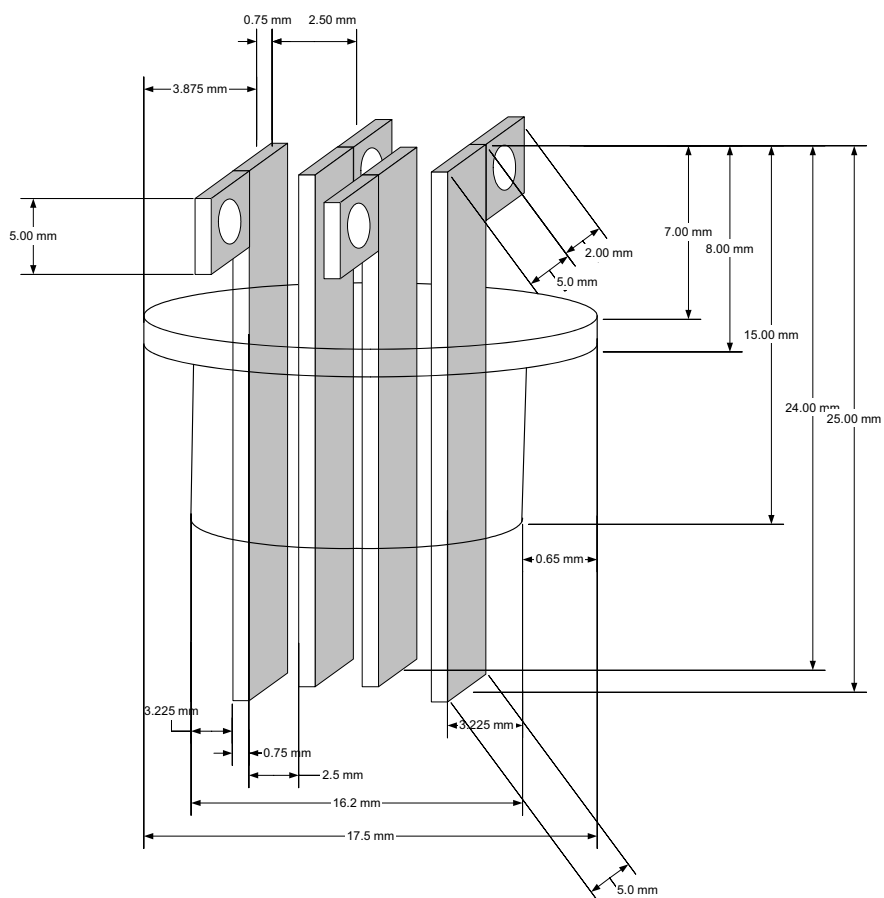


Figure 4.3 Fabrication schematic of probe interface. The probe interphase was specifically designed to fit into a well containing a biological cell sample.



Figure 4.4 Picture of fabricated probe interface. This specific probe interface fits into a 24 sample well (see figure 4.10). Two probe interface types were considered: two leads and four leads. The four lead probe was not used because subsequent experiments found that the two inner probes did not take cell sample measurements but only measured extra-cellular material. This resulted from cells sticking to the bottom of the sample wells, where the middle leads could not properly test.

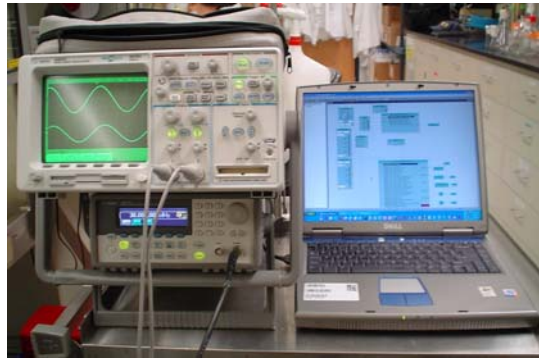


Figure 4.5 Figure of measurement and experimental equipment used to send an input and record an output of the cell sample. The function generator (bottom left) sends a sinusoidal input into the cell sample. The oscilloscope (top left) measures the input and registers the output of the cell sample. The laptop (on the right) directs the input and output, and records the measurements at every sample time.

Measurements were recorded at a variety of frequencies and at multiple sample times. There was a delay from the time each sinusoidal input was used to excite the cells and the time each measurement was taken. This was done to make sure the measurement represented the output while in steady-state. The system was carefully built so that no transients were recorded. Figure 4.6 shows the programming flow chart for the recording of measurements. The measurement acquisition process steps are summarized below:

- Function generator sends a signal into the cell (i.e., a sine wave with 1Vpp amplitude and 1MHz frequency).
- Delay of 0.5 seconds to let the transients die out and reach steady-state.
- Oscilloscope re-scales for optimal measurement resolution.
- Oscilloscope records input, output, frequency and phase change.
- Function generator advances to the next frequency (i.e., a sine wave with 1Vpp amplitude and 2MHz frequency).
- Process is repeated until the entire frequency range specified has been covered.

This process was repeated for every cell sample.

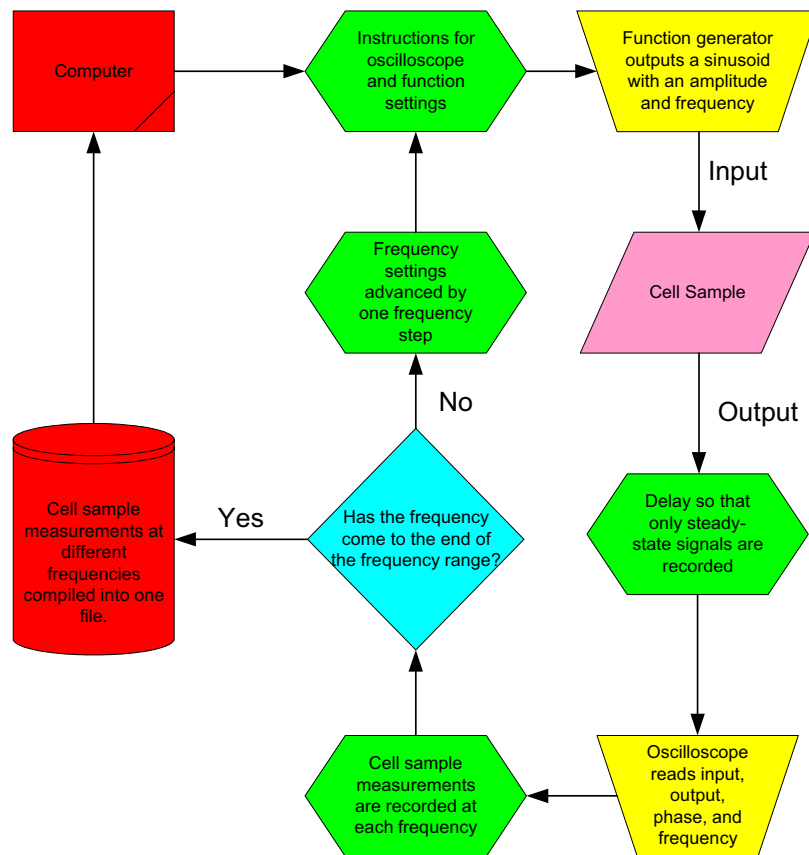


Figure 4.6 The flowchart depicts the process of taking different cellular measurements automatically. The computer specifies the input of the function generator. The output is read by the oscilloscope and recorded into a computer file at each frequency. The automated process then moves on to the next frequency increment to take a measurement until measurements from the entire frequency range are taken.

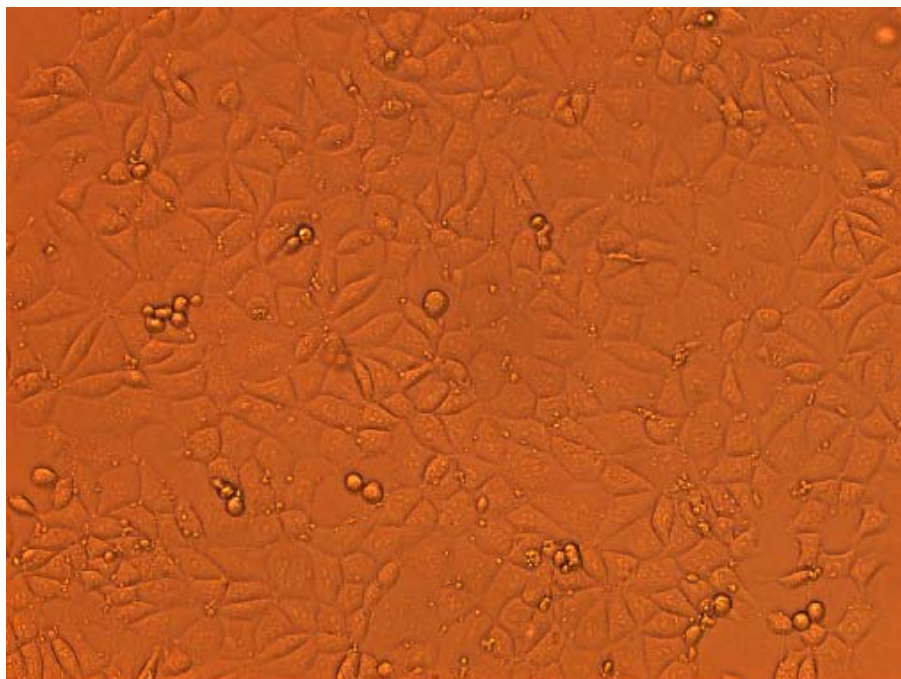


Figure 4.7 Control HEL-30 sample at 10x magnification.

4.2 Cell-type Samples

There were two main cell-types that were tested in this experiment. The HEL-30 cell-type was used to model the smoother. It is a keratinocyte cell made immortal. It is basically an epidermal cell that originated on the tail of a rodent. The HEL-30 is mainly used to model skin behavior. The PC-12 is a lung type cell and was used to test the ability to distinguish cell types. This type of cell models nervous system characteristics. Refer to Chapter 2 for a more in-depth background on the sample cells. Figure 4.7 and 4.8 display HEL-30 cells and PC-12 cells respectively.

The cells were grown in the same sample plate wells that were later used to take measurements. Each sample plate consisted of 24 wells, with two wells left untested for control purposes, so there were 22 samples per plate. In total, 14 sample plates were tested, resulting in 308 total cell samples. Figure 4.10 depicts a 24 well cell sample plate, while a cell sample is being tested.

All cell samples (including the control cell samples) were subjected to the MTT test for mitochondrial activity. Figure 4.9 shows HEL-30 cells with the MTT marker used for

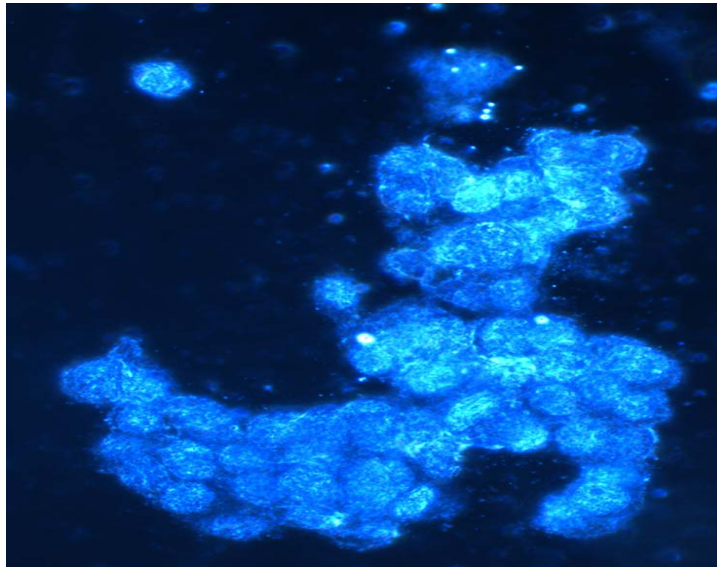


Figure 4.8 Control PC-12 cell sample at 60x magnification.

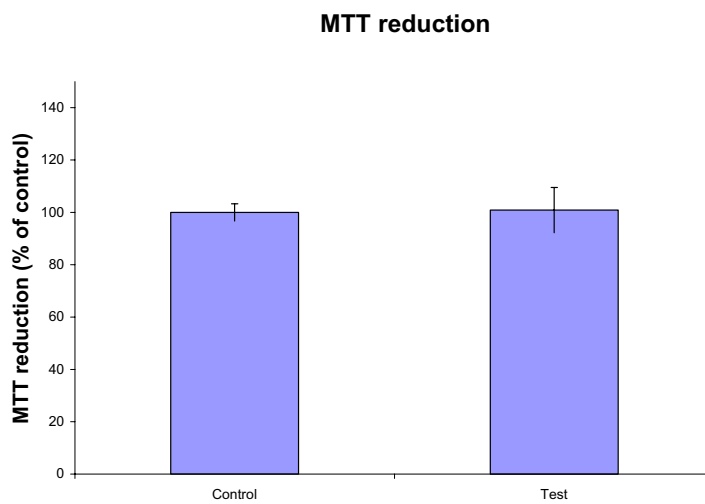


Figure 4.9 Figure displaying results of MTT tests. This is a comparison between the normalized data of the 308 samples tested with an input signal and the control test samples, which were not excited by an electrical input.

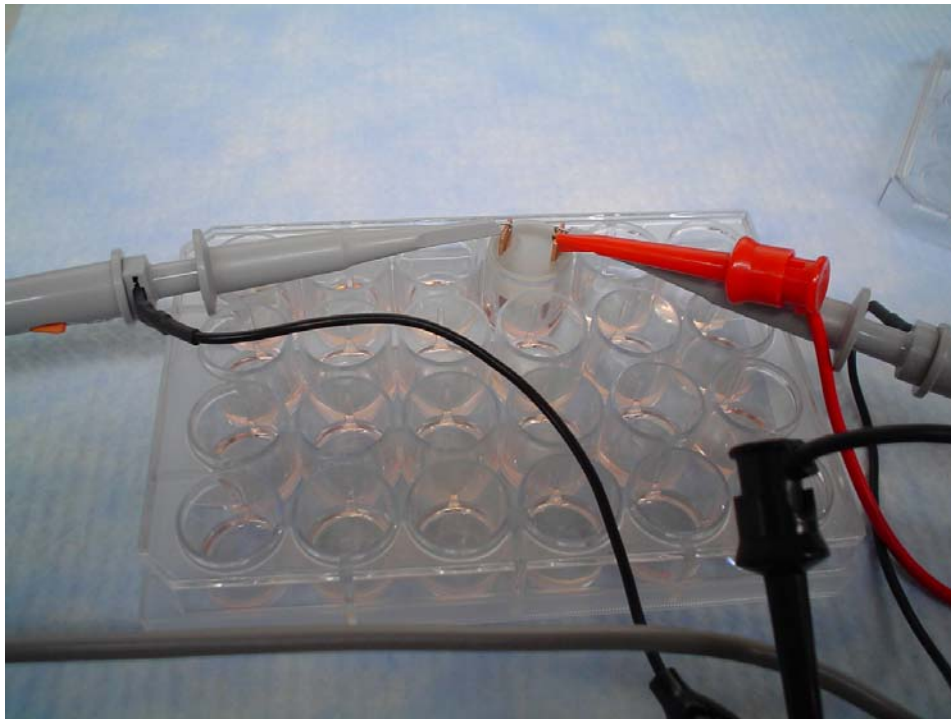


Figure 4.10 Depiction of 24 well cell sample plate. Each well contains either a sample of HEL-30 cells or PC-12 cells. Probes are connected to test the electrical characteristics of an individual cell sample within the plate.

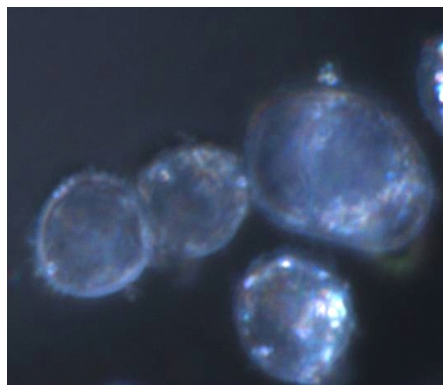


Figure 4.11 HEL-30 control cell without MTT marker. Photographs used to compare the structure of the cell of anomilies.

testing. When this marker was irradiated with a spectrometer, it emitted a specific light spectrum depending on mitochondrial activity (reddish purple delineates no mitochondrial activity while a greenish glow depicts normal mitochondrial activity). It was important to determine if the cells lived through the measurement process for many reasons. Dead cells would change in electrical properties which would make the measurement of the response of the cell sample invalid. If cells died, it would also imply that the process could not be used in-vivo. Based on this, it was important to choose parameters that would ensure the survival of the cell samples. Figure 4.12 is a comparison of all the cell tests in every plate as compared to the control samples. As shown, 100 % of the cell samples survived the testing procedure. It can be seen that the tested samples have slightly larger than 100% mitochondrial activity. This could be due to a slight rounding off of the data numbering, or the fact that the electrical input stimulated the cells in some way. Regardless of the reason, it is well within boundaries of healthy cells (too much increase in mitochondrial function could be a sign of mutation of the cells, effectively making it cancerous).

4.2.1 Cell Test Samples. For research purposes, it was important to find the ability of the cell to survive under different input parameters. Literature suggested the types of inputs that cells could handle (i e., sinusoids up to 46 Vpp with a frequency range between 10KHz and 1MHz), but none of this literature directly pertained the cell-type samples that were used in this research. Also, tests had to be done to see the time it took the transients of the initial signal to die out such that the output of the cell sample

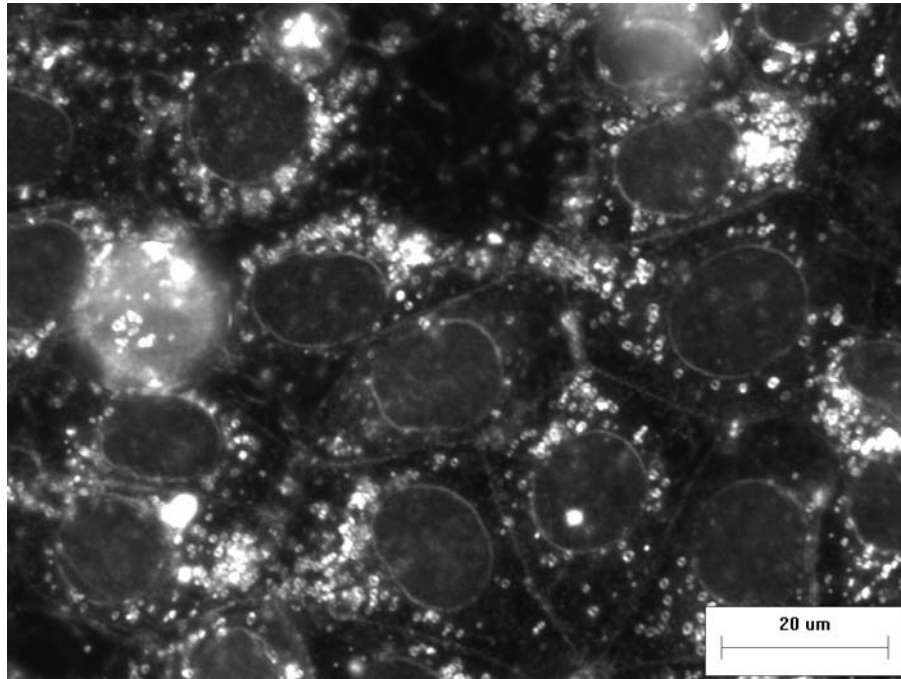


Figure 4.12 HEL-30 cell control samples with MTT marker.

reached steady-state. For this purpose, some samples were subjected to extreme inputs. Table 4.1 and Table 4.2 show initial tests done on the HEL-30 cells to determine viable inputs. Cells were tested at a temperature of 52°C . The period column delineates the total time the cells were tested. Once it was established that the cell could survive for a lengthy period of testing (up to 615 seconds), the time was no longer recorded.

The rest of the cell sample plates' frequency range and amplitude for HEL-30 cells are summarized in Table 4.3. Note the variety of changes in amplitudes, frequency ranges, and frequency steps. The main reason for these variations in testing amplitudes and frequency ranges was the need to obtain useful output data. At the beginning of the experimentation, measurements found in literature were used, but it was found that responses were more significant in other frequency ranges. The initial frequency range used was from 10KHz to 1MHz as stated in much of the literature (1, 2, 10, 11, 41). No significant signal response was found in this frequency range as shown in Figure 4.13. There was no discernible frequency variation in amplitude or phase; so a different frequency range with a more discernible response was required.

Table 4.1 This table denotes the results of Cell Sample Plate 1. HEL-30 cell samples were tested. There were no control samples in this plate because boundaries needed to be tested.

Sample (#)	Amplitude (Vpp)	Frequency Tested (Hz)	Period (s)
1	1.0	10K-50M @ 10K steps	N/A
2	1.0	80 M	300
3	1.0	10K-1M @ 20K steps	N/A
4	1.0	10K-1M @ 20K steps	N/A
5	1.0	10K-1M @ 20K steps	N/A
6	1.0	10K-1M @ 20K steps	N/A
7	1.0	10K-1M @ 20K steps	N/A
8	1.0	10K-1M @ 20K steps	N/A
9	1.0	10K-1M @ 20K steps	N/A
10	1.0	10K-1M @ 20K steps	N/A
11	1.0	10K-1M @ 20K steps	N/A
12	1.0	10K-1M @ 20K steps	N/A
13	1.0	10K-1M @ 20K steps	N/A
14	1.0	10K-1M @ 20K steps	N/A
15	1.0	10K-1M @ 20K steps	N/A
16	1.0	10K-1M @ 20K steps	N/A
17	1.0	10K-1M @ 20K steps	N/A
18	1.0	10K-1M @ 20K steps	N/A
19	1.0	10K-1M @ 20K steps	N/A
20	1.0	10K-1M @ 20K steps	N/A
21	1.0	10K-1M @ 20K steps	N/A
22	1.0	10K-1M @ 20K steps	N/A
23	0.1	10K-60M @ 20K steps	N/A
24	0.1	10K-60M @ 20K steps	N/A

Table 4.2 This table denotes the results of HEL-30 Cell Sample Plate 2. This plate was mainly tested to find input boundaries that could be used for experimentation.

Sample (#)	Amplitude (Vpp)	Frequency Tested (Hz)	Period (s)
1	N/A (control)	N/A (control)	N/A
2	N/A (control)	N/A (control)	N/A
3	100m	10K-3M @ 10K steps	600
4	100m	10K-3M @ 10K steps	600
5	100m	10K-3M @ 10K steps	600
6	100m	10K-3M @ 10K steps	600
7	100m	10K-3M @ 10K steps	600
8	100m	10K-3M @ 10K steps	600
9	100m	10K-3M @ 10K steps	600
10	100m	10K-3M @ 10K steps	600
11	100m	10K-3M @ 10K steps	600
12	100m	10K-3M @ 10K steps	600
13	100m	10K-3M @ 10K steps	600
14	100m	10K-3M @ 10K steps	600
15	100m	10K-3M @ 10K steps	600
16	100m	10K-3M @ 10K steps	600
17	100m	10K-3M @ 10K steps	600
18	100m	10K-3M @ 10K steps	600
19	100m	10K-3M @ 10K steps	600
20	100m	10K-3M @ 10K steps	600
21	100m	10K-3M @ 10K steps	600
22	100m	10K-3M @ 10K steps	600
23	100m	10K-3M @ 10K steps	600
24	100m	10K-3M @ 10K steps	600

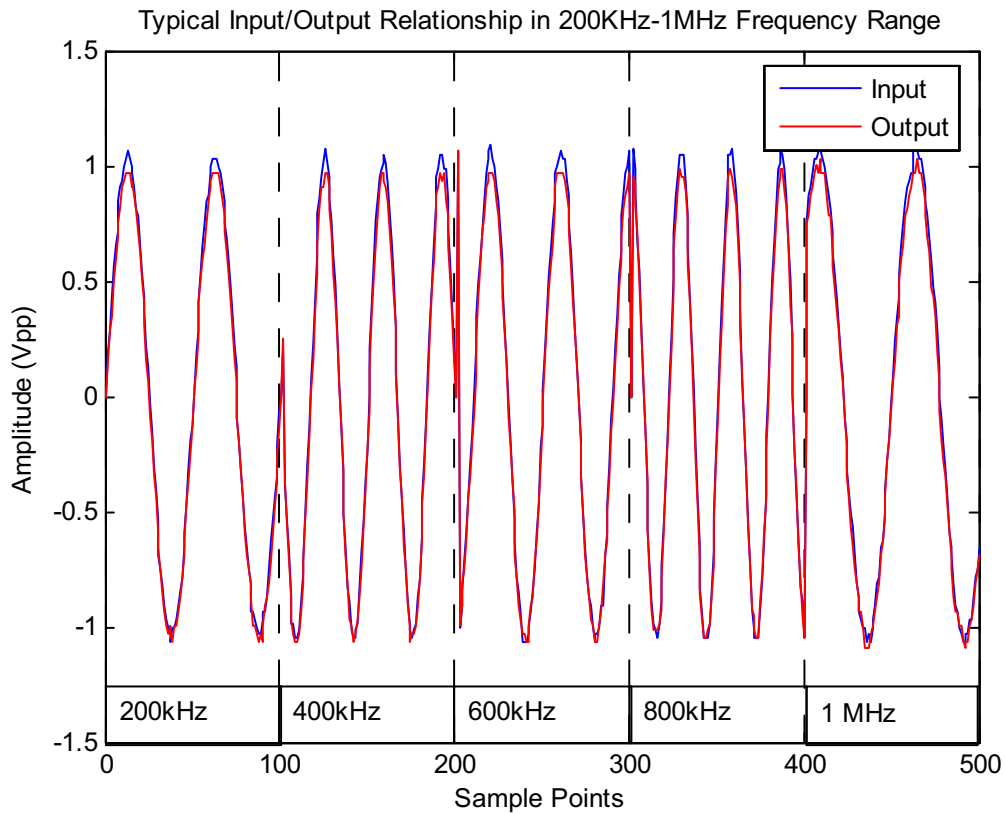


Figure 4.13 Typical frequency response over a 200KHz-1MHz range with a 2Vpp amplitude. There is no significant response change between the input and the output. It was for this reason that a range of 1MHz to 80 MHz in the β dispersion frequency range was chosen. X label denotes sample points (100 per frequency measurement). Frequencies labeled in their specific partitions.

Table 4.3 This table denotes the input that each HEL-30 cell sample plate was subjected to. The cell samples that have already been displayed are referenced from other tables. There were only 22 test samples in each plate because 2 test samples were always used for control

Plate (#)	Amplitude (Vpp)	Frequency Tested (Hz)	Period (s)
1	refer to Table 4.1	refer to Table 4.1	refer to Table 4.1
2	refer to Table 4.2	refer to Table 4.2	refer to Table 4.2
3	0.1	10K-1M @ 5K steps	615
4	0.025	10K-1M @ 10K steps	204
5	0.025	10K-60M @ 500K steps	N/.A
6	0.025	10K-20K @ 0.5K steps	N/A
7	0.025	10K-3M @ 500K steps	N/A
8	0.025	10K-3M @ 10K steps	N/A
9	0.25	1M-70M @ 5M steps	N/A
10	0.25	1M-70M @ 5K steps	N/A
11	0.25	1M-75M @ 1M steps	N/A

Frequency ranges were not the only input variation in the experiment. Based on the literature (11), a 25mV amplitude would guarantee linearity in the system. It was found that this voltage did not provide any significant signal changes except for noise. Furthermore, at low amplitudes, the oscilloscope could not read the frequency measurements. Frequency measurements were vital to the processing of the model; so research at this amplitude had to be abandoned.

The cell samples that produced the most significant responses and provided a good measure of the amplitudes, were the cell samples in plate 11. These samples were taken at an amplitude of 250 mV and a frequency range of 1MHz to 80MHz (with frequency change steps of 1MHz). The following figures show the input and output relationship of a representative sample in plate 11. As seen in Figure 4.14 and Figure 4.15, the input output relationship does not show a significant response until 40MHz is reached. After this point, the frequency response is very significant. Once it was established that this specific amplitude and frequency range gave good measurements regarding the HEL-30 cell samples, the last three plates involving PC-12 samples were subjected to these same inputs. Table 4.4 shows the amplitude and frequency range of the last 3 sample plates. Figures 4.16 and 4.17 show a representative input and output sample from plate 14.

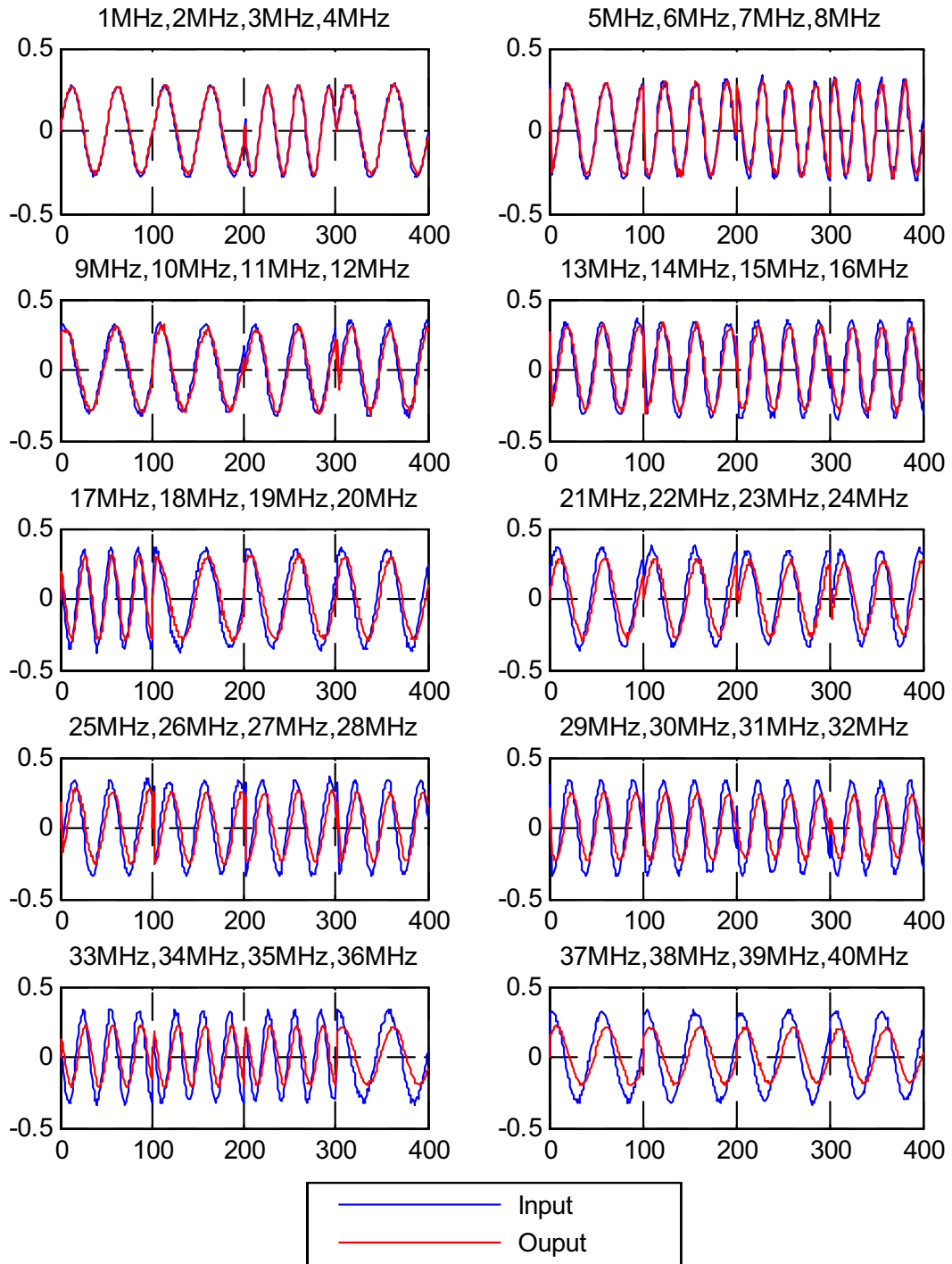


Figure 4.14 Input/output relationships of representative HEL-30 cell samples used in the system modeling. Top scale and dividers denote frequencies and boundaries respectively. Bottom scale denotes number of sample points. Y scale denotes units in volts (V). This figure denotes a frequency range of 1MHz-40MHz at 1MHz steps.

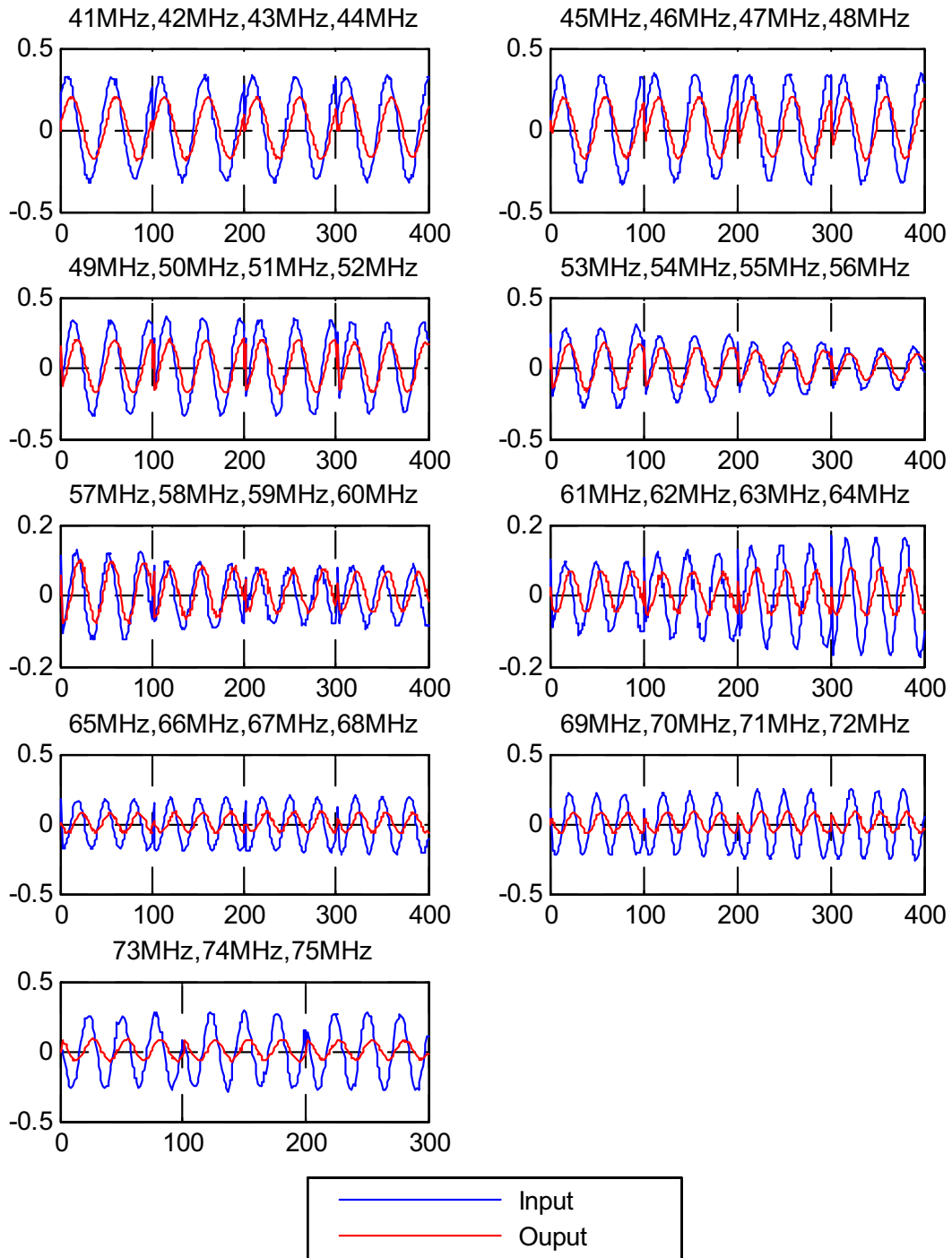


Figure 4.15 Input/output relationships of representative HEL-30 cell samples used in the system modeling. Top scale and dividers denote frequency changes. Bottom scale denotes number of sample points. Y scale denotes units in volts (V). This figure denotes a frequency range of 41MHz-75MHz at 1MHz steps.

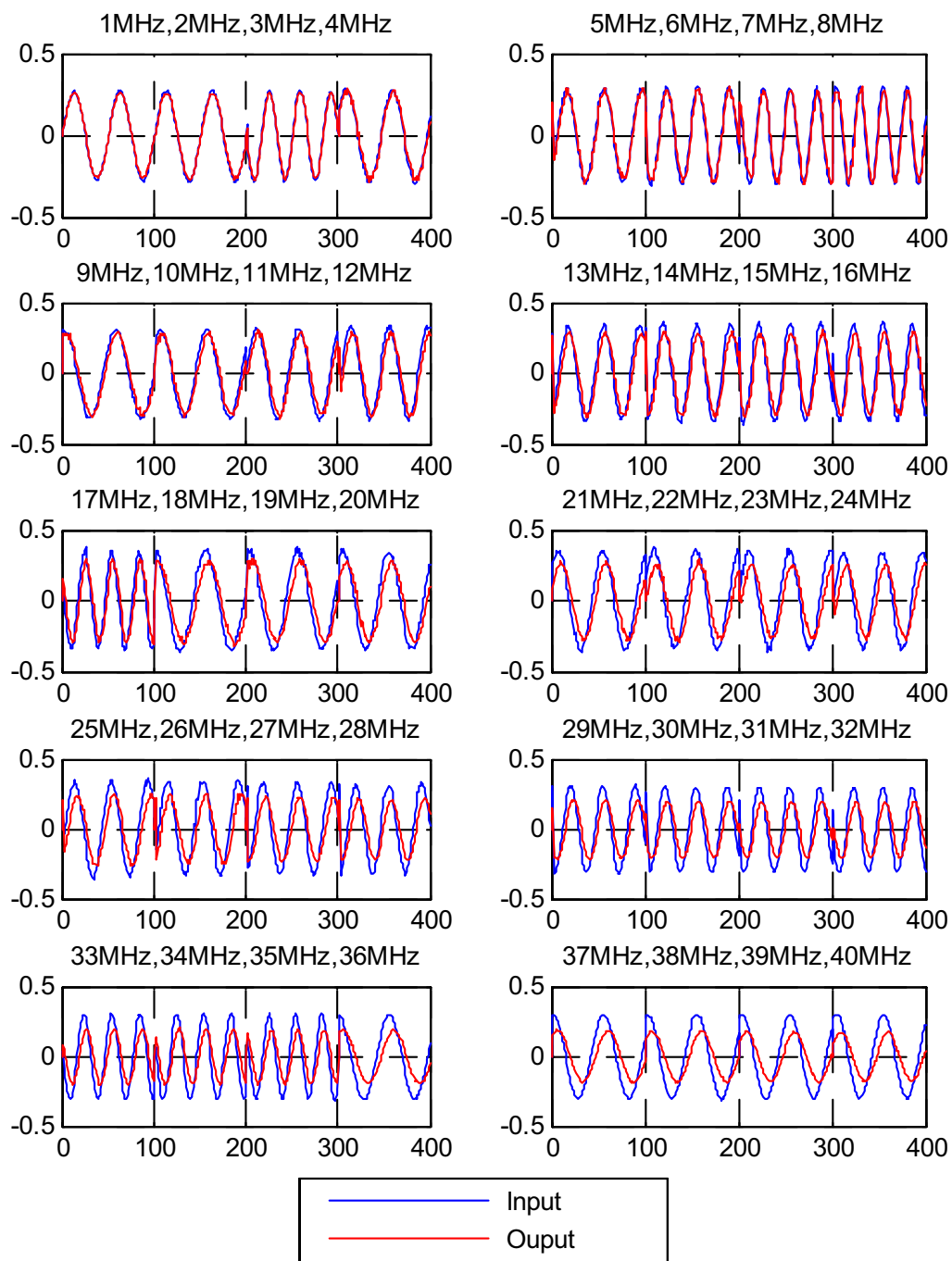


Figure 4.16 Input/output relationships representative of PC-12 cell samples. Top scale and dividers denote frequency. Bottom scale denotes number of sample points. Y scale denotes units in volts (V). This is from a frequency range 1MHz-40MHz at 1MHz steps and an amplitude of 250 mVpp.

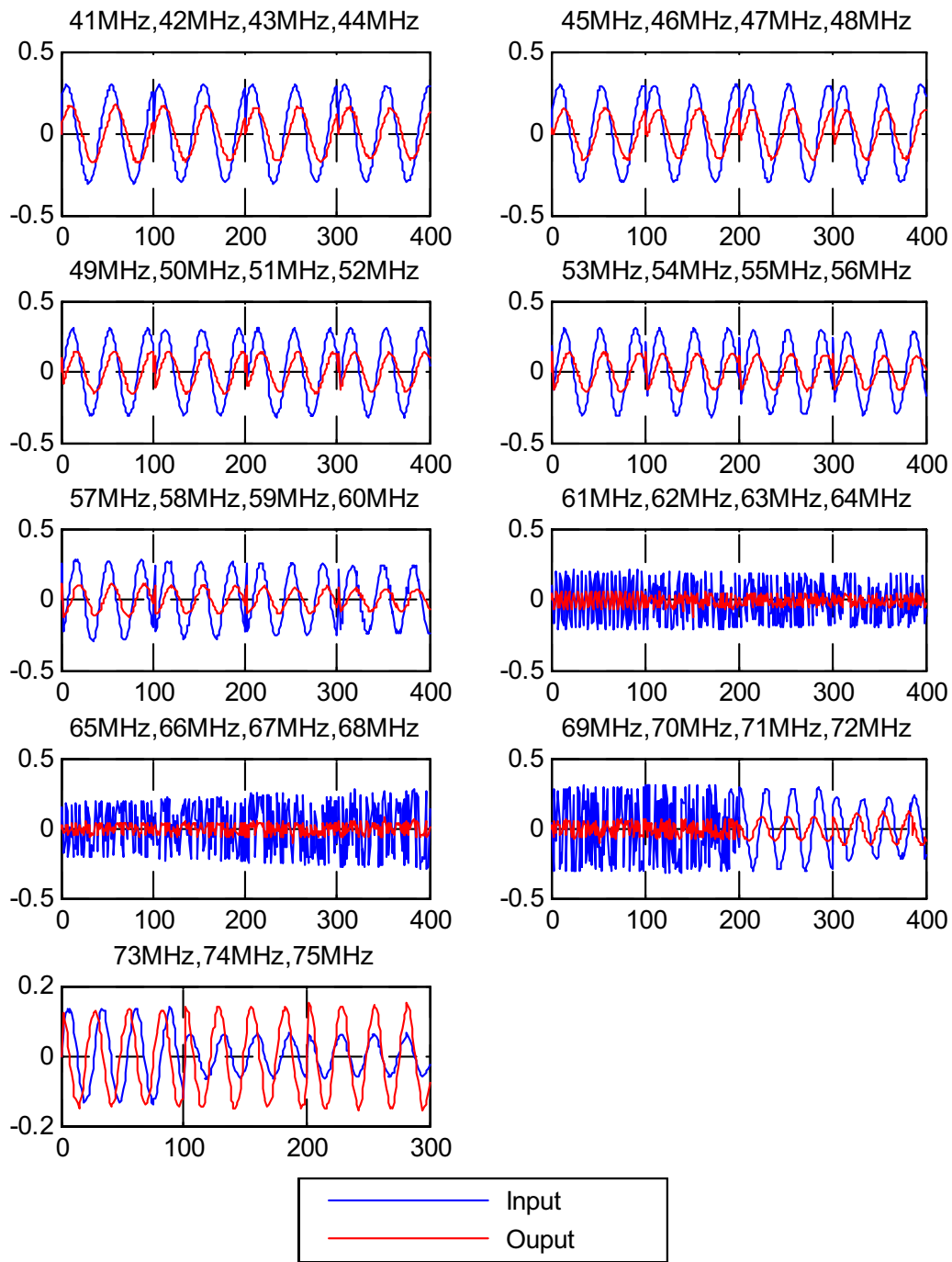


Figure 4.17 Input/output relationships of representative PC-12 cell samples. Top scale and dividers denote frequency. Bottom scale denotes number of sample points. Y scale denotes units in volts (V). This is from a frequency range 41MHz-75MHz at 1MHz steps and an amplitude of 250 mVpp.

Table 4.4 This table denotes inputs that PC-12 sample plates were subjected to. MTT test column delineates survival of all test samples. There were only 22 test samples in each plate because 2 test samples were always used for control

Plate (#)	Amplitude (Vpp)	Frequency Tested (Hz)	Period (s)
12	0.25	1M-75M @ 1M steps	N/A
13	0.25	1M-75M @ 1M steps	N/A
14	0.25	1M-75M @ 1M steps	N/A

The next step in the experimental process was to make sure that both cell-types did not produce the same output characteristics despite identical inputs. Figures 4.18 and 4.19 denote the comparison between HEL-30 and PC-12 cell samples despite the fact that they have the same input. One can easily see the differences between the HEL-30 and PC-12 output characteristics when compared to one another. In this plot, one can definitely see the different cellular characteristics, especially once a higher frequency range is reached. When higher frequencies are reached, both signals seem to display a noise component. These are only sinusoidal signals sampled at a different resolution. The oscilloscope opted for a different resolution because it could not trigger onto a single signal so it allowed a greater variety of samples to be shown as some frequencies base on the variance of the output. It can be seen that both cell display such similar characteristics.

4.3 System Modeling

Once it was realized that sample plate 11 had the cell samples with the most discernible frequency response, the 22 cell samples were put into a MATLAB[®] program named Ident (21). This Graphic User Interface (GUI) has the capacity of taking input/output frequency data to produce a model via the ARX method. Refer to Chapter 3 for a discussion of the ARX algorithm. Figure 4.20 shows a picture of the GUI. The left side of the figure depicts the inputs and outputs loaded into the program. The right side of the figure depicts the models built via ARX model estimation.

The ident tool produced a variety of models that were suitable matches based on their input/output characteristics. Figure 4.21 depicts the models generated by the input/output data. Based on the model characteristics, one model was chosen to be used

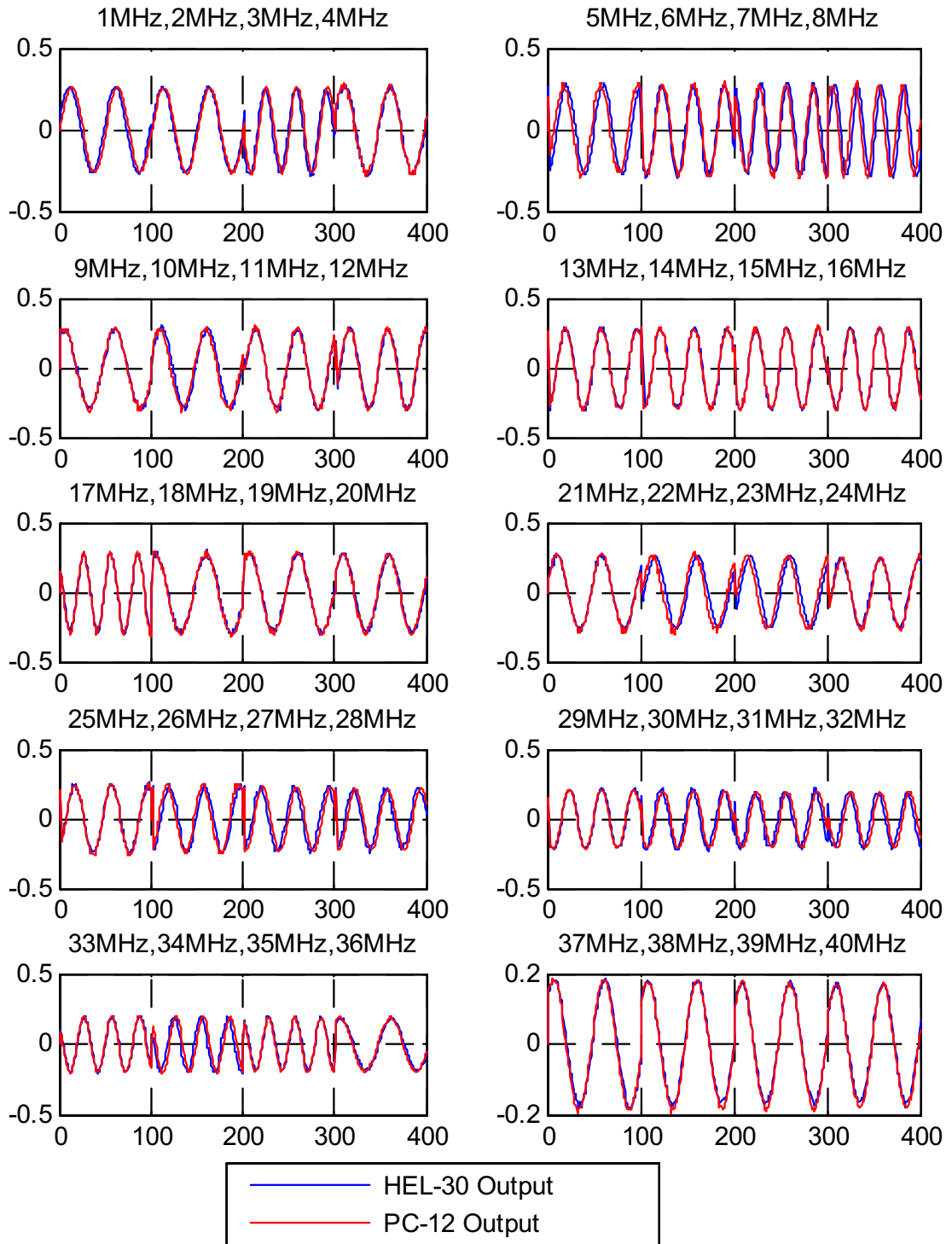


Figure 4.18 Comparison of PC-12 sample and HEL-30 sample outputs (Blue denotes HEL-30 samples while Red denotes PC-12 samples). Upper scale denotes frequency changes. Lower scale denotes sample steps. Y scale denotes amplitude in volts (V). These plots show response over a frequency range of 1MHz-40MHz. 4-21

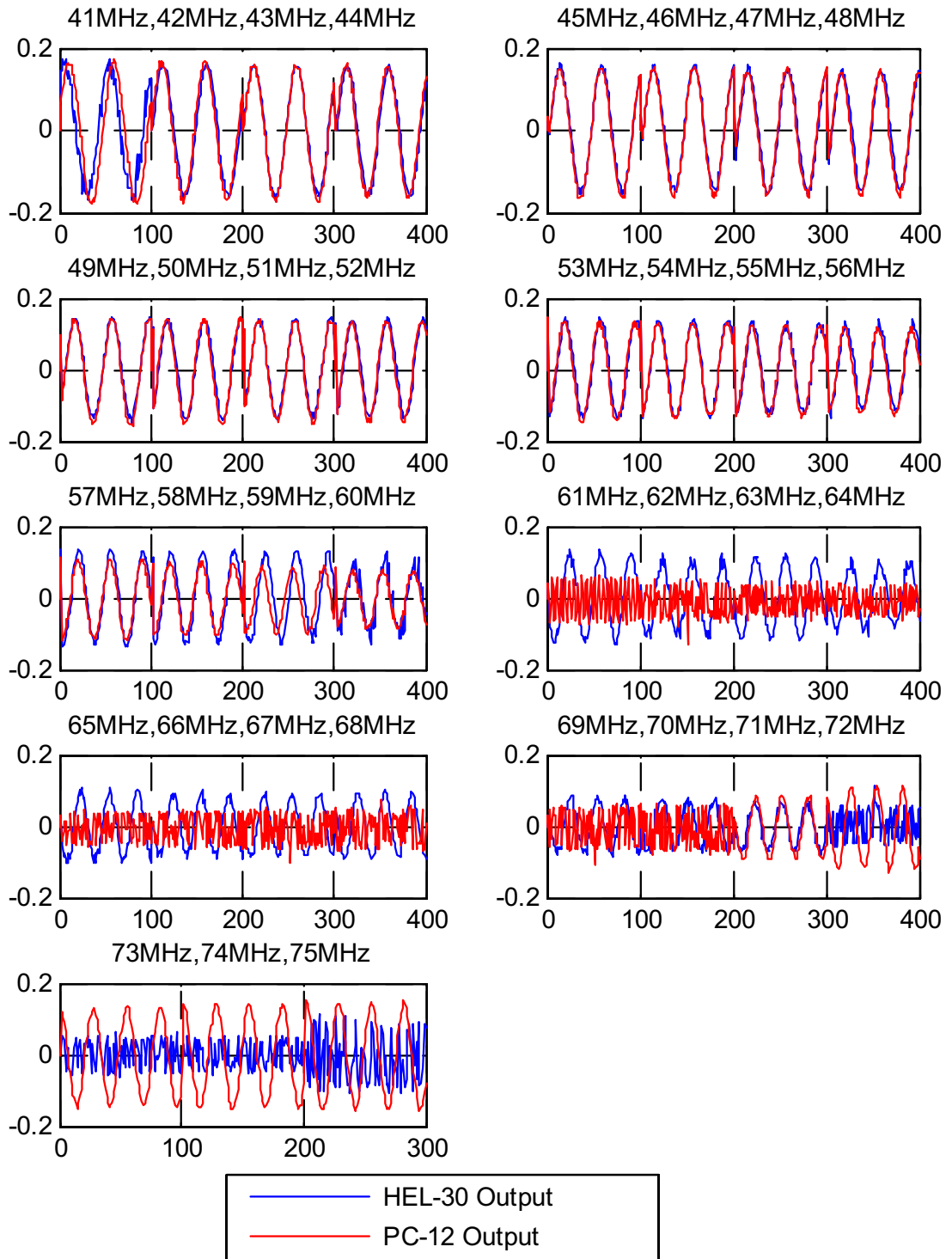


Figure 4.19 Comparison of PC-12 sample and HEL-30 sample outputs (Blue denotes HEL-30 samples while Red denotes PC-12 samples). Upper scale denotes frequency changes. Lower scale denotes sample steps. Y scale denotes amplitude in volts (V). These plots show response over a frequency range of 41MHz-75MHz.

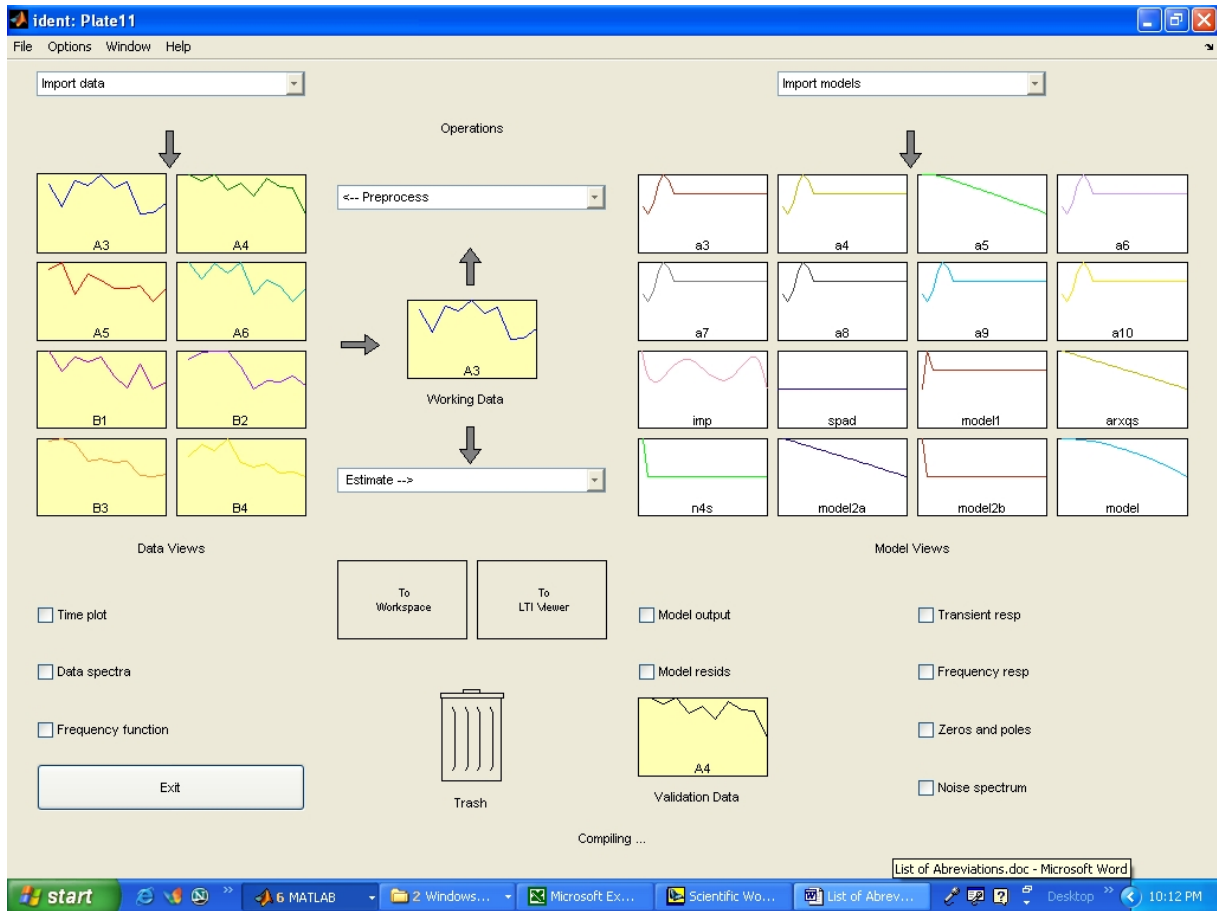


Figure 4.20 Figure of Ident, a GUI used within MATLAB[®] to build system models based on ARX models. This tool is used to estimate transfer functions based on input and output measurements.

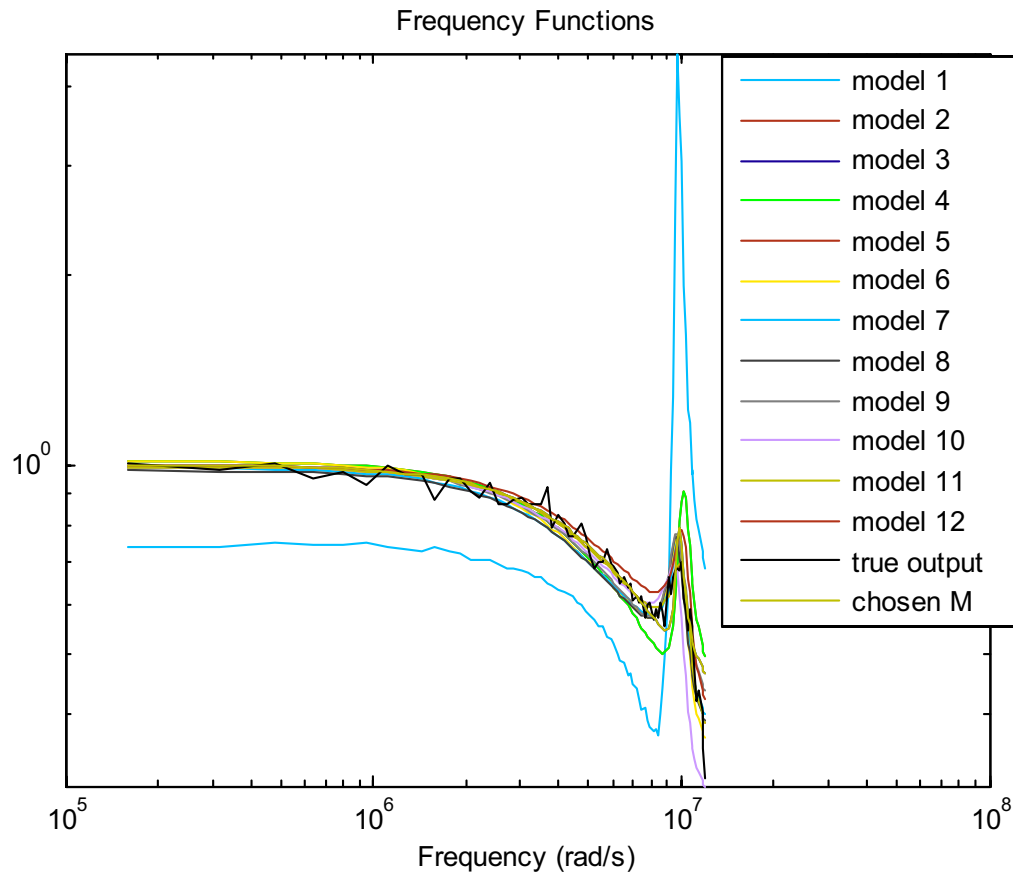


Figure 4.21 The figure depicts 13 different models that very closely resemble the output characteristics of the samples at different frequencies. These models were produced by different iterations of the ARX algorithm. From these models, one was chosen as best depiction. The line in black is the system measured response, the smooth multi-colored lines depict the different models.

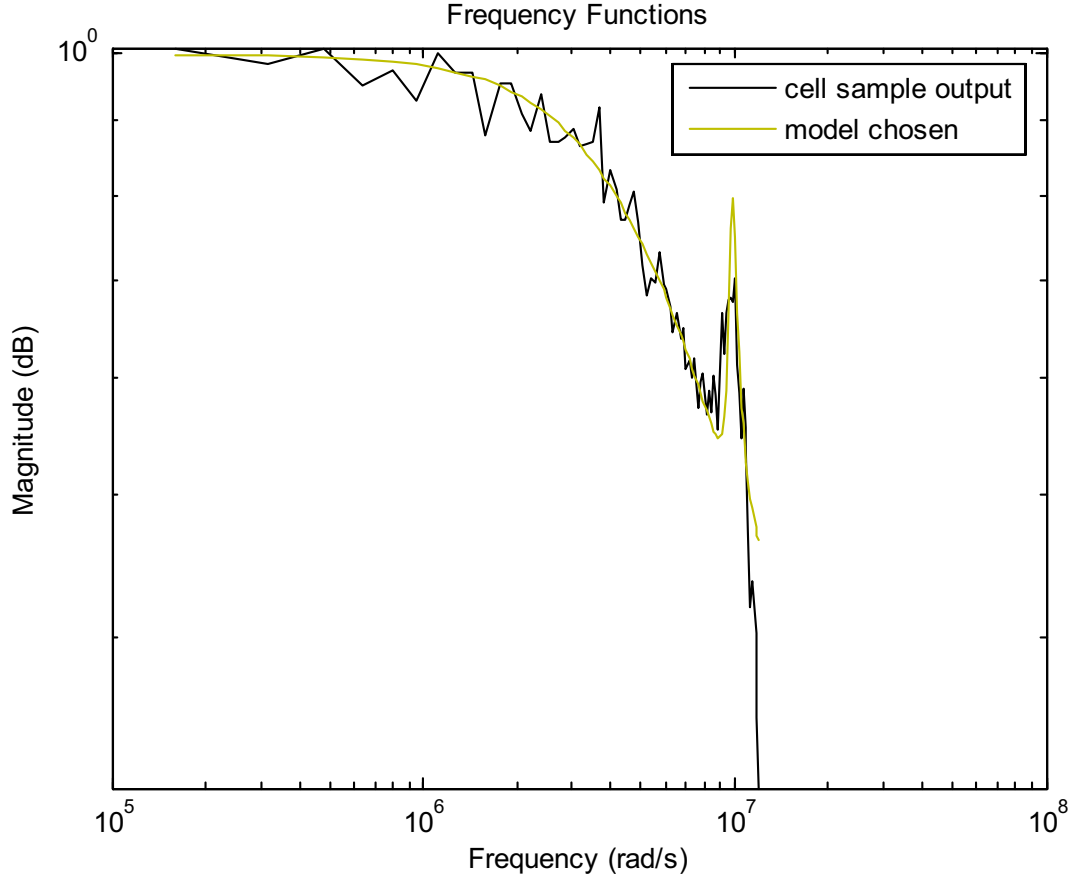


Figure 4.22 Figure depicts the model that was to be used in the development of the stochastic smoother.

in the development of the smoother. Figure 4.22 depicts the model chosen based on its similarity to the sample data.

The model was chosen based on two criteria; it was the model that best fit the measurement output from the cell and it was also the model that had a \mathbf{D} matrix ≈ 0 (more to follow on this subject). The model chosen produced the following differential equation:

$$A(q)y(t) = B(q)u(t) + e(t) \quad (4.1)$$

$$A(q) = 1 - 4q^{-1} + 6.001q^{-2} - 4.001q^{-3} + q^{-4} \quad (4.2)$$

$$B(q) = -0.0006025 + 0.001807q^{-1} - 0.001807q^{-2} + 0.0006021q^{-3} \quad (4.3)$$

Loss function $V_N(\theta)$ (refer to Equation 3.20) was calculated to be:

$$V_N(\theta) = 1.09032e^{-27}$$

Based on this differential equation, the following state space model was created:

$$\mathbf{x}(t_{i+1}) = \mathbf{\Phi}(t_{i+1}; t_i)\mathbf{x}(t_i) + \mathbf{B}(t_i)\mathbf{u}(t_i) + \mathbf{\Gamma}_d(t_i)\mathbf{w}_d(t_i) \quad (4.4)$$

$$y(t_i) = \mathbf{H}(t_{i-1})x(t_{i-1}) + \mathbf{D}(t_{i-1})u(t_{i-1}) \quad (4.5)$$

$$\mathbf{\Phi} = \begin{bmatrix} 4 & 1 & 0 & 0 \\ -6.001 & 0 & 1 & 0 \\ 4.001 & 0 & 0 & 1 \\ -1 & 0 & 0 & 0 \end{bmatrix} \quad (4.6)$$

$$\mathbf{B} = \begin{bmatrix} -0.0006039 & 634e^{-14} \\ 0.001809 & -1.445e^{-13} \\ -0.001808 & 9.635e^{-14} \\ 0.0006026 & -2.409e^{-14} \end{bmatrix} \quad (4.7)$$

$$\mathbf{H} = \begin{bmatrix} 1 & 0 & 0 & 0 \end{bmatrix} \quad (4.8)$$

$$\mathbf{D} = \begin{bmatrix} -0.00060252 & 408e^{-14} \end{bmatrix} \approx \begin{bmatrix} 0 & 0 \end{bmatrix} \quad (4.9)$$

The \mathbf{D} matrix was approximated to zeros because the feed through items, or extra outputs, would make the calculations for the estimation of the stochastic smoother more difficult. Given that the numbers were not very significant, an approximation to zero was logical. This is the state-space model in discrete form.

4.4 Modeling of Stochastic Smoother

Once the state model in discrete form was determined, the next step was to use this model in implementing the smoother. The forward filter in the smoother developed from

the HEL-30 sample response used the following initial values:

$$\hat{\mathbf{x}}(t_0) = \mathbf{0} \quad (4.10)$$

$$\mathbf{P}(t_0) = \mathbf{0} \quad (4.11)$$

Where $\hat{\mathbf{x}}(t_0)$ is the initial measurement estimate and $\mathbf{P}(t_0)$ is the initial covariance. From this point forward, $\hat{\mathbf{x}}(t_0)$ and $\mathbf{P}(t_0)$ are propagated and updated using Equations (3.47) to (3.51). The values of $\hat{\mathbf{x}}(t_0)$ and $\mathbf{P}(t_0)$ were set to 0. This is by no means the best case scenario because a covariance matrix is not transposable if set to 0. Setting the covariance equal to zero implies that the measurement is perfect as is. This situation is rarely true. By saying that a perfect measurement is attained there is a chance that the filter equations become singular. Equation (3.51) may become negative which would imply a non-existent negative covariance. The values were chosen based on the fact that all initial sample points were set to zero. This was done to counteract instrument behavior. Every time the oscilloscope took measurements, it would set each initial sample to a very high value ($10e^{37}$ volts) regardless of input. This huge value did not allow the filter to acquire an estimate. To allow the filter to estimate after a couple of samples, each initial sample value was set to zero. Since the value was set, it was determined that a perfect knowledge of this initial value was the correct assumption.

$$\Phi(t_{k+1}, t_k) = \begin{bmatrix} 4 & 1 & 0 & 0 \\ -6.001 & 0 & 1 & 0 \\ 4.001 & 0 & 0 & 1 \\ -1 & 0 & 0 & 0 \end{bmatrix} \quad (4.12)$$

$$\mathbf{\Gamma}_d(t_k) = \begin{bmatrix} 1 & 0 & 0 & 0 \\ 0 & 1 & 0 & 0 \\ 0 & 0 & 1 & 0 \\ 0 & 0 & 0 & 1 \end{bmatrix} \quad (4.13)$$

$$\mathbf{Q}_d(t_k) = 0.1 \quad (4.14)$$

$$\mathbf{H}(t_k) = \begin{bmatrix} 1 & 0 & 0 & 0 \end{bmatrix} \quad (4.15)$$

$$\mathbf{R}(t_k) = 10 \quad (4.16)$$

The values for \mathbf{Q}_d and \mathbf{R} were obtained based on fine tuning of the system. The value \mathbf{Q}_d pertains to the covariance of the zero-mean Gaussian noise pertaining to the model, while \mathbf{R} is the covariance of the zero-mean Gaussian noise relating to the measurement. Each of them is basically a measure of how much confidence should be given to each of these components (\mathbf{Q}_d pertains to how accurate the model is, while \mathbf{R} pertains to the accuracy of the measurement). In this case \mathbf{R} was obtained by analyzing the variance of the instrument accuracy. This variance was then squared to obtain \mathbf{R} . There was no way to know the adequacy of the model based on the fact that this was the first time it had been used. Due to the lack of empirical data pertaining to the accuracy of the model, values of \mathbf{Q}_d were varied until an accurate estimate was obtained. While this is not the optimal method for smoother tuning, the lack of research did not allow for a more accurate option. The values for the backward filter were calculated using Equations (3.52) to (3.56). The smoothed estimates were calculated using Equations (3.60) to (3.64)

Figure 4.23 and Figure 4.24 represent the comparison of the smoothed estimate of the measurement versus actual output measurement of an HEL-30 cell sample. As Figure 4.24 shows, the filter starts giving sub-standard estimates at the higher frequencies. This is due to mismodeling at high frequencies.

Figure 4.25 and Figure 4.26 represent the comparison of the smoothed estimate of the measurement versus the actual output measurement of a representative PC-12 cell sample. The system was not built based on the characteristics of this cell-type. As a result, accurate estimation is not expected. From these figures it can be seen that, while the filter estimates cell sample output values well over some frequency ranges, cell sample estimation is not as accurate as it had been for the HEL-30 cell estimation in Figure 4.23 and Figure 4.24.

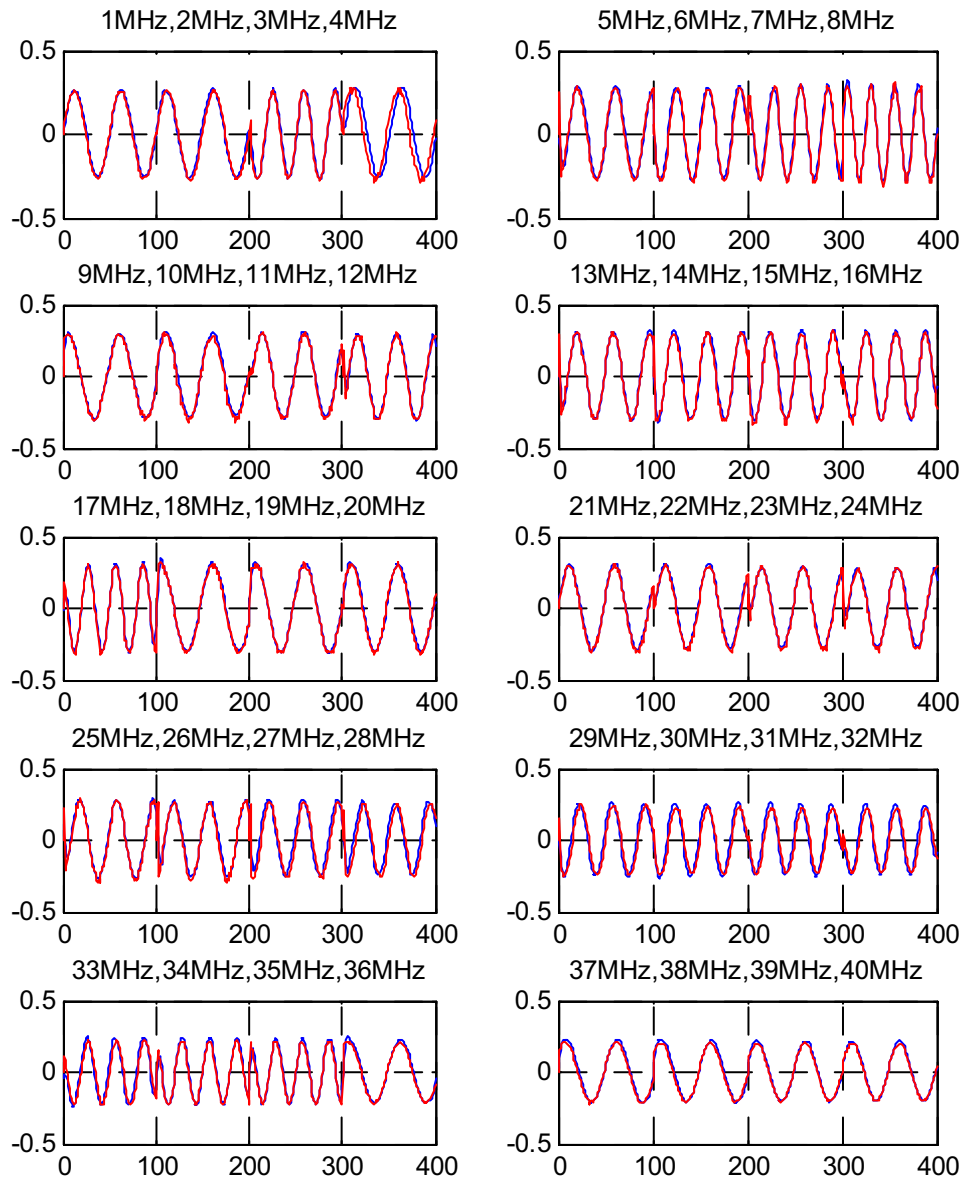


Figure 4.23 This figure shows the difference between the smoothed output estimated and the measured output of a representative HEL-30 cell sample. Red shows the cell sample output. Blue shows the estimate output. Upper scale denotes frequencies. Lower scale shows sample intervals. Y scale shows magnitude in volts (V).

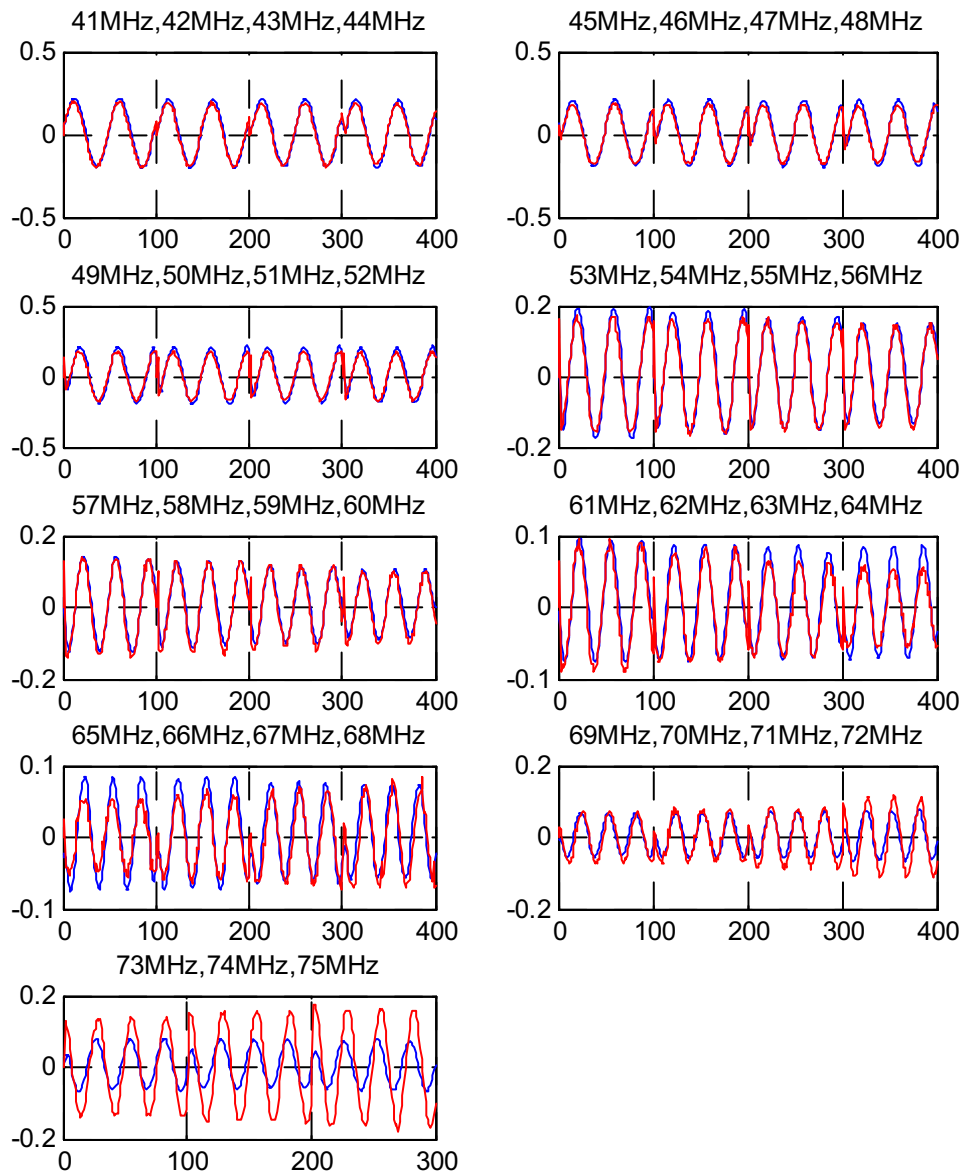


Figure 4.24 This figure shows the difference between the smoothed output estimated and the measured output of a representative HEL-30 cell sample. Red shows the cell sample output. Blue shows the estimate output. Upper scale denotes frequencies. Lower scale shows sample intervals. Y scale shows magnitude in volts (V).

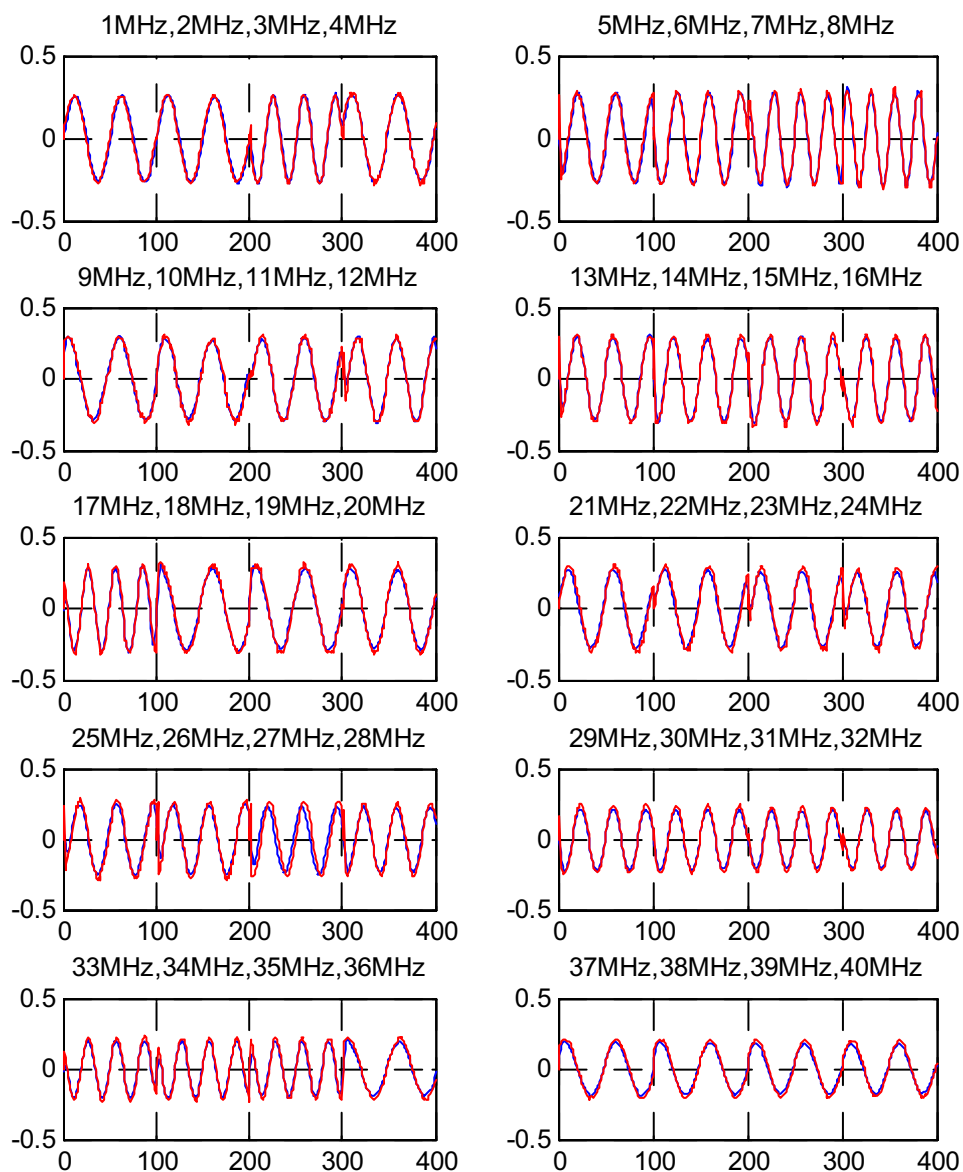


Figure 4.25 The figure shows the difference between the smoothed output estimate and the measured output of a representative PC-12 cell sample. Red shows the cell sample output. Blue shows the estimated output. Upper scale denotes frequencies. Lower scale shows sample intervals. Y scale shows magnitude in volts (V).

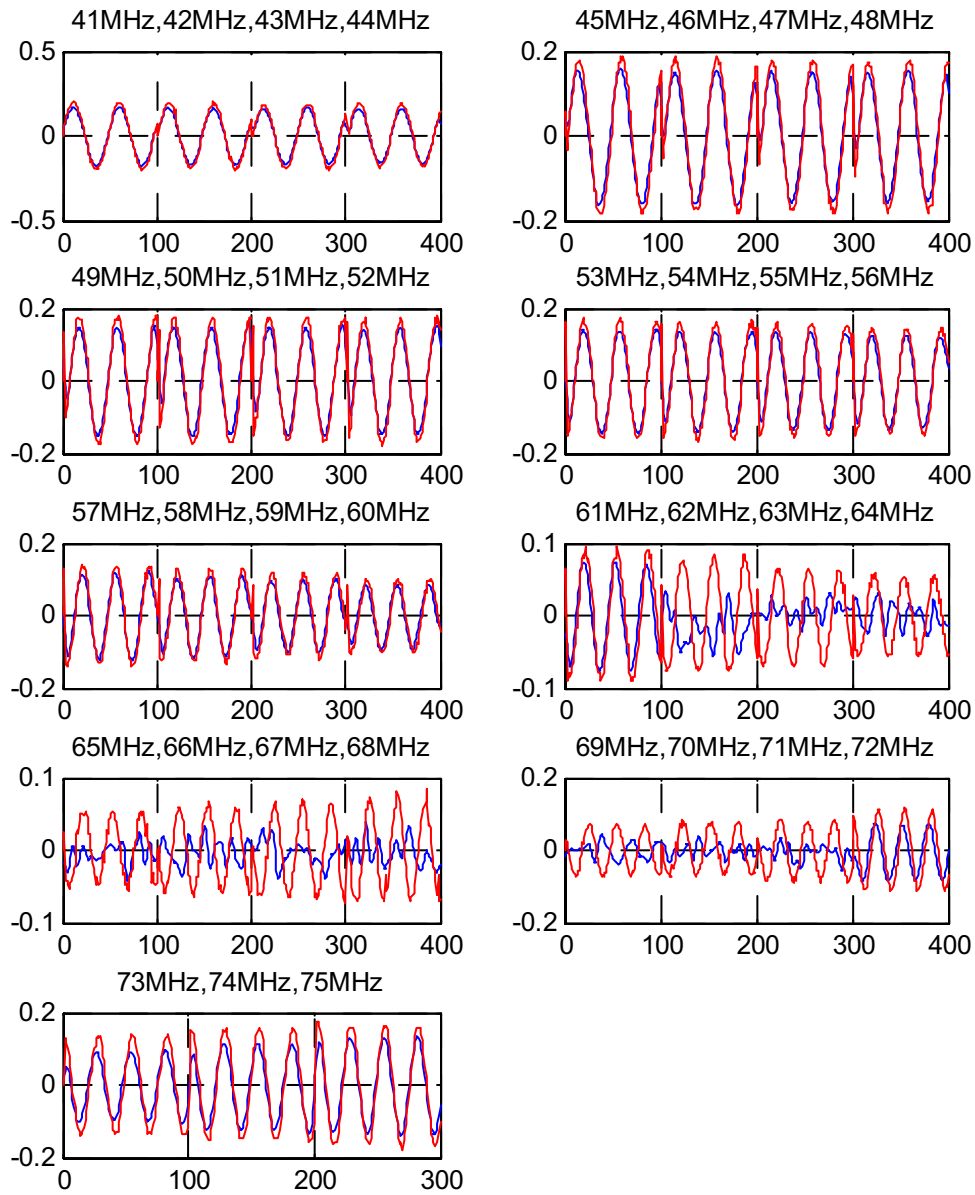


Figure 4.26 The figure shows the difference between the smoothed output estimate and the measured output of a representative PC-12 cell sample. Red shows the cell sample output. Blue shows the estimated output. Upper scale denotes frequencies. Lower scale shows sample intervals. Y scale shows magnitude in volts (V).

4.5 Residual Analysis

One can compare the difference between the estimated results of the samples of both cell-types and the output measurements of the oscilloscope. While this would be a way to identify the different cell samples, this research effort opted doing residual analysis instead. While residual analysis is not the only method available that could be used to identify cells, it was used in this case because it was readily available and easily implemented. With this in mind, the research effort focused on identification by studying the residual results acquired from the estimates and the measurement outputs. Residuals are defined as the difference between an estimated value and an actual value. For more on residuals, refer to Sections 3.2.1 and 3.2.2. Residuals are important because they show the adaptability of the filter to the system. A low residual shows that a filter is adapting accurately, while a high residual shows that a filter is not estimating the response correctly (22). Naturally, it would be ideal if the filter could accurately estimate the output of the HEL-30 cell samples, and not be able to estimate the PC-12 cell sample output.

4.5.1 Residual Results. Typical residuals of both cell samples in Plate 11 (HEL-30 cells), and Plate 14 (PC-12 cells) are compared in Figure 4.27. An empirical threshold was placed in order to separate low residuals from high residuals. The smoother can estimate a measurement rather closely, but will seldom provide a residual value that is exactly zero. Therefore an empirical threshold of 7mV was used to distinguish "large" residuals from "small" residuals. An issue of concern was the fact that even though the residuals in the HEL-30 samples were consistently lower than the residuals of the PC-12 samples, the HEL-30 sample residuals were continually above the threshold through all frequencies. A blown up plot such as Figure 4.28 and Figure 4.29 illustrate why this happened. It can be observed by looking at the plot that residuals of both types of cell samples spike when there is a frequency change. During a frequency change, the filter has a harder time making the correct estimate, but soon recovers. The tuning of the filter helped reduce the spikes at the frequency changes, but not enough to remove them completely. Other than the spikes, it was observed that the residuals of the HEL-30 cell samples were consistently lower than the residuals estimated with the PC-12 samples.

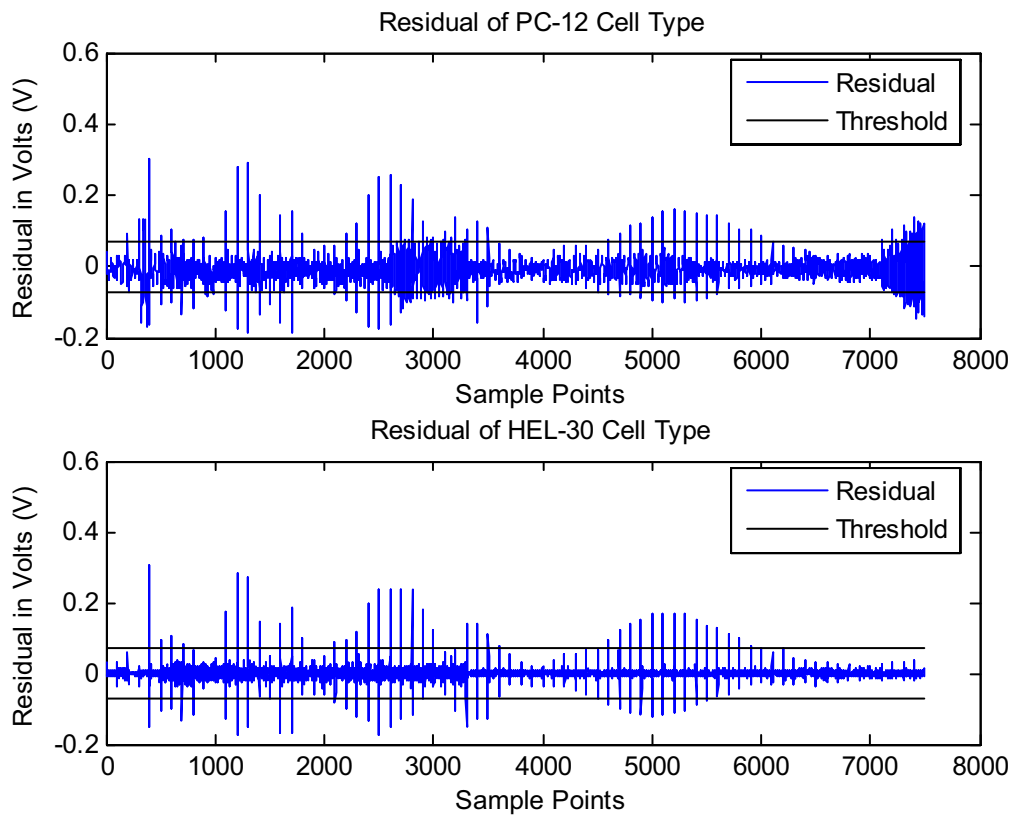


Figure 4.27 Typical comparison between residuals from HEL-30 cell sample and PC-12 cell sample. Black line delineates allowable threshold error in the estimate.

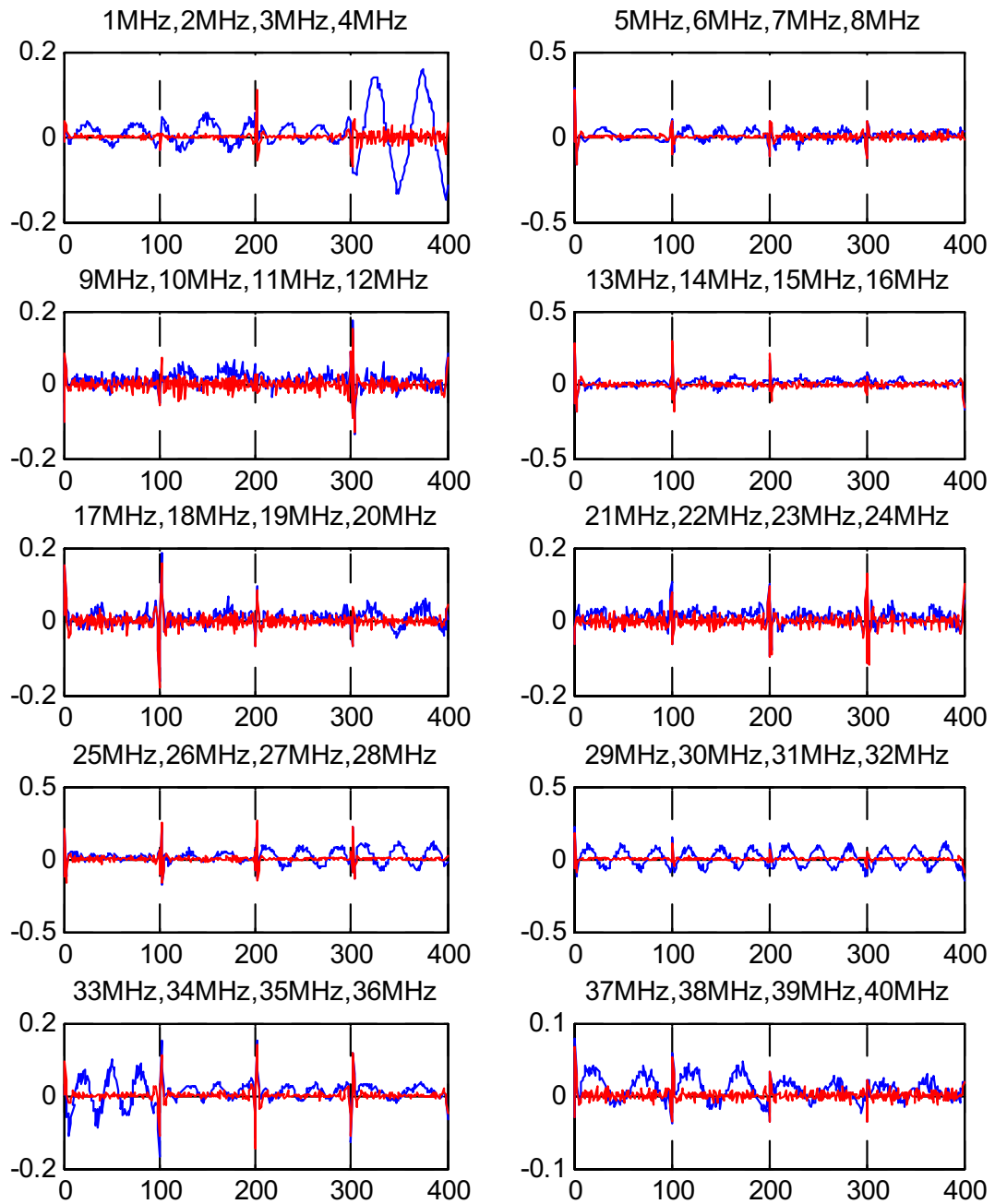


Figure 4.28 Plot of comparison between residual values of HEL-30 cell sample (Red), and PC-12 sample (Blue). Upper scale measured the frequency. Lower scale shows sample point. Y scale is amplitude in volts (V).

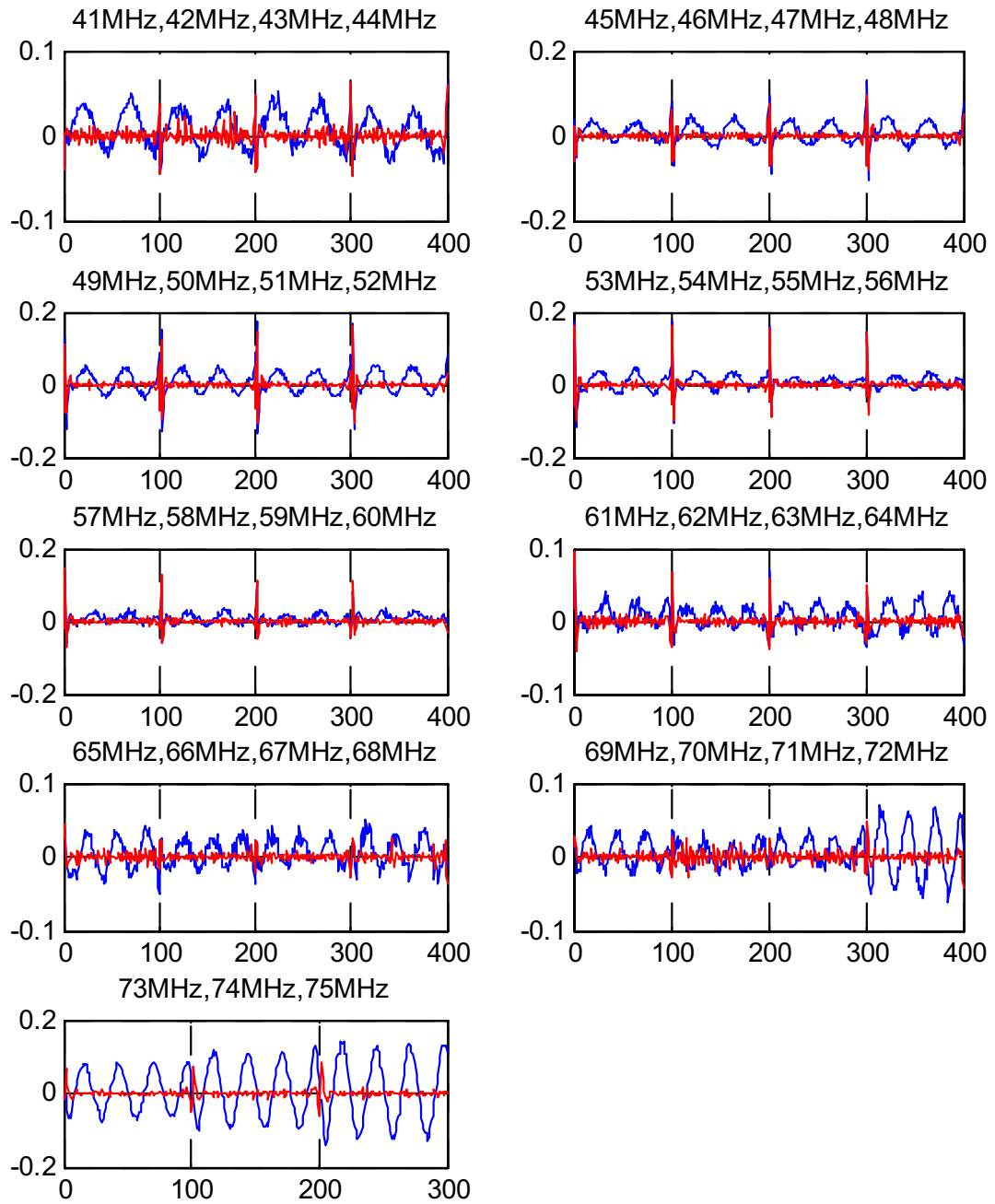


Figure 4.29 Plot of comparison between residual values of HEL-30 cell sample (Red), and PC-12 sample (Blue). Upper scale measured the frequency. Lower scale shows sample point. Y scale is amplitude in volts (V).

4.5.2 *Results from Windowing.* Some of the high residual values had to be removed from the data at the frequency boundaries in order to properly use the data for cell identification. To remove the high residuals that only occurred at frequency boundaries, a windowing method was devised. This windowing method made use of binary logic to address the issue of samples being above the threshold for short durations.

The routine for windowing looks at each sampled residual and organizes them into a defined value calculated by Equation (4.17),

$$\mathbf{m}(t_i) = \begin{cases} 1, & \mathbf{r}(t_i) \geq c \\ 0, & \mathbf{r}(t_i) < c \end{cases} \quad (4.17)$$

where $\mathbf{m}(t_i)$ is indicator value on whether the residual is above or below the threshold, c . For the purposes of this research, events were defined as a residual being above the threshold.

Finally, identification is established based on a hypothesis. This hypothesis states that if, at any time, there are a predefined number of consecutive events (a number of concurrent $\mathbf{m}(t_i) = 1$ values in a predefined window area), then a cell sample mismatch decision is declared:

$$\begin{cases} \mathbf{h}(t_i) = 1 & \sum_{i-w}^i \mathbf{m}(t_i) \geq w \\ \mathbf{h}(t_i) = 0 & \sum_{i-w}^i \mathbf{m}(t_i) < w \end{cases} \quad (4.18)$$

where w is the window size and $\mathbf{h}(t_i)$ is a hypothesis assigned a binary value based on whether it is true or false at any individual sample time.

For the purposes of this study, a threshold was defined as $c = 7\text{mV}$. The window size was defined as $w = 5$. Figure 4.30 depicts a flow-diagram describing the logic process.

Figure 4.31 is a representative plot of the residuals having been subjected to windowing. It is extremely clear in the plot that the PC-12 cell samples are consistently instancing the predefined hypothesis at different frequencies. Looking at Table 4.5 it can be observed that HEL-30 cells have no true hypothesis points plotted. This is representative that the hypothesis is, and should be, false with cell samples that match the model-derived



Figure 4.30 Flow diagram describing the process of windowing. Windowing is a method to determine if residuals are consistently above a certain threshold.

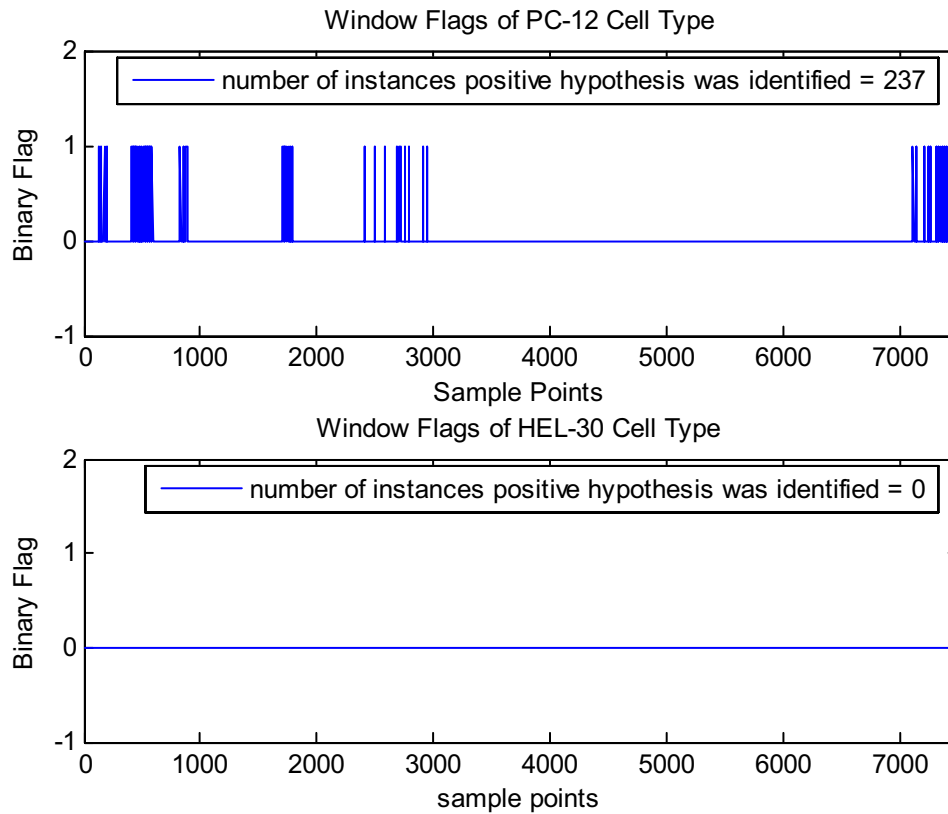


Figure 4.31 Window plot representing flags from windowing the data in residual plots from Plate 14 and Plate 11.

smoother. If at anytime the estimates have a residual higher than the threshold (i.e., when there is a frequency change), it takes the smoother less than five sample periods to start estimating accurately again. This is not the case with the samples of the PC-12 cells, which are consistently breaking the threshold between 1MHz-30MHz and again between 70MHz and 75MHz.

While the representative window plot of Figure 4.31 is typical, there were some extreme cases. Figure 4.32 shows a PC-12 cell sample where the smoother had a very hard time estimating the output measurements. In total 465 instances of the residual breaking the threshold at five consecutive points were recorded. This figure does, however, show that the extra flags were instanced around the same frequency range as in Figure 4.31. Examining the actual residual plot for this flag plot (refer to Figure 4.33), it can be seen that most of the residuals barely break the threshold. But it can also be observed that the

Table 4.5 The table shows how many flags each of the samples in Plate 11 (made up of 21 HEL-30 samples), and Plate 14 (made up of PC-12 samples) raised as a result of their residuals not being below acceptable thresholds. Based on this data, it can be safe to assume that system identification is possible based on the number of times the residuals of the data exceed a specific limit

Sample #	Positive Hypothesis Instances Plate 11 (HEL-30)	Positive Hypothesis Instances Plate 14 (PC-12)
1	0	91
2	0	115
3	0	237
4	0	9
5	0	450
6	0	62
7	0	130
8	0	242
9	0	202
10	0	465
11	0	256
12	0	285
13	0	397
14	0	194
15	0	218
16	0	165
17	0	137
18	0	142
19	0	203
20	0	112
21	0	71

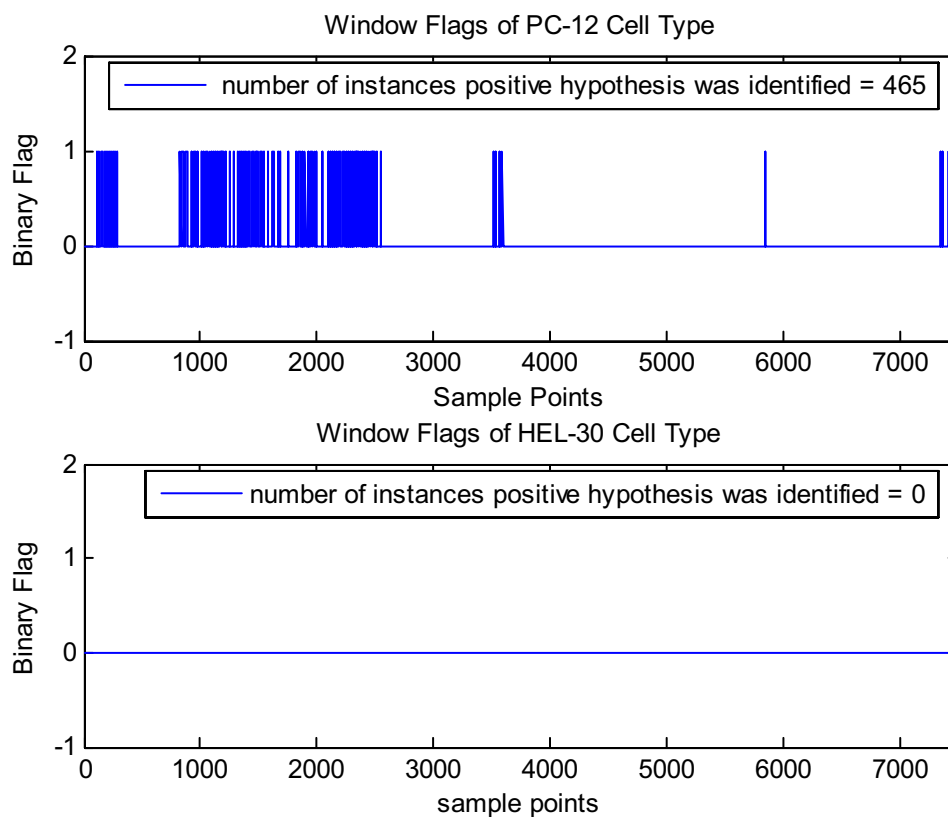


Figure 4.32 Window plot representing extreme amount of flags from windowing the data in residual plots from Plate 14 (top) and Plate 11 (bottom).

residual plot shows much higher residuals than shown plot in Figure 4.27. There could be many reasons for this phenomenon. It could be that for some reason the cellular response was unusually erratic. It could also be postulated that some biological phenomena beyond the scope of this research is represented in these measurements.

On the other side of the spectrum, Figure 4.34 shows a PC-12 cell sample that seems to have been very well estimated by the smoother (although still showing true hypothesis instances plotted). This sample could be considered an anomaly because while the previous plot on Figure 4.32, instanced a true hypothesis in an excessive number of sample points, Table 4.5 shows other samples where a commensurate number of samples identified a positive hypothesis. This is the only estimate, however, that identified a true hypothesis in only nine samples. Regardless of this observation, it can be shown that this

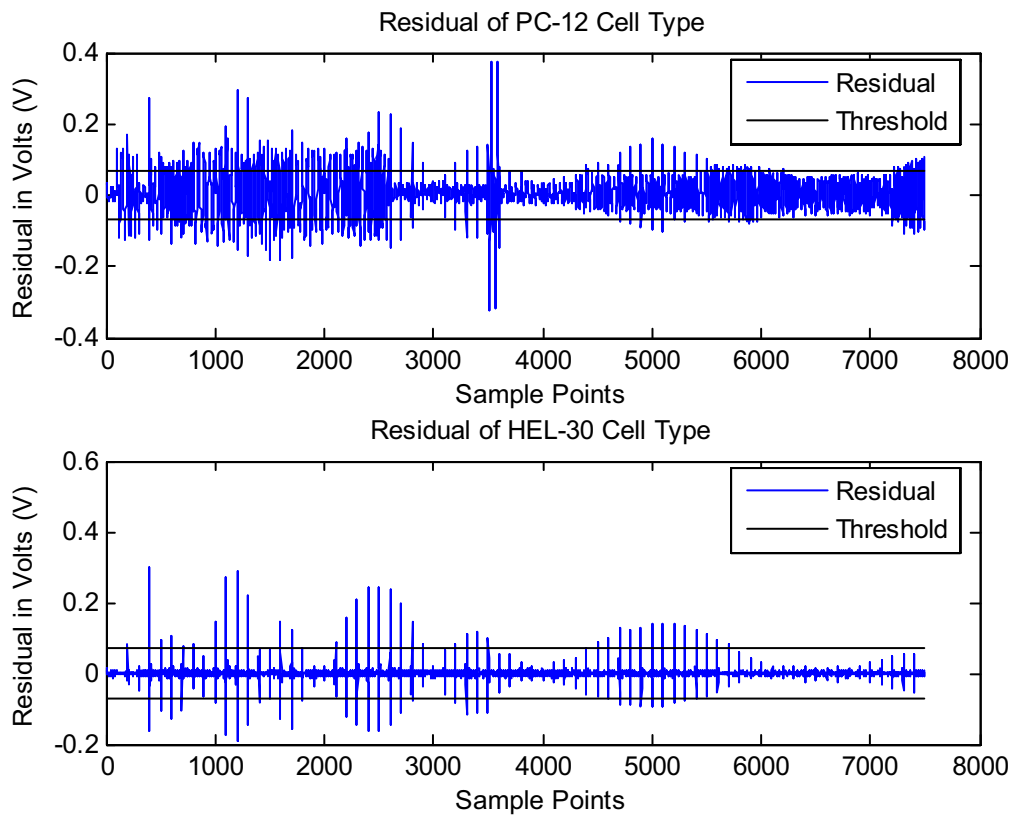


Figure 4.33 Comparison between residuals from HEL-30 cell sample and PC-12 cell sample. Black line delineates allowable threshold error in the estimate.

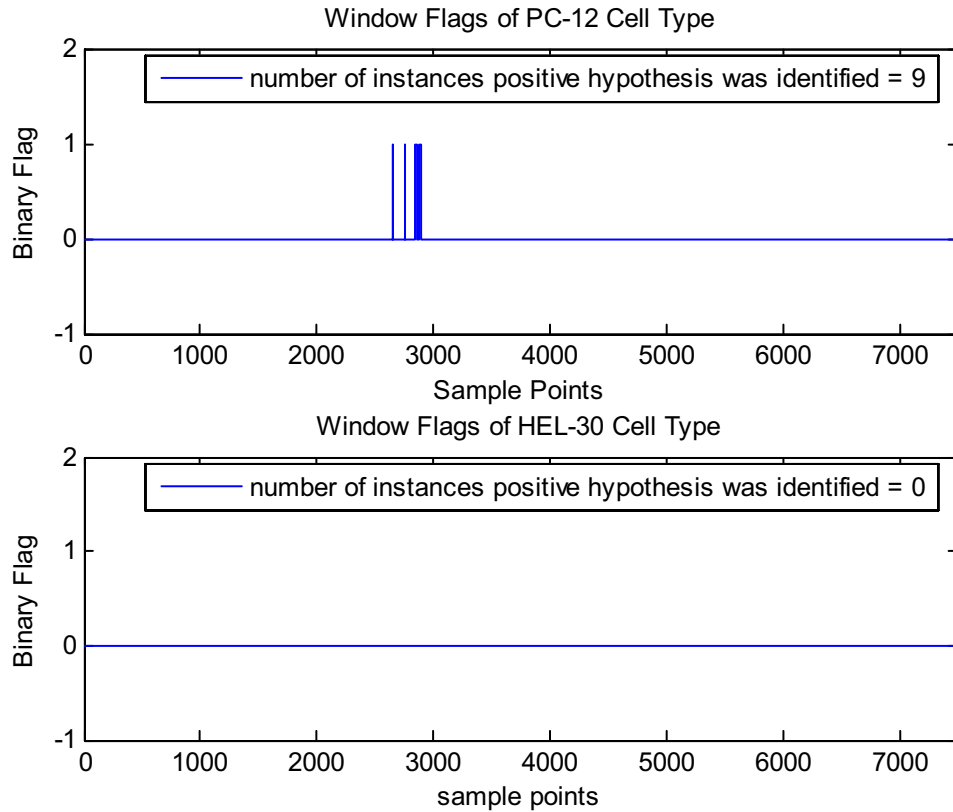


Figure 4.34 Window plot representing minute amount of flags from windowing the data in residual plots from Plate 14 (Top) and Plate 11 (bottom).

method for identifying cell samples is effective based on the two different cell-types used in this study. Residuals on Figure 4.35 show a significant difference between the estimated values of the two cell types, yet still below the empirical threshold.

Based on the information in Table 4.5, it is logical to surmise that a method made up of Electrical Impedance Spectroscopy and Stochastic Estimation and Control concepts can be implemented to successfully identify a cellular sample. The results of this research suggest that cellular sample identification is made possible by implementing a stochastic fixed interval smoother.

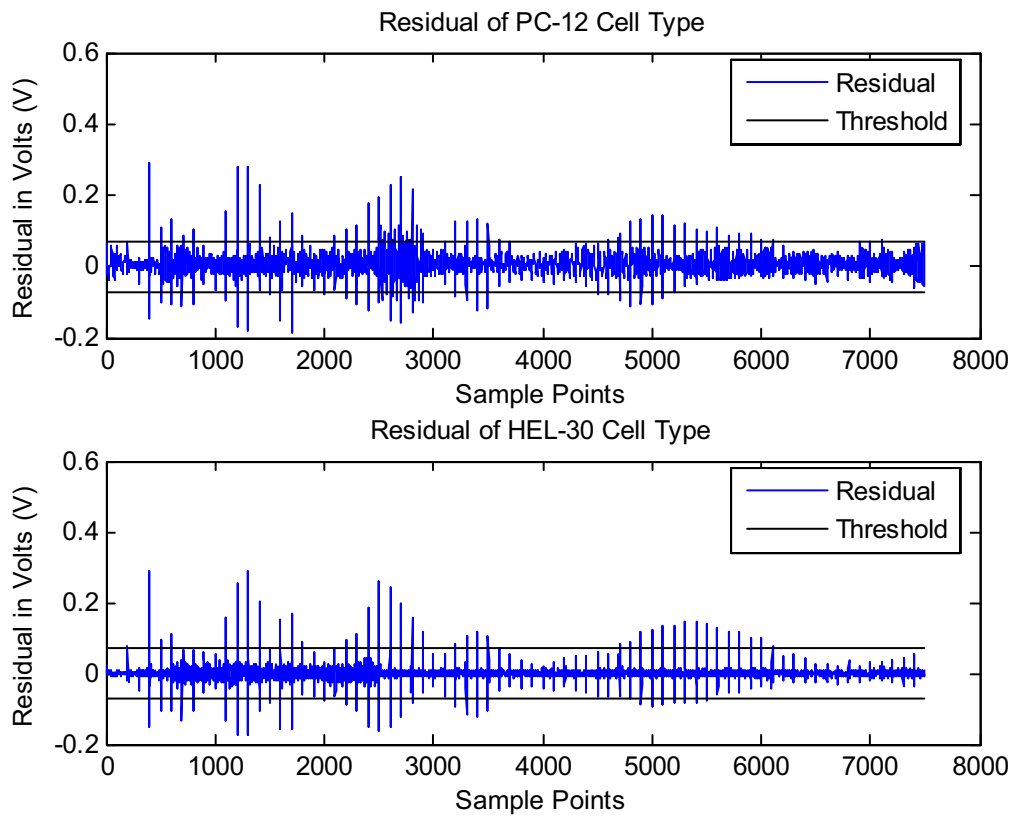


Figure 4.35 Comparison between residuals from HEL-30 cell sample and PC-12 cell sample. Black line delineates allowable threshold error in the estimate.

V. Conclusions and Recommendations

This chapter is written in order to summarize the work accomplished throughout this study. It will initially review and reinstate what the original goals of the project were. Section 5.2 will then continue to describe how the goals stated in Section 5.1 were met. The next section will delineate the benefits of continuing in this line of research. Finally, recommendations for future research will be made in the final section before the conclusion.

5.1 Restatement of Research Goals

The goals of this research were simple: to see if the synthesis of two disciplines, Electrical Impedance Spectroscopy (EIS) and Stochastic Estimation and Control (SEC) would provide a new type of experimental method that could identify cellular samples via their electrical characteristics. By using EIS theories, measurements that characterized the input and output of a cell sample could be used to build a transfer function that characterized the electrical behavior of a cell sample. Based on this transfer function, a fixed interval smoother could be developed and used to estimate samples of the system.

It was postulated that if the stochastic smoother (originally built from the transfer function of HEL-30 cell electrical characteristics) was able to properly estimate the output of the cell sample, other cell samples would be different enough so as not to be estimated well with the smoother. Identification of a cell-type would be based on the precision with which the smoother was able to estimate the output of such sample. An empirical threshold would be applied and, if the smoother matched the cell type, the residuals for such cell system would not exceed the threshold. This would be the basis of the identification of the cellular sample.

5.2 Summary of Results

When the residuals were first calculated (Figure 4.27), it was very hard to establish a threshold on the data that would provide distinguishability of the cells. The residual plot of the HEL-30 cells consistently showed lower residuals than the PC-12 cells.

Upon closer inspection, the residuals that were consistently higher than the threshold occurred during the times that the oscilloscope transitioned through different frequencies. The smoother had trouble estimating during frequency transitions, but it went back to estimating residuals to an acceptable threshold within one or two sample periods. Based on this observation, it was decided that a windowing algorithm could be used to more efficiently show where the residuals were above the threshold while at the same time eliminating those residuals that were created when the smoother tried to estimate over frequency boundaries.

The windowing algorithm developed to properly identify significant changes in residuals worked. It progressively compared every sample to the threshold. When a residual was below the threshold, it was plotted with a value of zero, denoting that the hypothesis for a mismatch had not been met. If the sample residual was above the threshold, then it would be labeled as an event. The hypothesis was that if a set window number of consecutive events were detected, then the hypothesis would become true. A true hypothesis denotes a model mismatch from the cell sample. In this way, any estimate that was above the threshold due to a frequency change was not recorded. By the same token, any estimate that was consistently above a residual threshold due to the fact that the model did not match the measurements was recorded. Table 4.5 clearly shows that the cellular samples used to build the model were estimated very accurately, while the cell samples from a different cell-type could not be estimated as accurately. From the data displayed on the table, one can see that only three cell samples had less than 90 detections of a true hypothesis. In the most extreme case, one PC-12 cell sample showed only 9 occasions where the system detected a true hypothesis (refer to Figure 4.34). This anomaly is likely due to equipment or measurement errors. Most of the PC-12 cellular samples were identified to have at least 100 true hypothesis detections. Based on the research, the flag-counting method could be used to correctly identify the HEL-30 cell sample from a PC-12 cell sample given their electrical characteristics. The bottom line is that 100% of the cell samples' residuals of the same cell-type used to develop the smoother did not break the threshold barrier for more than five samples in a row. While 100% of the cell

samples' residuals from another cell-type broke the threshold five times in a row at least in nine different occasions.

5.3 Significant Contributions of Research

This research could have many contributions both in the military and the civilian sector. This experimental method is new, therefore its capacities could not completely be explored at this point. There are however many avenues that could be used to expand this research.

5.3.1 The Military Sector. In the military sector, this research could be expanded in many directions. By being able to identify a cell-type from a sample, the military could build sensors that identify certain types of biological agents via their electrical characteristics. Also, research and development could use a very highly tuned version of this experimental method to develop a device that identifies different cell processes within the same cell-type.

Implementation of this experimental method could also be of practical use in the field based on the fact that it makes use of electrical impedance. Handheld devices could be developed that test for a specific biological phenomenon. Handheld devices that test for certain biological agents in the water could also be developed.

5.3.2 The Civilian Sector. Through this experimental method, a device could be developed for testing different types of benign or malignant cancers. Myoscopies would be a thing of the past, if tumors could be tested simply by introducing a Micro Electro Mechanical Systems (MEMS) device into the body to test for malignancy.

The civilian sector is looking for different tools to identify markers to learn more about new diseases. A cure for cancer, or even arthritis and Alzheimer's is not yet available, but there is research that suggests that these maladies could be prevented if they are detected in time. By developing this experimental method to look for different biological markers within the same cell-type, an inexpensive early-warning procedure could be developed.

5.4 Recommendation for Future Research

It is wise to point out that these are the first steps to developing a new type of experimental method. While it is admitted that this method is not ready for full implementation, this research has found that it has a lot of potential. Given this, recommendations for future research are as follows:

5.4.1 More Accurate Experimentation. There needs to be an improvement in the experimental method. While this project was accurate enough to notice a significant change between two cell-types, other cell-types may have electrical characteristics that more closely resemble the tested cell samples' electrical characteristics. Probes need to be developed specifically for this type of testing. While the probes in this research were accurate enough to take measurements, experimentation on the correct kind of probing of these cell samples could be developed. Also, research on different types of testing could be implemented (this research made use of two lead probes, but four-lead probing may be more accurate).

More accurate equipment could be used in the experimentation. This experiment used the best function generator, oscilloscope and interface, available given the economic constraints. Different companies have already developed probes, techniques and machines that will test EIS.

Finally, the stochastic smoother process could also be improved. While this research was very careful to make all the correct assumptions, there is no doubt that any experimental method could be improved. Given this, expansion on the modeling and stochastic theory would make a great impact in future accuracy of the results. Recommendations of this type would include to build a Multiple Model Adaptive Estimation (MMAE) filter. This filter makes use of more than one filter. This would be useful in many ways; it could help figure out which filter out of a multitude of filters gave the best estimate. Also, each filter could be tuned to estimate a different cell sample, making identification of multiple cell samples in one algorithm possible.

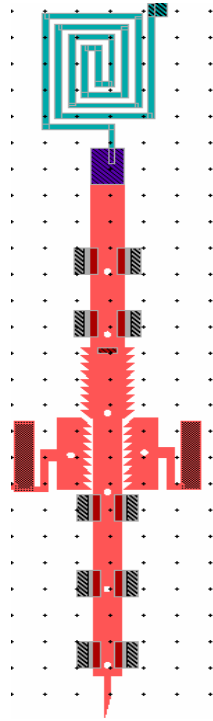


Figure 5.1 MEMS probe designed during this research but never implemented. Probe is $100\mu\text{m}$ long and $10\mu\text{m}$ wide and is made of polysilicon overlaid with gold. Probe thickness is $6\mu\text{m}$. Gold wire (Blue) connects probe to wire bonded gold pad.

5.4.2 MEMS. Recent research efforts by many people have gone towards the development of EIS via the use of MEMS probes (4, 9, 19, 36). At one point, this thesis would have tackled such an endeavour, but given the complexity of the research, it was decided that this effort had to be abandoned. Future research would definitely improve if this technology were implemented. Several different methods of fabricating MEMS probes for biological purposes have already been in industry. Numerous MEMS probes were fabricated for use in testing and one design is shown in Figures 5.1 and 5.2. By using MEMS in future studies, researchers could test a single cell instead of a cell sample (each cell sample consisted of about 70,000 cells). This would allow for increased accuracy in the estimation of different cells, and allow for testing of specific phenomena within the same cell type. Inherent problems in this type of research would include the signal interference from probes, isolation of a single cell, and fabrication of biologically friendly electrical devices.

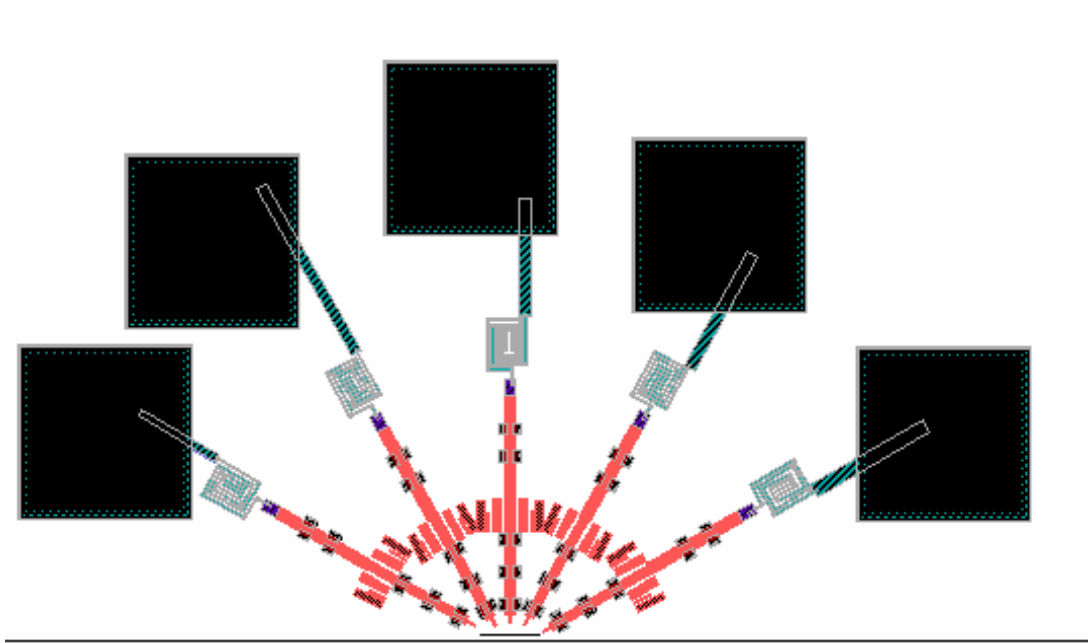


Figure 5.2 Probe array designed for cell testing. Given that different cells vary in size, this probe is designed to be fit around a cell and then probe from different angles for best measurement accuracy. Each of these probes are the same as in Figure 5.1.

5.4.3 Noninvasive Designs. In theory, any development of EIS could be extended to identification given correct modeling and stochastic algorithms. In the spirit of this, biological identification could be extended to noninvasive methods. A noninvasive method of EIS pertains to the theory of electromagnetism. If a specific electromagnetic field were interrupted by an eddy field (a field in the opposite direction), then there would be a change in the inherent current that produced the electromagnetic field. In theory, one could put a current through a coil to make an electromagnetic field. If that magnetic field gets too close to the skin, the skin's natural eddy field would change the magnetic field, which in turn would change the current going through a coil. This current could then be tested for magnitude and frequency changes (for a more detailed explanation, refer to Chapter 2). A stochastic filter could be put in place to identify the cell type. In this way any anomalies in the skin cells (i.e., certain types of skin cancers begin mutating skin cells without visual confirmation of such a change) could be identified and different maladies could be prevented.

5.5 Conclusion

In conclusion, the goal to find an experimental method that could be used to identify a cell-type via its electrical characteristics was a success. While the full implementation of this experimental method is premature, the procedures show promise for future research. There are many inherent benefits of this type of biological identification, both in the civilian sector and the military sector. There are still, however, many facets of research that will need to be exploited before the theories presented here can be used.

Bibliography

1. A. Malicha, T. B. Ohmb, M. Faciusa I. Kleinteicha M. Flecka D. Saunera R. Andersonc W.A. Kaisera. "Electrical Impedance Scanning as a New Imaging Modality in Breast Cancer Detection: A Short Review of Clinical Value on Breast Application, Limitations and Perspectives," *Elsenvier*, 75–82 (2003).
2. Aberg, Peter. *Skin Cancer as Seen by Electrical Impedance*. MS thesis, University of Stockholm, 2004.
3. Adrian W. Bott, Ph.D. "Electrochemical Impedance Spectroscopy Using the BAS-Zahner IM6 and IM6e Impedance Analyzers," *Current Separations* 17/8, 1–3 (1998).
4. Alastair H. Kyle, Carmel T. O. Chan, Andrew I. Michinton. "Characterization of Three-Dimensional Tissue Cultures Using Electrical Impedance Spectroscopy," *Biophysical Journal*, 2640–2648 (2005).
5. B. Frazier, C. Friedrich, R. D. Warrington. "The Miniaturization Technologies: The Past, Present and Future," *Industrial Electronics, Control and Instrumentation*, 3:1460–1465 (1994).
6. Blady, B'orje and Bo Baldetorp. "Impedance Spectra of Tumour Tissue in Comparison With Normal Tissue; A Possible Clinical Application for Electrical Impedance Tomography," *Physiol. Meas.*, 17:A105–A115 (1996).
7. Blady, O'orje and Bo Baldetorpz. "Impedance Spectra of Tumour Tissue in Comparison With Normal Tissue; A Possible Clinical Application for Electrical Impedance Tomography," *Physiol. Meas.*, 1–11 (1996).
8. Carmichael, J., Degraff W.G. Gazdar A.F. Minna J.D. and J.B Mitchell. "Evaluation of a tetrazolium-based semi automated colorimetric assay: Assessment of chemo sensitivity testing," *Cancer Res.*, 47:936–942. (1987).
9. Cole, Kenneth S. *Electric Phase Angle of Cell Membranes*. Technical Report, From the Department of Physiology, College of Pkysicians and Surgeons, Columbia Universily, New York, 1932.
10. D. O. Mendonca, M. N. Souza. "Application of Step Response Impedance Spectroscopy for Detection of Skin Irritation," *Proceedings of the 25th Annual International Conference of the IEEE Engineering in Medicine and Biology Society* (2003).
11. Evgenij Varsoukov, J. Ross Macdonald. *Impedance Spectroscopy, Theory, Experiments, and Applications*. John Wiley and Sons Inc., 2005.
12. Fumihito Arai, Tomohiko Sugiyama, Toshio Fukuda Hitoshi Iwata Kouichi Itoigawa. "Micro Tri-Axial Sensor for 3D Bio-Micromanipulation," *Proceedings of the 1999 IEEE International Conference on Robotics and Automation*, 2744–2749 (1999).
13. H. E. Ayliffe, S. D. Brown and R. D. Rabbitt. "Micro-Electric Impedance Spectra of Isolated Cells Recorded in Micro-Channels," *Proceedings of the Second Joint EMBS/BMES Conference*, 1692–1693 (October 23-26, 2002 2002).

14. Institute, The Rockefeller, "Journey Into the Cell." <http://www.rockefeller.edu/ru.home.php>, 1995.
15. Instruments, National, "GPIB Tutorial." <http://www.hit.bme.hu/people/papay/edu/GPIB/tutor.htm>, 1987.
16. Ionescu-Tirgoviste, C. and S. Pruna. "Non-Invasive Assessment of Peripheral Dysfunction of the Autonomic Nervous System," *IEEE Engineering in Medicine and Biology Society*, 1–2 (1988).
17. J.R. Macdonald, J.A.Garber. "Analysis of Impedance and Admittance Data for Solids and Liquids," *Journal of Biochem*, 124:1022–1030 (1977).
18. Judy, Jack W. *Biomedical Applications of MEMS*. Technical Report, University of California, 2000.
19. J.W, Judy. "Biomedical Applications of MEMS," 1–12 (2000).
20. Lennart Ljung, Torkel Glad. *Modeling of Dynamic Systems* (1 Edition). Englewood Cliffs, NJ: Prentice Hall, 1994.
21. Ljung, Lennart. *System Identification Toolbox*. MATLAB Manual.
22. Maybeck, Peter S. *Stochastic Estimation and Control, Vol. I*. Navtech, 1994.
23. McAdamst, E T and J Jossinett. "Tissue Impedance: A Historical Overview," *Physiol. Meas.*, A1–A13 (1995).
24. Ogata, K. *Discrete-Time Control Systems* (4th Edition). Upper Saddle River, New Jersey: Prentice Hall, 1995.
25. Ogata, Katsuhiko. *System Dynamics* (3rd Edition). Upper Saddle River, NJ.: Prentice Hall, 1998.
26. Ogata, Katsuhiko. *Modern Control Engineering* (4th Edition). Upper Saddle River, New Jersey: Prentice Hall, 2002.
27. Patterson, Robert and Todd Latterell. "Evaluation of a Commercial Impedance Spectroscopy Instrument: Inaccuracies and Their Corrections," *IEEE Clinical Engineering/Medical Informatics*, 651–652 (1995).
28. Prausnitz, Mark R. "Do High-Voltage Pulses Cause Changes in Skin Structure?," *Journal of Controlled Release*, 321–326 (1996).
29. R. D. Armsstrong, W.P. Race and H.R. Thrisk. "Determination of Electrode Impedance over an Extended Frequency Range by Alternating-Current Bridge Methods," *Electrochim. Acta*, 23:215 (1968).
30. R. Ivanic, M. Weis, T. Danilla and V. Tvarozek. "Thin Film Interdigitated Electrode Arrays Applicable for Non-Invasive Monitoring of Human Skin," *Advanced Semiconductor Devices and Microsystems, The Third International EuroConference*, 319–322 (2000).
31. Rejali, Darius, "Electricity: The Global History of a Torture Technology." www.academic.reed.edu, 1994.

32. Richard C. Petty, Stevan Kun and Robert A. Peura. "Tissue Ischemia Measurement Using Induced Current Impedance Spectroscopy: Non-Contact System Design," *24th Annual North East Bio-Engineering Conference*, 74–76 (1998).
33. S. M. Hussain, A. Javorina, A. M. Schrand H. Duhart S. F. Ali J. J. Schlager. "The Interaction of Manganese Nanoparticles (Mn-40 nm) with PC-12 Cells Induces Dopamine Depletion." 2006.
34. Saber M. Hussain, Carol M. Amato, David R. Mattie John J. Schlager. "In Vitro Toxicity of Silver Nanoparticles in a Mouse Keranocyte Cell Line.." Unpublished, 2006.
35. Salter, D. C. *Quantifying Skin Disease and Healing in Vivo Using Electrical Impedance Measurements*. Oxford: Sthe Slade Hospital, 1979.
36. Sebaek O. H, Joon Sung Lee, Ki-Hun Jeong and Luke P. Lee. "Minimization of Electrode Polarization Effect by Nanogap Electrodes for Biosensor Applications," *16th Annual International Conference on MEMS*, 52–55 (2003).
37. Todd E. Kerner, Keith D. Paulsen, Alex Hartov Sandra K. Soho and Steven P. Poplack. "Electrical Impedance Spectroscopy of the Breast: Clinical Imaging Results in 26 Subjects," *IEEE Transaction on Medical Imaging*, 638–645 (2002).
38. Vincent Senez, Takatoki Yamamoto, Tatsuhiro Fukuba Shinsuke Usui Jean-Marc Capron Serge Ostrovidov Teruo Fujii. "PDMS Based Microelectodfluidic Devices for Impedance Spectroscopy of single Cells and Tissues," (2003).
39. Weiland James D, Anderson David J, Pogatchinik Chris C-Boogard Jerry J. "Recessed Electrodes Formed by Laser Ablation of Parylene Coated, Micromachined Silicon Probes," *IEEE/EMBS Proceeding- 19th International Conference*, (O):2273–2277 (Oct. 30-Nov 2 1997 1997).
40. X. J Zhang, S. Zappe, R. W. Bernstein C. C. Chen O. Sabin M. Scott and O. Solgaard. "High-Precision Characterization of Embryo Positioning Force Using MEMS Optical Encoder," *7th International Conference on Miniaturized Chemical and Bio-medical Analysis Systems*, 805–808 (October 2003).
41. Yael A. Clickman, Orna Filo, Magda DAvid Avner Yayon Moris Topaz Bosmat Zamir Alexander Ginsburg Dganit Rozenman and Gad Kenan. "Electrical Impedance Scanning: A New Approach to Skin Cancer Diagnosis," *Skin Research and Technology*, 262–269 (2003).

REPORT DOCUMENTATION PAGE

*Form Approved
OMB No. 074-0188*

The public reporting burden for this collection of information is estimated to average 1 hour per response, including the time for reviewing instructions, searching existing data sources, gathering and maintaining the data needed, and completing and reviewing the collection of information. Send comments regarding this burden estimate or any other aspect of the collection of information, including suggestions for reducing this burden to Department of Defense, Washington Headquarters Services, Directorate for Information Operations and Reports (0704-0188), 1215 Jefferson Davis Highway, Suite 1204, Arlington, VA 22202-4302. Respondents should be aware that notwithstanding any other provision of law, no person shall be subject to a penalty for failing to comply with a collection of information if it does not display a currently valid OMB control number.

PLEASE DO NOT RETURN YOUR FORM TO THE ABOVE ADDRESS.

1. REPORT DATE (DD-MM-YYYY) 23-03-2006		2. REPORT TYPE Master's Thesis		3. DATES COVERED (From - To) Aug 2004 - Mar 2006	
4. TITLE AND SUBTITLE Biological System Impedance Identification Using Stochastic Estimation and Control				5a. CONTRACT NUMBER	
				5b. GRANT NUMBER	
				5c. PROGRAM ELEMENT NUMBER	
6. AUTHOR(S) Mendezaceves, Enrique, 2d Lt, USAF				5d. PROJECT NUMBER	
				5e. TASK NUMBER	
				5f. WORK UNIT NUMBER	
7. PERFORMING ORGANIZATION NAMES(S) AND ADDRESS(S) Air Force Institute of Technology Graduate School of Engineering and Management (AFIT/EN) 2950 Hobson Way WPAFB OH 45433-7765				8. PERFORMING ORGANIZATION REPORT NUMBER AFIT/GE/ENG/06-41	
9. SPONSORING/MONITORING AGENCY NAME(S) AND ADDRESS(ES) N/A				10. SPONSOR/MONITOR'S ACRONYM(S)	
				11. SPONSOR/MONITOR'S REPORT NUMBER(S)	
12. DISTRIBUTION/AVAILABILITY STATEMENT APPROVED FOR PUBLIC RELEASE; DISTRIBUTION UNLIMITED.					
13. SUPPLEMENTARY NOTES					
14. ABSTRACT Impedance spectroscopy, the measurement of the complex resistance of a biological body, is not a new technology; it has been around for many years and has been used to make electrical representations of different biological systems. The problem with this procedure is that models cannot be used for system identification. Stochastic estimation can complement a model produced by analyzing the input/output characteristics of a cell sample to account for modeling inadequacies produced by the linear modeling of electrical impedance spectroscopy alone. In this thesis, biological cell samples were submitted to a sinusoidal voltage at a different range of frequencies. The cell samples created an output which was used to model the electrical behavior of the biological system. This electrical representation was used to build a fixed-interval stochastic smoother. The stochastic smoother was then used to estimate the output measurements of different cell samples and ultimately identify a cell type based on the evaluation of the residuals produced.					
15. SUBJECT TERMS Stochastic Estimation and Control, Electrical Impedance Spectroscopy, Fixed-Interval Smoother, Biology, HEL-30, PC-12, Cellular Identification, Residual Monitoring.					
16. SECURITY CLASSIFICATION OF:		17. LIMITATION OF ABSTRACT		18. NUMBER OF PAGES	
REPORT U	ABSTRACT U	c. THIS PAGE U		UU	
				120	
				19a. NAME OF RESPONSIBLE PERSON Juan R. Vasquez, Lt Col, USAF (ENG)	
				19b. TELEPHONE NUMBER (Include area code) (937) 255-3636, ext 7231; e-mail: juan.vasquez@afit.edu	

Standard Form 298 (Rev. 8-98)
Prescribed by ANSI Std. Z39-18